

**CENOZOIC INTRUSIVE AND EXHUMATION HISTORY OF THE ELK AND
WEST ELK MOUNTAIN PLUTONS, SOUTHWEST COLORADO**

By

Rebecca V. Garcia

Submitted in partial fulfillment
of the requirements for the degree of
Master of Science in Geology

New Mexico Institute of Mining and Technology
Department of Earth and Environmental Science

Socorro, NM

August 2011

To my family and friends, thank you for your love and support.

ABSTRACT

The Elk and West Elk Mountains of southwest Colorado are dotted with middle Cenozoic plutons that can provide important geochronological and thermochronological data about the plutonic emplacement and exhumation interval between the end of Colorado Mineral Belt (CMB) magmatism and the onset of San Juan volcanic field activity. $^{40}\text{Ar}/^{39}\text{Ar}$ biotite and U/Pb zircon geochronology are used to determine intrusion age, whereas low temperature apatite fission-track (AFT) and apatite (U-Th)/He (AHe) thermochronology constrain the cooling history of the region. Exhumation patterns found in the data are used to evaluate possible links to present-day low seismic velocity zones in the upper mantle beneath western Colorado, specifically the San Juan Mountains. Intrusion ages based mainly on $^{40}\text{Ar}/^{39}\text{Ar}$ dates generally decrease from north to south and can be broadly grouped into ca. 34 Ma and 30 Ma suites. The AFT and AHe ages are either equivalent to or younger than their corresponding intrusion ages. In general, the majority of the plutons experienced slow cooling between 110 and 60°C after emplacement that reflects denudation. The two southernmost plutons (East Beckwith and Gunnison) cooled far more rapidly than the plutons to the north and were likely emplaced within 1-2 km of the present surface. Additionally, the low temperature data for these two plutons are equal within error to their $^{40}\text{Ar}/^{39}\text{Ar}$ biotite ages and demonstrate emplacement structurally above the ambient 70°C isotherm. The low temperature data from this study, along with regional AFT data, demonstrate distinct periods of cooling that indicate a

pulsed cooling and exhumation history across the Colorado Rocky Mountains. The regional and new data sets record periods of exhumation during late Cretaceous to early Cenozoic Laramide deformation, during the middle Cenozoic time (AFT data) and at ~6 – 8 Ma (AHe data). The most recent pulse of exhumation recorded by AHe data from the West Elk Mountains may be related to dynamic topography that developed above hot, buoyant mantle located below the San Juan volcanic field.

Keywords: CREST; (U-Th)/He; Fission Track; Argon; Elk Mountains

ACKNOWLEDGEMENTS

I would like to begin by thanking my advisors, Shari Kelley and Matt Heizler, along with the rest of my committee members, Bill McIntosh and Jeff Johnson, for their guidance and support on this project. Daniel Stockli of the University of Texas Austin provided me with (U-Th)/He ages for my samples and insight into their meaning. George Gehrels of the University of Arizona provided support and insight into my U/Pb dates that were analyzed in his laboratory. Mark Mansell and Lewis Gillard helped draft some of my figures in ARC GIS. Joshua Feldman and Matthew Zimmerer gave me immeasurable help in the field and in the understanding of many concepts. The CREST members: Karl Karlstrom, Jonathan MacCarthy, Brandon Schmandt, Magdalena Sandoval-Donahue, and Andres Aslan to mention a few. I would especially like to thank my family and friends for their constant support and encouragement: Michael Garcia, Lucille Garcia, Gabriel Garcia, Jesse Trullijo, Trinidad Vigil, Laura Rosales, Shoba Maraj, Breanna Hennessy, Christina Forbes, Shari Houston, and Lara Owens.

I would also like to thank the following institutions for providing funding for this work:

National Science Foundation - CREST Project (Proposal # 0607693)

Minority Fellowship (New Mexico Institute of Mining and Technology)

CONTENTS

LIST OF TABLES	V
LIST OF FIGURES	VII
INTRODUCTION	1
1. GEOLOGIC BACKGROUND	4
1.1 REGIONAL SETTING	4
1.2 REGIONAL GEOLOGIC HISTORY	8
1.3 ELK AND WEST ELK MOUNTAINS	10
2. METHODS	19
2.1 SAMPLING	19
2.2 MINERAL SEPARATION	20
2.3 U/Pb	21
2.4 $^{40}\text{Ar}/^{39}\text{Ar}$	23
2.5 APATITE FISSION-TRACK	24
2.6 (U-Th)/He	26
2.7 MODELING	28
3. RESULTS	32
3.1 EMPLACEMENT HISTORY	32

3.1.1 U/Pb: Zircon	32
3.1.2 ⁴⁰ Ar/ ³⁹ Ar: Hornblende	32
3.1.3 ⁴⁰ Ar/ ³⁹ Ar: Biotite	34
3.1.4 ⁴⁰ Ar/ ³⁹ Ar: K-Feldspar	37
3.2 COOLING HISTORY	41
3.2.1 Apatite Low Temperature Thermochronology	41
3.2.1.1 Qualitative Observations	41
3.2.1.2 Quantitative Observations	47
4. DISCUSSION	53
4.1 EMPLACEMENT HISTORY	53
4.2 COOLING HISTORY	60
4.3 REGIONAL THERMOCHRONOLOGY	63
CONCLUSION	70
APPENDIX A: GEOCHRONOLOGY DATA	72
APPENDIX B: LOW TEMPERATURE THERMOCHRONOLOGY DATA.....	94
APPENDIX C: ADDITIONAL DATA.....	103
REFERENCES.....	137

LIST OF TABLES

TABLE 1.1: PUBLISHED AGES. PREVIOUS GEOCHRONOLOGY CONDUCTED IN THE ELK AND WEST ELK MOUNTAINS.	15
TABLE 1.2: HEAT FLOW DATA FROM DECKER ET AL. (1988) AND REITER ET AL. (1975)....	16
TABLE 3.1: SUMMARY TABLE. ERRORS ARE SPECIFIED FOR EACH DATING TECHNIQUE. ARGON AGES ARE REPORTED AS INTEGRATED AGES.....	33
TABLE A.1: U/Pb ZIRCON ANALYTICAL DATA.....	73
TABLE A.2: HORNBLLENDE ⁴⁰ Ar/ ³⁹ Ar ANALYTICAL DATA.	76
TABLE A.3: BIOTITE ⁴⁰ Ar/ ³⁹ Ar ANALYTICAL DATA.	81
TABLE A.4: ⁴⁰ Ar/ ³⁹ Ar K-FELDSPAR ANALYTICAL DATA.....	88
TABLE B.1: APATITE FISSION-TRACK DATA.	95
TABLE B.2: APATITE (U-Th/He) DATA. ANALYZED BY D. STOCKLI AND R. KISLITSYN AT THE UNIVERSITY OF KANSAS. GRAY HIGHLIGHTING INDICATES RUNS THAT WERE OMITTED DURING AVERAGING.....	98
TABLE B.3: AVERAGE EXHUMATION RATES CALCULATED FROM LINEAR REGRESSIONS OF THE DATA PLOTTED ON THE AGE VS. ELEVATION PLOTS (FIGURE 3.4).	101
TABLE B.4: COOLING RATES CALCULATED FOR EACH SAMPLE BETWEEN DIFFERENT ISOTHERMS.....	102
TABLE C.1: SAMPLE DESCRIPTION. BOTH THE FRESH (F) AND WEATHERED (W) COLOR IS	

GIVEN FOR EACH SAMPLE	104
TABLE C.2: REGIONAL APATITE FISSION-TRACK DATA. AGES MOSTLY COMPILED FROM KLEIN ET AL. (2009). DATA USED FOR FIGURE 4.8.....	117
TABLE C.3: REGIONAL OLIGOCENE PLUTON LTT DATA. MAPPED ON FIGURE 4.7.	136

LIST OF FIGURES

FIGURE 1: MAP OF WESTERN COLORADO SHOWING THE LOCATIONS OF MID-TERTIARY VOLCANIC UNITS FROM THE SAN JUAN AND WEST ELK VOLCANIC FIELDS (38 – 23 MA, ORANGE), TERTIARY-AGE PLUTONS (36 – 25 MA, PINK) AND LARAMIDE-AGE PLUTONS (75 – 45 MA, MAGENTA). SKY BLUE OUTLINE REPRESENTS THE COLORADO MINERAL BELT BASED ON LATE MESOZOIC-CENOZOIC MAGMATISM (TWETO AND SIMS, 1963). THIN, BLACK, DASHED POLYGONS OUTLINE THE MAJOR MOUNTAIN RANGES AND TOPOGRAPHIC FEATURES. A GENERALIZED LOCATION OF THE RIO GRANDE RIFT IS OUTLINED BY THE SAN LUIS VALLEY AND THE ARKANSAS RIVER VALLEY GRABEN (STIPPLED PATTERN). GP: GRIZZLY PEAK CALDERA; TLB: TWIN LAKES BATHOLITH; MP: MOUNT PRINCETON; WP: WHITEROCK PLUTON; BC: BONANZA CALDERA; BCG: BLACK CANYON OF THE GUNNISON; GHM: GRAND HOGBACK MONOCLINE. THE BLACK BOX OUTLINES THE AREA OF STUDY. MAP AFTER LIPMAN ET AL (1969), LIPMAN (2007), AND FELDMAN (2010)..... 2

FIGURE 1.1: MAP OF WESTERN COLORADO OVERLAIN ON THE IMAGED SEISMIC TOMOGRAPHY (MEAN OF 60 AND 100 KM). GENERALIZATION OF MID-TERTIARY VOLCANIC UNITS FROM THE SAN JUAN AND WEST ELK VOLCANIC FIELDS (38 – 23 MA, ORANGE), TERTIARY-AGE PLUTONS (36 – 25 MA, PINK) AND LARAMIDE-AGE PLUTONS (75 – 45 MA, MAGENTA). THIN, BLACK, DASHED POLYGONS OUTLINE THE MAJOR MOUNTAIN RANGES AND TOPOGRAPHIC FEATURES. A GENERALIZED LOCATION OF THE

RIO GRANDE RIFT IS OUTLINED BY THE SAN LUIS VALLEY AND THE ARKANSAS RIVER VALLEY GRABEN (STIPPLED PATTERN). GP: GRIZZLY PEAK CALDERA; TLB: TWIN LAKES BATHOLITH; MP: MOUNT PRINCETON; WP: WHITEROCK PLUTON; BC: BONANZA CALDERA; BCG: BLACK CANYON OF THE GUNNISON; GHM: GRAND HOGBACK MONOCLINE. MAP AFTER LIPMAN ET AL (1969), LIPMAN (2007) AND FELDMAN (2010). TOMOGRAPHY FROM SCHMANDT & HUMPHREYS (2010)..... 5

FIGURE 1.2: PLUTON AGE RELATIONSHIPS IN THE ELK AND WEST ELK MOUNTAINS. SOME ADDITIONAL PLUTONS FROM THE SAWATCH RANGE ARE INCLUDED AS PART OF THE “INTRUSIVE ROCKS UNDIVIDED” GROUP OF OBRADOVICH ET AL. (1969). REDWELL STOCK (P) IS ALSO INCLUDED AS PART OF GROUP 4 (THOMAS AND GALEY, 1982). MAP MODIFIED FROM OBRADOVICH ET AL. (1969)..... 11

FIGURE 1.3: MAPPED HEAT FLOW VALUES FOR THE FIELD AREA. VALUES FROM DECKER ET AL. (1988) AND REITER ET AL. (1975) KEYED TO TABLE 1.2. MAP MODIFIED FROM OBRADOVICH ET AL. (1969)..... 17

FIGURE 3.1: REPRESENTATIVE $^{40}\text{Ar}/^{39}\text{Ar}$ BIOTITE SPECTRA FROM EACH MOUNTAIN. ERRORS REPORTED AT 2σ 35

FIGURE 3.2: $^{40}\text{Ar}/^{39}\text{Ar}$ K-FELDSPAR SPECTRA WITH CORRESPONDING BIOTITE WHERE APPLICABLE. (A) 09ELK-S3 (3649 M) FROM MT. SOPRIS PLOTTED WITH THE BIOTITE SPECTRA FOR 09ELK-S2 (3777 M). (B) 08ELK5 (3543 M) FROM CAPITOL PEAK PLOTTED WITH THE BIOTITE SPECTRA FOR 08ELK6 (3386 M). (C) 08ELK7 (3229 M) FROM CAPITOL PEAK PLOTTED WITH THE BIOTITE SPECTRA FOR 08ELK6 (3386 M). (D) 08ELK8 (4295 M) FROM SNOWMASS MOUNTAIN PLOTTED WITH THE BIOTITE SPECTRA FROM THE SAME SAMPLE. ERRORS REPORTED AT 2σ 39

FIGURE 3.2 (CONTINUED): $^{40}\text{Ar}/^{39}\text{Ar}$ K-FELDSPAR SPECTRA WITH CORRESPONDING BIOTITE WHERE APPLICABLE. (E) 08ELK13 (3691 M) FROM SNOWMASS MOUNTAIN PLOTTED WITH THE BIOTITE SPECTRA FROM THE SAME SAMPLE. (F) 09ELK-R1 (3410 M) FROM RAGGED MOUNTAIN (NO AVAILABLE BIOTITE AGE FOR THIS PLUTON). (G) 09ELK-R6A (1882 M) FROM RAGGED MOUNTAIN (NO AVAILABLE BIOTITE AGE FOR THIS PLUTON). ERRORS REPORTED AT 2σ 40

FIGURE 3.3. AHe AGE, eU, AND GRAIN SIZE COMPARISONS. (A) AGE VS. eU. (B) AGE VS. eU WITH RESPECT TO GRAIN SIZE. (C) AGE VS. GRAIN SIZE (R). (D) GRAIN SIZE VS. eU ... 43

FIGURE 3.4: AGE VS. ELEVATION PLOTS FOR EACH TRAVERSE. THE K-FELDSPAR AGE IS A MINIMUM AGE. 44

FIGURE 3.5: SIMILAR ELEVATION AGE PLOT OF THE FIELD AREA. THE DATA POINTS REPRESENT THE DIFFERENT PLUTONS (LEFT TO RIGHT: GUNNISON, BECKWITH, MARCELLINA, RAGGED, AND SOPRIS). 46

FIGURE 3.6: SIMPLE THERMAL HISTORY MODELS FOR RAGGED MOUNTAIN USING THE HeFTy INVERSE MODELING PROGRAM (KETCHAM, 2007). THE SURFACE TEMPERATURE IS SET $\sim 10^\circ\text{C}$. THE INITIAL CONDITION FOR (A) AND (B) RANGES FROM 31 – 34 MA AND $\sim 300^\circ\text{C}$. THE INITIAL CONDITION FOR (C) – (F) IS 28.3 MA AND $\sim 275^\circ\text{C}$. (A) 3641M, (B) 3410 M, (C) 3280 M, (D) 3071 M, (E) 2900 M, AND (F) 1882 M. GREEN LINES (ACCEPTABLE PATH), PINK LINES (GOOD PATH), BLACK LINE (BEST-FIT MODEL), BLUE LINE (WEIGHTED MEAN PATH), AND THE ORANGE DOTTED LINE (CONSTRAINT PATH). 48

FIGURE 3.7: THERMAL HISTORY MODELS FOR RAGGED MOUNTAIN EXPLORING A REHEATING EVENT ~ 12 MA USING HeFTy (KETCHAM, 2007). THE SURFACE

TEMPERATURE IS SET $\sim 10^{\circ}\text{C}$. THE INITIAL CONDITION FOR (A) AND (B) IS ~ 38 MA AND $\sim 300^{\circ}\text{C}$. THE INITIAL CONDITION FOR (C) – (F) IS 28.3 MA AND $\sim 275^{\circ}\text{C}$. (A) 3641M, (B) 3410 M, (C) 3280 M, (D) 3071 M, (E) 2900 M, AND (F) 1882 M. GREEN LINES (ACCEPTABLE PATH), PINK LINES (GOOD PATH), BLACK LINE (BEST-FIT MODEL), BLUE LINE (WEIGHTED MEAN PATH), THE ORANGE DOTTED LINE (CONSTRAINT PATH) AND BLUE BOXES (CONSTRAINT BOXES). 49

FIGURE 3.8: DESIGN MESH FOR THE MULTIPLE INTRUSIONS HEAT MODEL. EACH PLUTON WAS INTRUDED ACCORDING TO THEIR EMPLACEMENT AGES. 51

FIGURE 3.9: SIMPLE THERMAL HISTORY MODEL FOR 08ELK08 (4295 M, SNOWMASS MOUNTAIN) USING THE HEFTY INVERSE MODELING PROGRAM (KETCHAM, 2007). THE SURFACE TEMPERATURE IS SET $\sim 10^{\circ}\text{C}$. THE INITIAL CONDITION IS 33.7 MA AND 350°C . GREEN LINES (ACCEPTABLE PATH), PINK LINES (GOOD PATH), BLACK LINE (BEST-FIT MODEL), BLUE LINE (WEIGHTED MEAN PATH), AND THE ORANGE DOTTED LINE (CONSTRAINT PATH)..... 52

FIGURE 4.1: GEOLOGIC MAP OF THE FIELD AREA. THE INTRUSION AGES ARE $40\text{Ar}/39\text{Ar}$ BIOTITE AGES EXCEPT FOR THE $40\text{Ar}/39\text{Ar}$ K-FELDSPAR AGE FOR RAGGED MOUNTAIN (*) AND THE AFT AGE FOR MOUNT GUNNISON (**). THE LEGEND FOR THE MAP IS ON NEXT PAGE. BASE GEOLOGY MAP FROM TWETO AND SCHOENFELD (1979). 54

FIGURE 4.1 (CONTINUED): LEGEND FOR GEOLOGIC MAP OF FIELD AREA. 55

FIGURE 4.2: REGIONAL PLUTONIC HISTORY. THE GRAY BARS HIGHLIGHT DIFFERENT PERIODS OF MAGMATISM IN THE REGION. DATING TECHNIQUES: K-AR (OBRADOVICH AND THOMAS AND GAYLE), U/Pb (FELDMAN), $^{40}\text{Ar}/^{39}\text{Ar}$ BIOTITE (THIS STUDY). 57

FIGURE 4.3: REGIONAL PLUTONIC TRENDS. PLUTONS FROM THE ELK, WEST ELK AND SAWATCH RANGE WERE MAPPED ALONG WITH THEIR INTRUSIVE AGE DATA. THE DATES ARE COLOR-CODED BY DATING TECHNIQUE (U/Pb: BLACK; AR/AR: RED; K-AR: GREEN; ZFT: BLUE; AND AFT: BROWN). THE LETTERS ON THE MAP CORRESPOND TO THEIR LOCATION NAME: A. MOUNT SOPRIS; B. SNOWMASS PLUTON; C. RAGGED MOUNTAIN; D. MARCELLINA MOUNTAINS; E. EAST BECKWITH MOUNTAIN; F. MOUNT GUNNISON; G. TREASURE MOUNTAIN DOME; H. WHITEROCK PLUTON; I. CRESTED BUTTE PLUTON; J. LITTLE ANNIE SILL AND RICHMOND HILL; K. ITALIAN MOUNTAIN COMPLEX; L. LINCOLN CREEK STOCK; M. TWIN LAKES BATHOLITH; N. MOUNT PRINCETON BATHOLITH; O. GRIZZLY PEAK CALDERA; P. REDWELL STOCK. DIRECTIONAL ARROWS INDICATE YOUNGING PATTERNS. MAP AFTER OBRADOVICH ET AL. (1969)..... 58

FIGURE 4.4: MAP SHOWING THE CMB AND MIDDLE CENOZOIC VOLCANIC FIELDS AND CALDERAS (CHAPIN, IN PRESS). DARK GRAY = MIDDLE CENOZOIC VOLCANIC FIELDS; LIGHT GRAY = BASIN FILL OF RIO GRANDE RIFT AND BASIN AND RANGE PROVINCE.. 59

FIGURE 4.5: GENERALIZED CROSS SECTION OF THE STUDY AREA. THE GEOCHRONOLOGY FOR EACH MOUNTAIN IS LISTED AT THE TOP OF THE FIGURE. GEOLOGY INTERPRETED FROM GASKILL AND GODWIN (1966A), GASKILL AND GODWIN (1966B), GODWIN (1968), MUTSCHLER (1970), STREUFERT (1999), AND TWETO AND SCHOENFELD (1979)..... 61

FIGURE 4.6: AHe AGE VS. ELEVATION PLOTS. (A) DATA FROM THIS STUDY AND TWO ADDITIONAL AHe AGE TRANSECTS FROM THE TWIN LAKES AREA (FELDMAN, 2010). (B) MCKEON (2009). 64

FIGURE 4.7: THERMOCHRONOLOGY MAP OF OLIGOCENE PLUTONS IN THE ELK, WEST ELK AND SAN JUAN MOUNTAINS. BOTH AFT AND AHe DATA FROM THIS STUDY AND MCKEON (2009) ARE MAPPED. (A) TOMOGRAPHY DEPTH SLICE IS AT 100 KM BY MCCARTHY ET AL. (2010). (B) TOMOGRAPHY DEPTH SLICE IS A MEAN OF 60 – 100 KM BY SCHMANDT AND HUMPHREYS (2010). FIGURE KEYED TO TABLE C.3. 65

FIGURE 4.8: REGIONAL AFT DATA WITH TOMOGRAPHY MAP. (A) TOMOGRAPHY DEPTH SLICE IS AT 100 KM BY MCCARTHY ET AL. (2010). (B) TOMOGRAPHY DEPTH SLICE IS A MEAN OF 60 – 100 KM BY SCHMANDT AND HUMPHREYS (2010). FIGURE KEYED TO TABLE C.2. 67

FIGURE A.1: $^{40}\text{Ar}/^{39}\text{Ar}$ HORNBLende SPECTRUM FOR SNOWMASS MOUNTAIN. 75

FIGURE A.2: $^{40}\text{Ar}/^{39}\text{Ar}$ BIOTITE SPECTRA FOR SNOWMASS MOUNTAIN FOR THE BIOTITE-CHLORITIZED BIOTITE EXPERIMENT ON SAMPLE 08ELK08. (A) VISIBLY PRISTINE BIOTITE SAMPLE. (B) VISIBLY ALTERED BIOTITE SAMPLE. 77

FIGURE A.3: $^{40}\text{Ar}/^{39}\text{Ar}$ BIOTITE SPECTRA FOR CAPITOL PEAK. 78

FIGURE A.4: $^{40}\text{Ar}/^{39}\text{Ar}$ BIOTITE SPECTRA FOR SNOWMASS MOUNTAIN. 79

FIGURE A.5: $^{40}\text{Ar}/^{39}\text{Ar}$ BIOTITE SPECTRA FROM MOUNT SOPRIS (A), RAGGED MOUNTAIN (B), MARCELLINA MOUNTAIN (C-D), E. BECKWITH MOUNTAIN (E-F), AND MOUNT GUNNISON (G). 80

FIGURE A.6: $^{40}\text{Ar}/^{39}\text{Ar}$ K-FELDSPAR SPECTRA THAT WAS TOO COMPLICATED TO PROVIDE GOOD AGE DATA. 87

FIGURE C.1: MOUNT SOPRIS SAMPLE PHOTOGRAPHS. 109

FIGURE C.2: CAPITOL PEAK SAMPLE PHOTOGRAPHS. 110

FIGURE C.3: SNOWMASS MOUNTAIN SAMPLE PHOTOGRAPHS. 111

FIGURE C.4: RAGGED MOUNTAIN SAMPLE PHOTOGRAPHS..... 112

FIGURE C.5: MARCELLINA MOUNTAIN SAMPLE PHOTOGRAPHS..... 113

FIGURE C.6: EAST BECKWITH MOUNTAIN SAMPLE PHOTOGRAPHS..... 114

FIGURE C.7: MOUNT GUNNISON SAMPLE PHOTOGRAPHS..... 115

FIGURE C.8: SAMPLE LOCATION MAP. GEOLOGY FROM TWETO (1979). 116

This thesis is accepted on behalf of the
Faculty of the Institute by the following committee:

Shari A. Kelley, Research Advisor Date

Matthew T. Heizler, Research Advisor Date

William C. McIntosh, Academic Advisor Date

Jeffrey B. Johnson Date

I release this document to the New Mexico Institute of Mining and Technology.

Rebecca V. Garcia Date

INTRODUCTION

The multi-institutional, interdisciplinary project known as CREST (Colorado Rockies Experiment and Seismic Transect; Karlstrom et al., 2011) focused on (1) imaging the geometry of seismic velocity anomalies in the mantle beneath the Rocky Mountains of west central Colorado and (2) investigating possible temporal and spatial correlations between these mantle anomalies and Cenozoic magmatism and exhumation. The tomographic data from CREST combined with seismic data from previous studies revealed low seismic velocity anomalies beneath the San Juan volcanic field and the Front Range just west of Denver (MacCarthy et al., 2010; Schmandt and Humphreys, 2010). Several geodynamic models scaled to the observed velocity variation (~11% for V_s , 6% for V_p) suggest that significant upper mantle convective flow (1 to 5 cm/yr) is probably ongoing and has the potential to cause surface uplift of several hundreds of meters (Karlstrom et al., 2011; Moucha et al., 2009; van Wijk et al., 2010). One of the goals of this study is to constrain the timing of initiation of uplift and erosion related to possible Neogene upper mantle density modification and convection beneath western Colorado using thermochronology.

A secondary goal of this study is to add to the few K-Ar and zircon FT data (Obradovich et al., 1969 and Cunningham et al., 1994) from plutons in western Colorado, specifically in the Elk and West Elk Mountains (Figure 1). Additional data will refine the understanding of the timing and depth of pluton emplacement, and subsequent

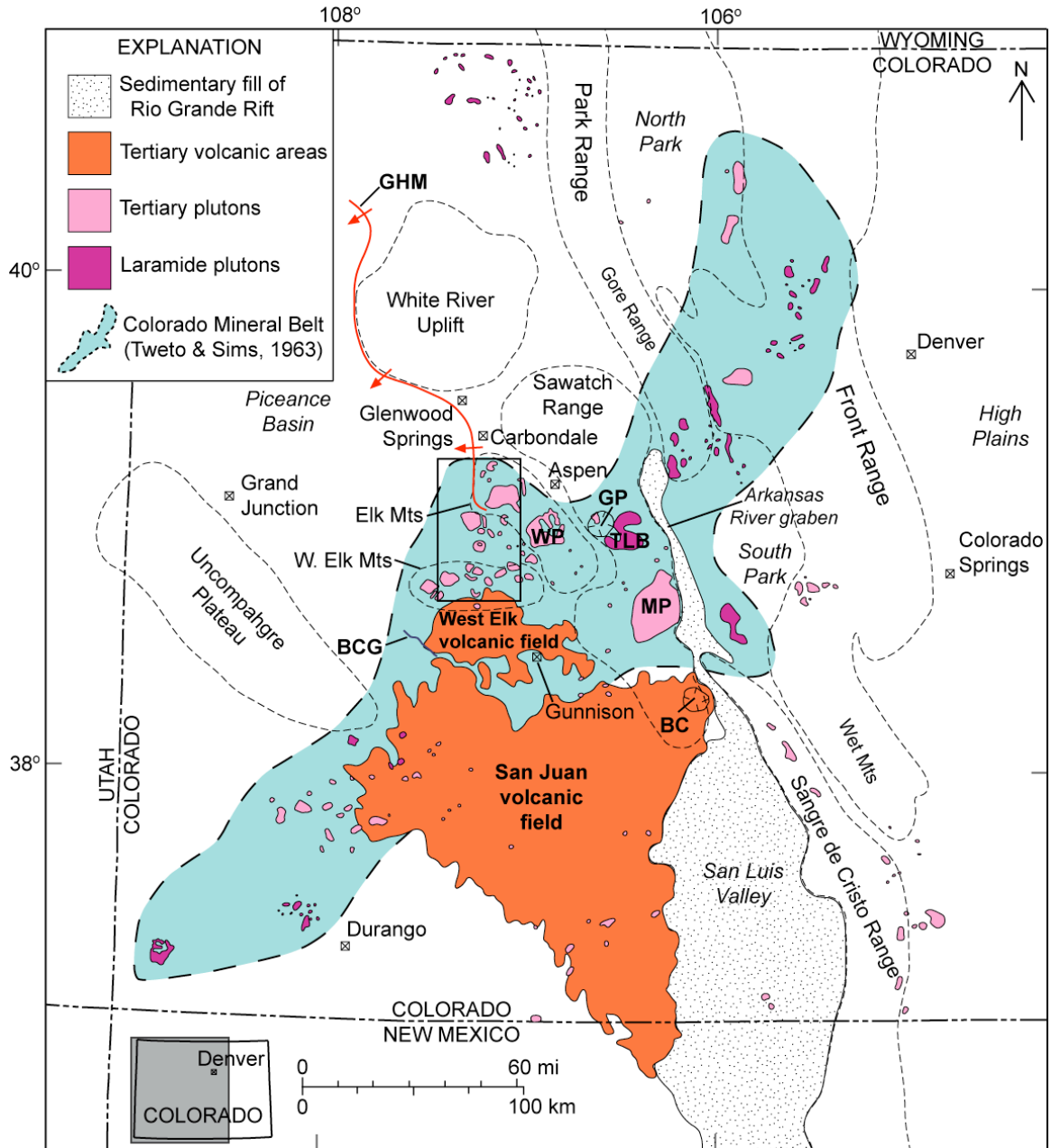


Figure 1: Map of western Colorado showing the locations of mid-Tertiary volcanic units from the San Juan and West Elk volcanic fields (38 – 23 Ma, orange), Tertiary-age plutons (36 – 25 Ma, pink) and Laramide-age plutons (75 – 45 Ma, magenta). Sky blue outline represents the Colorado Mineral Belt based on Late Mesozoic-Cenozoic magmatism (Tweto and Sims, 1963). Thin, black, dashed polygons outline the major mountain ranges and topographic features. A generalized location of the Rio Grande Rift is outlined by the San Luis valley and the Arkansas River valley graben (stippled pattern). GP: Grizzly Peak caldera; TLB: Twin Lakes batholith; MP: Mount Princeton; WP: Whiterock pluton; BC: Bonanza caldera; BCG: Black Canyon of the Gunnison; GHM: Grand Hogback Monocline. The black box outlines the area of study. Map after Lipman et al (1969), Lipman (2007), and Feldman (2010).

exhumation during the transitional interval between the end of 75-40 Ma Colorado Mineral Belt (CMB) magmatism and the onset of ~35 - 5 Ma San Juan volcanic field (SJVF) activity.

Therefore, samples were collected from seven mountain peaks composed of late Eocene to Oligocene plutons in the Elk and West Elk Mountains. U/Pb zircon geochronology and $^{40}\text{Ar}/^{39}\text{Ar}$, apatite fission-track and (U-Th)/He thermochronology data determined from these samples are used to obtain a regional perspective of emplacement ages, cooling history and the processes that affected the rate of cooling of the plutons. Simple thermal models of pluton emplacement and cooling were used to gauge the relative importance of isotherm relaxation after intrusive events versus cooling caused by exhumation in interpreting the LTT data.

CHAPTER 1

GEOLOGIC BACKGROUND

1.1 Regional Setting

The Elk and West Elk Mountains are located in west central Colorado roughly between the town of Carbondale to the north and the Black Canyon of the Gunnison to the south (Figure 1). Regionally, the ranges are bounded by several Laramide features (the White River uplift and the Grand Hogback monocline (GHM) to the north and the Piceance Basin to the west), along with the Sawatch Range to the east, the San Juan volcanic field to the south and the Uncompahgre Plateau to the west.

The plutons of the West Elk and Elk Mountain belong to a larger series of plutons emplaced within the bounds of the enigmatic CMB. The CMB is a northeast trending belt of ~75 – 40 Ma plutons and associated mineral districts in western and central of Colorado. The CMB intersects the northern Rio Grande Rift (RGR), a rift valley extending north from Chihuahua, Mexico through New Mexico and into central Colorado (Chapin, 1979). This intersection coincides with some of the highest elevation mountains in the Rockies and lies within a transition zone between low seismic velocity anomalies to the northeast (Aspen Anomaly) and to the south (San Juan Anomaly) (Figure 1.1) (Schmandt and Humphreys, 2010). The location of the CMB has been attributed to the presence of: (1) Proterozoic shear zones (Tweto and Sims, 1963), (2) a dilated segment

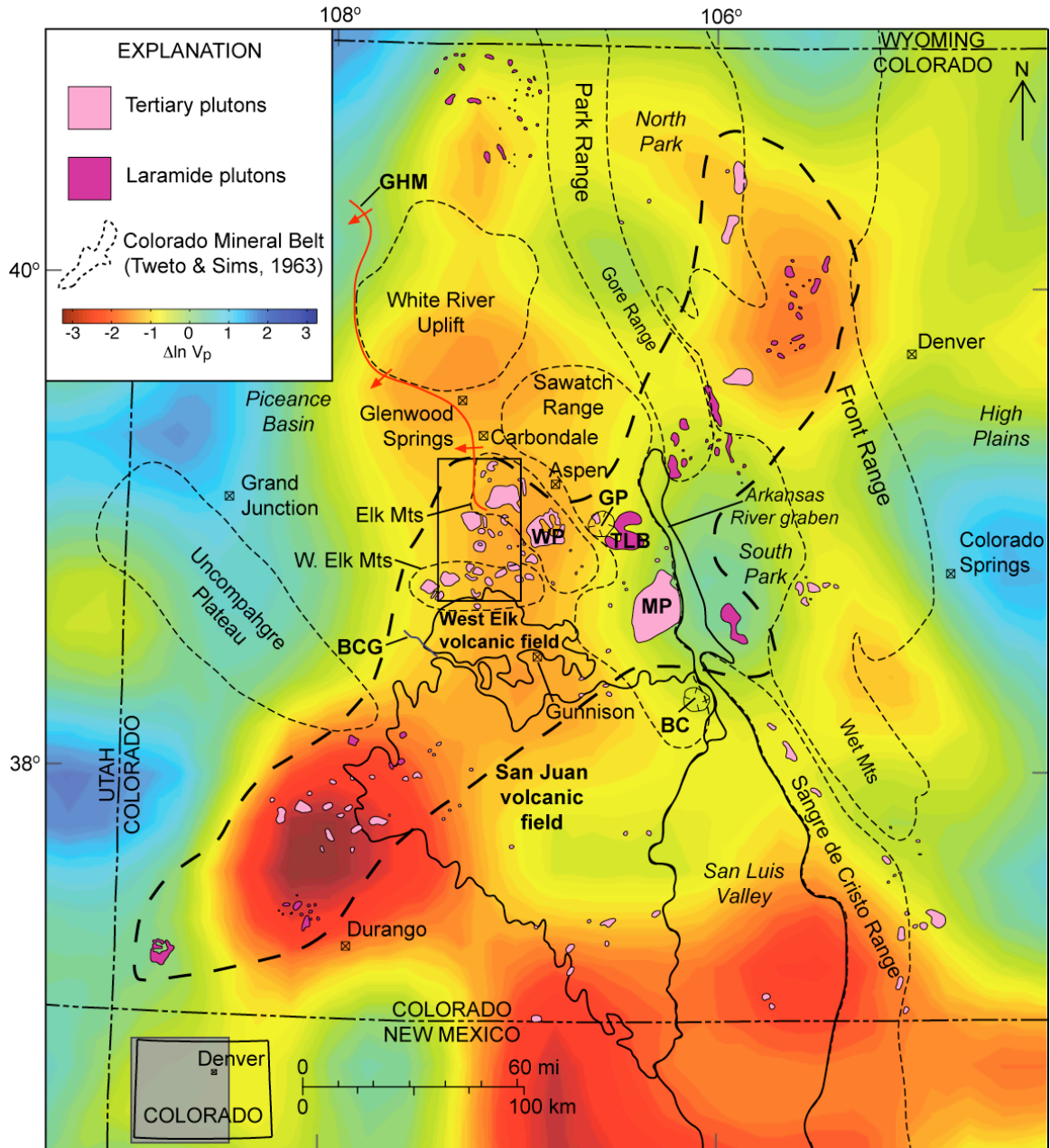


Figure 1.1: Map of western Colorado overlain on the imaged seismic tomography (mean of 60 and 100 km). Generalization of mid-Tertiary volcanic units from the San Juan and West Elk volcanic fields (38 – 23 Ma, orange), Tertiary-age plutons (36 – 25 Ma, pink) and Laramide-age plutons (75 – 45 Ma, magenta). Thin, black, dashed polygons outline the major mountain ranges and topographic features. A generalized location of the Rio Grande Rift is outlined by the San Luis valley and the Arkansas River valley graben (stippled pattern). GP: Grizzly Peak caldera; TLB: Twin Lakes batholith; MP: Mount Princeton; WP: Whiterock pluton; BC: Bonanza caldera; BCG: Black Canyon of the Gunnison; GHM: Grand Hogback Monocline. Map after Lipman et al (1969), Lipman (2007) and Feldman (2010). Tomography from Schmandt & Humphreys (2010).

boundary in the Farallon flat slab (Chapin, in press), or (3) localized shear-parallel small-scale convection (Jones et al., 2011).

Tweto and Sims (1963) were some of the first scientists to hypothesize that subduction-related late Cretaceous to Oligocene CMB magmas and associated mineralizing fluids leaked along a zone of crustal weakness that formed during Proterozoic time. A 1300 km wide belt of Proterozoic juvenile crust extending from Wyoming to Mexico was formed by the accretion of a series of arcs and oceanic terranes onto the Laurentian plate between 2.0 and 1.8 Ga (Karlstrom and Bowring, 1988). Northeast-striking suture zones, representing craton growth, evolved into prominent shear zones that cross the length of the orogen. In Colorado, some of these shear zones were overprinted by mylonitic and ultramylonitic shear zone segments forming the Colorado Mineral Belt shear zone system (ca. 1.45-1.3 Ga) (McCoy et al., 2005). According to Tweto and Sims (1963), both the Elk and West Elk Mountains lie within the maximum boundaries of the CMB, with ore deposits confined to the eastern part of the mountain ranges.

Chapin (in review) argues that a much more recent event, namely the subduction of the Farallon slab, was the primary control of the CMB. The CMB developed within a ~1200 km wide late Cretaceous-Paleogene magma gap overlying subhorizontally subducted segments of the Farallon Plate. The unique nature of this particular magmatic gap is due to a dilated segment boundary that was warped by the overriding, thick Archean craton in Wyoming during acceleration of Farallon-North American convergence. The CMB cuts indiscriminately across the geologic grain of Colorado in a northeast-trending pattern, seemingly independent of the tectonic elements crossed by the

belt. Proterozoic shear zones (Tweto and Sims, 1969) provided some local influence, but were not the primary control. Chapin (in review) states that the igneous rocks in the CMB can be broken down into three main age groups: Late Cretaceous – middle Eocene (Laramide, ca. 75 – 43 Ma); middle Cenozoic (ca. 43 – 18 Ma); and late Cenozoic (ca. 18 – 0 Ma). Flat slab rollback causes a younging trend to the west, southwest that is recorded between 37 and 23 Ma. The remaining plutonism is due to the extension of the Rio Grande rift through the CMB in the Leadville area.

While both of the aforementioned explanations on the origin of the CMB are coupled with the flat slab theory as the cause of the subsequent magmatism, Jones et al. (2011) take a completely different approach. These authors note that the flat-slab hypothesis has difficulty predicting specific observation about the Laramide and the CMB (i.e., timing of subduction conflicts with some events in the continental interior, late Cretaceous subsidence, means of generating the igneous activity in the CMB). Therefore, Jones et al. (2011) set about explaining an alternative hypothesis for the Laramide orogeny and in turn the CMB. The Farallon slab underwent shallowing subduction during the late Cretaceous due to acceleration of the North American plate as it moved west/southwestward. This shallow slab locally interacts with a keel in the thick Archean lithosphere under Wyoming and interrupts the asthenospheric counterflow causing the arc to shut down. Dynamic stresses from the slab-keel interaction drive subsidence off the edge of the Archean craton, allowing the formation of the Western Interior Seaway. The narrowed asthenospheric wedge above this shallow slab segment induces small-scale convection parallel to plate motion and becomes an upwelling limb of localized magmatism, thus creating the CMB. Jones et al. (2011) assume little or no

time transgression to the igneous activity, which differs from the flat-slab hypothesis of a time transgression from northeast to southwest during the Middle and Late Cenozoic due to slab rollback.

1.2 Regional Geologic History

The high elevation mountain ranges, complex structures, voluminous magmatism, and lucrative ore deposits of the Colorado Rocky Mountains are all products of a diverse geologic history. Some of the main events affecting the area include the late Cretaceous to Paleogene compressional Laramide orogeny, the latest Eocene to Miocene ignimbrite flare-up, and Oligocene to Miocene extension that formed the Rio Grande Rift.

As mentioned above, Proterozoic events imparted a northeast striking structural grain in the region. Later, Pennsylvanian to Permian Ancestral Rocky Mountains deformation created a series of northwest-striking uplifts and basins. These ancient highlands were roughly situated at the current locations of the Front Range and San Juan Mountains/Uncompahgre Plateau. The material shed from these mountains was deposited in the northwest trending Eagle Basin, including the thick redbeds of the Pennsylvanian-Permian Maroon Formation.

The Laramide orogeny, a mountain building event that formed the modern Rocky Mountains and triggered large scale faulting, magmatism and mineralization, began in the area ~75 Ma ago (Bryant and Naeser, 1980) and continued through the early Cenozoic. The most widely accepted theory for the cause of the orogeny is related to late Cretaceous subduction of the Farallon plate beneath the North American plate and its eastward flattening from ~70 to 57 Ma (Lipman et al., 1971; Snyder et al., 1976; Coney

& Reynolds, 1977). However, as mentioned above, Jones et al. (2011) invokes a hydrodynamic model of slab–continental lithosphere interaction as a means for the evolution of the Laramide orogeny. No matter which conjecture is more accurate, multiple structures related to this event formed in the Elk and the Sawatch Ranges, including the SW-vergent Elk Range thrust zone, the Castle Creek fault zone and the Sawatch monocline, which all have a general north-south orientation with some northwest variations (Bryant, 1979). The nearby Piceance Basin to the west and the White Mountain uplift along with the Grand Hogback monocline to the northwest also formed during Laramide deformation.

Removal of the Farallon Plate at the end of Laramide deformation is thought to have caused the ignimbrite flare-up (36 – 23 Ma, Lipman, 2007). The flare-up was triggered by the isolation of the North American lithosphere from the asthenosphere during flat slab subduction, causing both refrigeration and hydration of the North American plate (Humphreys et al., 2003; Farmer et al., 2008). Around 40 Ma, the Farallon slab became unstable. As the slab foundered and began to pull away from the base of the North American plate, hot dry asthenosphere (relative to the hydrated overriding lithosphere) came into contact with the refrigerated lithosphere, generating large volumes of magma. Farmer et al. (2008) argues for magma sources from both continental lithospheric mantle and the sub-lithospheric mantle in order to match the entire volume and duration of volcanism. This amount of magma loss would result in dedensification of the mantle. Multiple Oligocene intrusions in the Elk and West Elk Mountains, along with the San Juan, Mogollon-Datil, and Sierra Madre Occidental volcanic fields, formed during this time (Obradovich, 1969). Additional volcanic activity

can also be found in the Sawatch Range (Mount Princeton, Grizzly Peak, and Bonanza).

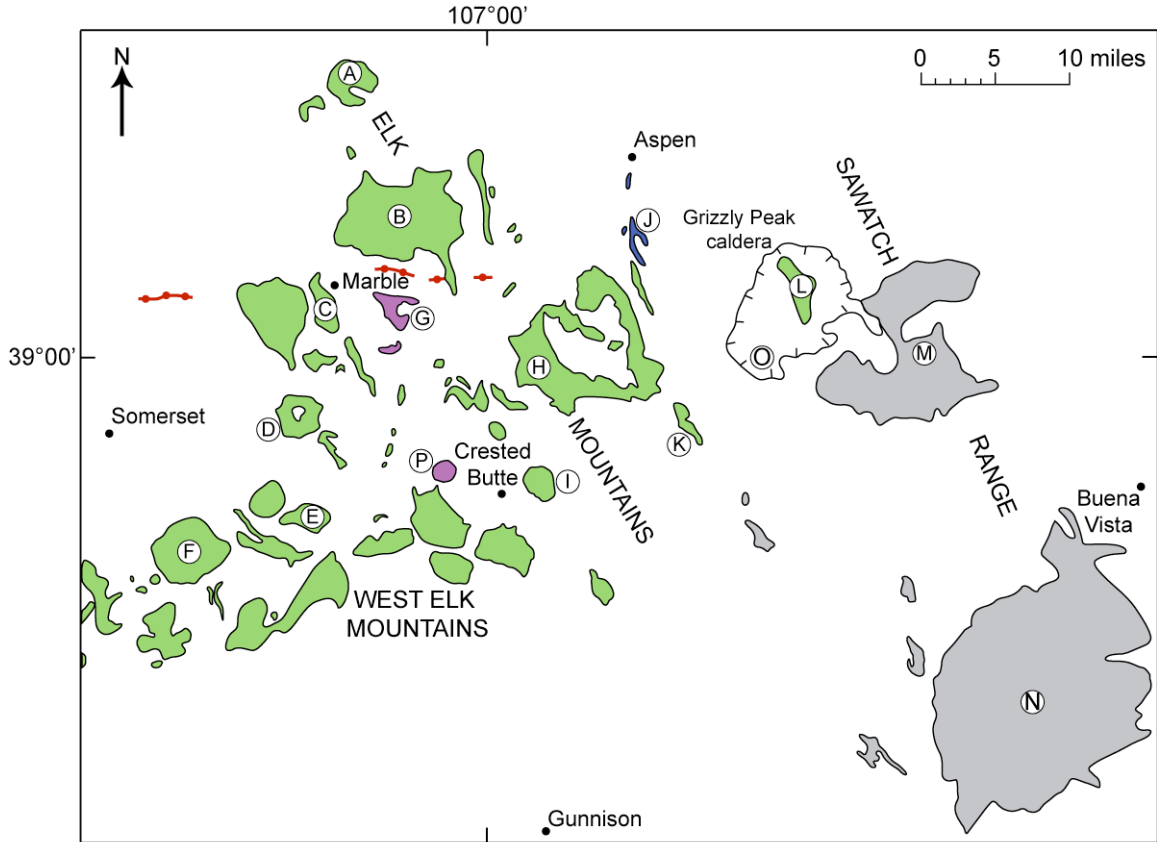
The SJVF is a region of voluminous, volcanism in the San Juan Mountains that can be divided into three general periods of activity between ~35 and 5 Ma (Lipman et al., 1970; Lipman et al., 1976). The first period of activity occurred 35 – 30 Ma with the eruption of intermediate-composition lavas and breccias. Around 30 Ma, volcanic activity changed to explosive ash-flow tuff eruptions until ~26 Ma with concurrent eruptions of local andesitic-silicic lava flows (26.4 Ma). The final phase between ~26 and 5 Ma consisted of a bimodal suite of silicic rhyolites and mafic alkalic lavas.

During the middle Cenozoic the crustal stresses changed from one of compression to extension. The Rio Grande Rift system began to open up at this time causing widespread mafic magmatism in Colorado, New Mexico and western Texas (Chapin and Cather, 1994). Tectonic activity associated with rifting gradually diminished during the late Tertiary and Quaternary.

1.3 Elk and West Elk Mountains

The post-Paleozoic intrusive plutons of the Elk and West Elk Mountains and the western margin of the Sawatch Range can be broken down into four groups (Figure 1.2): (1) late Cretaceous (67 – 72 Ma [Obradovich et al., 1969]) felsic porphyritic intrusions of the Aspen mining district, (2) granodioritic plutons of Oligocene age, (3) Miocene and Pliocene porphyritic gabbro and lamprophyre dikes, and (4) a soda granite stock of latest Miocene or earliest Pliocene age.

High angle faulting and emplacement of the group 1 porphyries accompanied uplift of the Sawatch Range during the Laramide orogeny. The timing of deformation



- (A): Locality
- A. Mount Sopris
 - B. Snowmass pluton
 - C. Ragged Mountain
 - D. Marcellina Mountain
 - E. East Beckwith Mountain
 - F. Mount Gunnison
 - G. Treasure Mountain dome
 - H. Whiterock pluton
 - I. Crested Butte pluton
 - J. Little Annie sill & Richmond Hill
 - K. Italian Mountain complex
 - L. Lincoln Creek stock
 - M. Twin Lakes batholith
 - N. Mount Princeton batholith
 - O. Grizzly Peak caldera
 - P. Redwell stock
- | | | | |
|-----------------|---|--|--|
| Tertiary | } | | Group 4 plutons:
Granite of Treasure Mountain |
| | | | Group 3 plutons:
Gabbro porphyry, lamprophyre and basalt dikes |
| | | | Group 2 plutons:
Granodiorite stocks lacoliths, sills & dikes |
| Late Cretaceous | } | | Group 1 plutons:
Porphyries of Aspen mining district |
| | | | Intrusive rocks undivided |

Figure 1.2: Pluton age relationships in the Elk and West Elk Mountains. Some additional plutons from the Sawatch Range are included as part of the “Intrusive rocks undivided” group of Obradovich et al. (1969). Redwell stock (P) is also included as part of group 4 (Thomas and Galey, 1982). Map modified from Obradovich et al. (1969).

must be younger than 75 – 73 Ma because of age constraints provided by marine Cretaceous rocks that covered the area (Obradovich et al., 1969). The ages obtained from the porphyritic intrusions (72 – 67 Ma) located near the Aspen-mining district are similar to porphyritic intrusions of the Leadville district. The Elk Range thrust fault (ERTF), a system of northeast dipping faults, probably formed during the time of high angle faulting by means of westward gravity sliding of sedimentary units (Bryant and Martin, 1988). The ERTS is structurally bounded to the east by the margin of the Sawatch Range and to the north by the Grand Hogback Monocline (GHM).

Post-middle Eocene and pre-Oligocene faults and folds related to the Grand Hogback Monocline are cut by undeformed group 2 Oligocene plutons that make up the largest volume of exposed intrusive rocks in the area (Obradovich et al., 1969). The larger volume granodiorite stocks (Mount Sopris, Snowmass, and Whiterock) were the initial plutons to be emplaced in thick Pennsylvanian-Permian sedimentary rocks of the Elk Mountains (~34 Ma), with the ERTF acting as a control for emplacement. After crystallization of the larger plutons, smaller dikes, sills and laccoliths were intruded into Jurassic and Cretaceous age sedimentary rocks in the Elk, West Elk and Ruby Range Mountains (located between the Elk and West Elk Ranges, Figure 1). The emplacement of these plutons was accompanied and followed by renewed high-angle faulting. The majority of the faults in the West Elk Mountains is oriented east west and controlled the emplacement of similarly trending Oligocene plutons.

Some of the smaller granodiorite stocks of the Elk region have a more mafic granodiorite border that represents early phases of intrusion. Some of the porphyritic granodiorite plutons have quartz diorite xenoliths that are interpreted as products of early

crystallization at depth. Both the mafic borders and xenoliths suggest that the initial undifferentiated magmas had mafic to intermediate compositions (Lipman et al., 1969).

CMB related ore deposits occur as north to northeast trending veins and are confined to the eastern part of the Elk and West Elk Mountains (Tweto and Sims, 1963). Since mineralization mostly occurred in conjunction with Laramide intrusions, the hydrothermal process should not affect ages of the sampled Oligocene plutons from this study. However, the 12 Ma (Obradovich et al., 1969) Crystal pluton, located next to the Ragged Mountain pluton and the Snowmass pluton, was accompanied by mineralization and contact metamorphism, therefore possibly complicating the interpretation of the thermochronology data from Ragged and Snowmass mountains. Similarly, the 16 – 18 Ma molybdenum-bearing granite pluton at Redwell Basin near Mt. Emmons is surrounded by alteration zones and younger base metal deposits (Thomas and Galey, 1982). This intrusion is largely in the subsurface and has been identified primarily by drilling. The known diameter of the intrusion is 1.4 km.

Volcanic activity followed in the West Elk Mountains producing dacitic and andesitic materials from these differentiated plutons that eventually constituted the West Elk Breccia. The source vents of these eruptions are unknown, most likely due to erosion of cauldron collapse structures (Lipman et al., 1969). Dacitic porphyry dikes cut the granodiorite plutons in the Ruby Range and the West Elk Breccia. However, K-Ar dating of the dikes is not possible due to altered biotite (Obradovich et al., 1969).

Group 3 mafic dikes cut group 2 Oligocene plutons during the Miocene in parts of the Elk Mountains, Ruby Range and Treasure Mountain dome area. The mafic dikes appear to be younger than most tectonic features in the area and may correlate with basalt flows

in surrounding regions. However, they seem to be older than the group 4 plutons that not only cut the mafic dikes of group 3 but also Oligocene dikes from group 2. Group 4 is represented by the Crystal pluton, a soda granite that intruded Proterozoic and Paleozoic rocks southwest of Marble, Colorado, which produced the Treasure Mountain dome that is 6 miles in diameter that displays evidence of extensive contact metamorphism.

The epizonal plutonism in the Elk and West Elk Mountains is similar in age, sequence of volcanic activity, and evolution of chemistry compared to the predominately volcanic San Juan region (Lipman et al., 1969). The peak of activity for the San Juan volcanic field (SJVF) was from 35 – 26 Ma (Lipman & McIntosh, 2008), while K-Ar ages of the Elk Mountain intrusions range from 34 – 29 Ma (Obradovich et al., 1969) (Table 1.1). The igneous rocks of both regions are of intermediate compositions with a change to bimodal activity during middle to late Cenozoic crustal extension. The San Juan Mountains are largely made up of ash flow tuffs and intermediate composition breccias and lavas. The tuffs are compositionally zoned, indicating eruptions from a zoned magma chamber. The lavas and breccias are chemically similar to epizonal stocks and laccoliths that intrude volcanic piles in part of the volcanic field. Lipman et al. (1969) even consider that the intrusions in the Elk Mountains may have been additional feeders for volcanic deposits in the San Juan volcanic field.

The depth of emplacement of igneous rocks in the Elk Mountains, which cannot always be figured out by means of stratigraphic reconstruction, has been constrained by a fluid inclusion investigation (Cunningham, 1976). Fluid inclusions in the intrusive rocks of the Italian Mountain Complex (Figure 1) were used to evaluate changes in temperature, pressure and chemistry of the evolving aqueous phase during and

Table 1.1: Published Ages. Previous geochronology conducted in the Elk and West Elk Mountains.

Rock Unit	Longitude	Latitude	Rock Type	Dating Technique	Mineral	Published Age (Ma)	Author
Little Annie sill	-106.8250	39.11861	Quartz muscovite porphyry	K-Ar	Muscovite	72.2 ± 2.2	Obradovich, 1969
Pando Porphyry, Hayden Peak	-106.8006	39.10556	Aplite	K-Ar	Biotite (a) Biotite (b)	70.0 ± 2.3 67.4 ± 2.2	Obradovich, 1969
Snowmass pluton	-107.0406	39.11750	Granodiorite	K-Ar	Biotite	34.1 ± 1.4	Obradovich, 1969
Whiterock pluton	-106.8378	39.00972	Granodiorite	K-Ar	Biotite	33.9 ± 1.0	Obradovich, 1969
Lincoln Creek stock	-106.6414	39.08889	Granodiorite porphyry	K-Ar	Biotite	33.9 ± 1.1	Obradovich, 1970
Snowmass Creek sill	-107.0189	39.18528	Granodiorite porphyry	K-Ar	Biotite	31.2 ± 1.1	Obradovich, 1969
Crested Butte laccolith	-106.9433	38.88889	Granodiorite porphyry	K-Ar	Biotite	29.1 ± 1.0	Obradovich, 1969
Mount Sopris stock	-107.1453	39.27028	Quartz monzonite	FT	Zircon	34.3 ± 4.1	Cunningham et al., 1994
Mount Sopris stock	-107.1453	39.27028	Quartz monzonite	K-Ar	Biotite	34.2 ± 0.8	Cunningham et al., 1994
Italian Mountain intrusives (Pearl Pass)	-106.7531	38.94778	Quartz monzonite	FT	Zircon	33.0 ± 1.8	Cunningham & Naeser, 1975
Red Lady (Redwell stock)	-107.057	38.892	Granite	K-Ar	Biotite Serците	17.2 17.9	Thomas & Galey, 1982
Redwell stock	-107.055	38.890	Granite	K-Ar	Biotite	17.3	Thomas & Galey, 1982
Redwell stock	-107.052	38.893	Granite	K-Ar	Biotite Serците	16.4 15.8	Thomas & Galey, 1982
Crystal Pluton	-107.1189	39.05444	Soda granite porphyry	K-Ar	Biotite	12.5 ± 0.6	Obradovich, 1969
Crystal Pluton	-107.1214	39.05167	Soda granite porphyry	K-Ar	Biotite	12.3 ± 0.6	Obradovich, 1969

subsequent to solidification of the magma. The fluid inclusions from the Italian Mountain Complex suggest a depth of emplacement between 950 – 2700 m. The higher estimate (2700 m) implies modest erosion in the Elk Mountains since middle Oligocene time.

Decker et al. (1988) and Reiter et al. (1975) measured unusually high heat flow values (86 – 150 mWm⁻²) in the West Elk Mountains between Crested Butte and

Table 1.2: Heat flow data from Decker et al. (1988) and Reiter et al. (1975).

Locality	Map code	North Latitude (DD)	West Longitude (DD)	Elevation (m)	Depth Range (m)	Thermal Conductivity (W/mK)	Geothermal Gradient (°C/km)	Heat Flow (mW/m ²)	
Gothic	GOT1	38.988	106.945	3250	220 - 860	3.29	39.2	112	
	GOT2	38.988	106.945	3232	300 - 380	3.59	36.5	108	
	GOT3	38.988	106.945	3262	160 - 680	3.41	39.0	105	
							Mean values:	108	
Lake Irwin	LI	38.900	107.112	3290	300 - 900	3.30	39.5	129	
North Pole Basin	NPB1	39.022	107.092	3665	210 - 235	4.27	23.1	100	
	NPB2	39.023	107.090	3649	300 - 350	3.54	26.5	96	
							Mean values:	96	
Paradise Pass	PP1	38.995	107.058	3445	280 - 900	3.13	27.6	90	
	PP2 (DH-1)			3380	100 - 210	2.94	26.5	65	
							Weighted mean values:	86	
							Mean values:	90	
Redwell Basin	RB1	38.892	107.057	3462	710 - 1360	3.69	36.7	150	
	RB2	38.890	107.055	3359	860 - 1410	3.70	36.3	148	
	RB3	38.892	107.053	3327	840 - 1440	3.69	36.8	149	
	RB4		38.890	107.060	3439	800 - 1100	3.29	42.0	155
						1200 - 1500	3.69	35.8	143
	RB5		38.893	107.052	3350	200 - 820	3.18	45.0	160
						820 - 920	3.53	33.5	132
						Mean values:	150		
Crested Butte*	CB	38.917	107.117	3640	300 - 580	3.19	29.18 ± 0.06	93	
					580 - 740	3.31	32.56 ± 0.2	108	
							Mean values:	100	

Marble (Table 1.2; Figure 1.3). The fact that the heat flow changes rapidly from 150 to 86 mWm⁻² over a distance of ~15 km is indicative of a shallow source in the crust.

Decker et al. (1988) suggest that some of the F-rich intrusions have relatively high radioactivity, causing higher heat production values that could account for most of the excess flux at Redwell Basin (RB; Miocene intrusion 16 – 18 Ma), and the North Pole Basin (NPB)- Treasure Mountain area.

Residual heat flow, interpreted as heat flow coming from the mantle and crust once the effects of radioactive heat generation is removed, is high (70-105 mWm⁻²) at the intersection of the Rio Grande rift and the CMB in the Leadville-northern Sawatch Range-Elk Mountain area. The residual heat flow is also high beneath the San Juan Mountains (60 mWm⁻²) Decker et al. (1988) speculates that these heat flow anomalies are due to the transient cooling effects of unexposed Late Cenozoic (<10 Ma) granite intrusions in the upper crust. The high heat flow values also correspond with -300 to

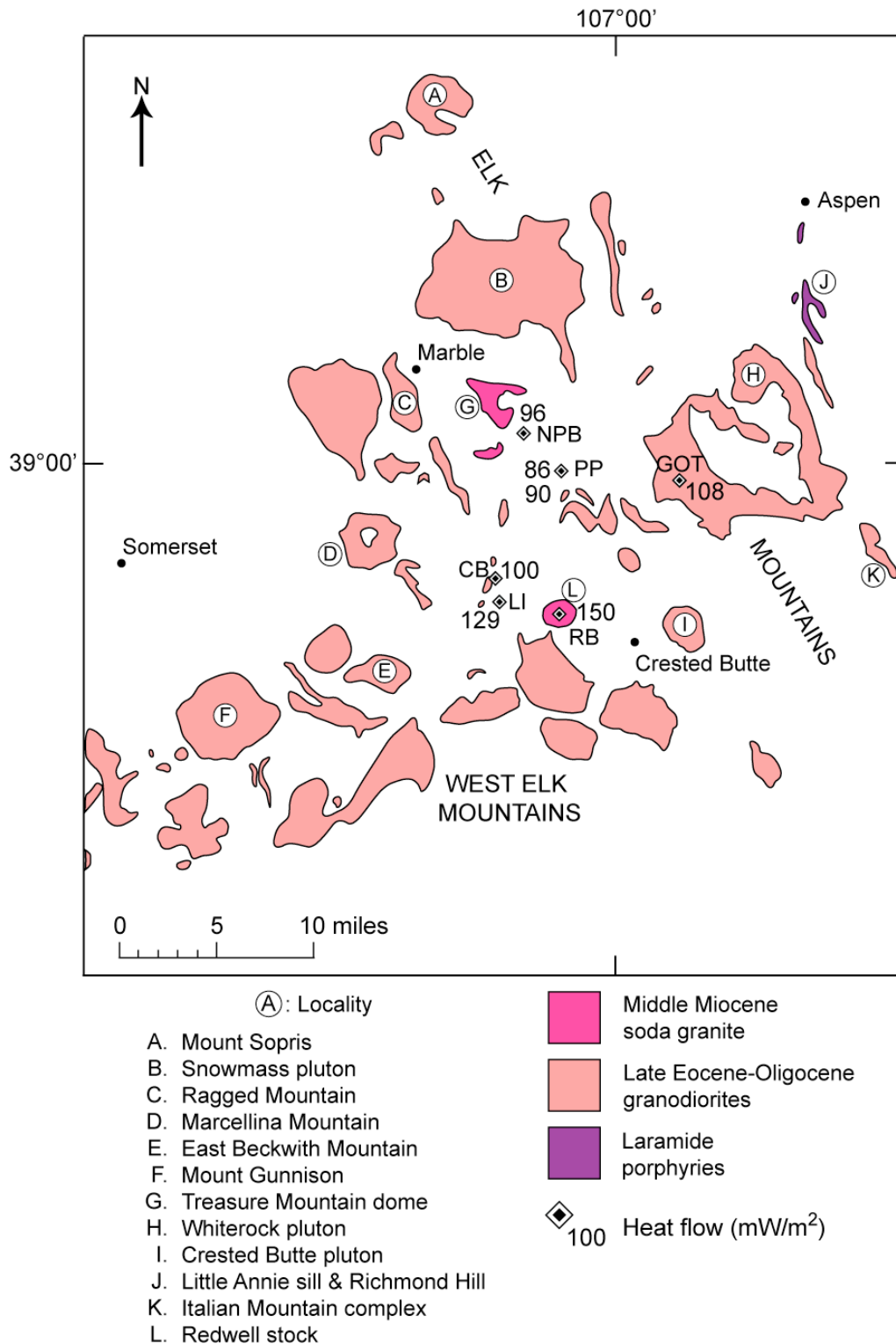


Figure 1.3: Mapped heat flow values for the field area. Values from Decker et al. (1988) and Reiter et al. (1975) keyed to Table 1.2. Map modified from Obradovich et al. (1969).

-325 mgal gravity lows, also suggesting the presence of low-density rocks in the upper crust.

Reiter (2008) analyzed smoothed gravity and heat flow data along an east-west profile across the Piceance Basin, through the Elk Mountains, and into the Rio Grande rift. Reiter (2008) noted that the broad half-width of the change from high heat flow/low gravity in the Leadville area to lower heat flow/high gravity in the Piceance Basin is indicative of a source in the mantle (depths of 60-70 km). Reiter (2008) also recognized low density, highly radiogenic, crustal sources near Leadville.

CHAPTER 2

METHODS

2.1 Sampling

$^{40}\text{Ar}/^{39}\text{Ar}$ (hornblende, biotite, and K-feldspar), apatite fission-track (AFT), and apatite (U-Th)/He (AHe) dating methods are used in constraining the thermal histories of the Oligocene plutons in the Elk and West Elk Mountains. U/Pb zircon geochronology is also used to ascertain the intrusion history of the Snowmass stock, the largest pluton sampled in this study.

Seven vertical traverses were collected from six different, high relief plutons that trend NE-SW along the maximum extent of the Colorado Mineral Belt defined by Tweto and Sims (1963). This sampling strategy was used in order to determine if there are differences in the timing and rate of cooling with distance relative to the surface projections of the low seismic velocity mantle anomalies (Aspen and San Juan). In addition, we hope to obtain improved thermochronologic coverage in this part of the Colorado Rocky Mountains. The spatial and temporal patterns of emplacement and cooling may reveal previously unrecognized aspects of the igneous and tectonic history of the area. All the plutons sampled have a granodioritic composition with some variations either due to zoned magma chambers or cooled margins. Some of the samples were affected by chlorite alteration, giving the rocks a greenish hue, especially on Mt.

Sopris. Samples were collected at ~150 m (500ft) intervals with extra sampling at phase changes in the rocks based on mineral assemblage or texture (Table C.1). The Mount Sopris traverse samples 2.3 km of vertical relief with the highest sample taken at 3944 m and the lowest sample at 3107 m. A lower elevation sample, not from the main traverse, was collected at 1622 m from a small intrusion that lies to the SW of Mount Sopris. However, this sample yielded no apatite or datable biotite. The Snowmass stock comprises of two vertical traverses: one from Capitol Peak (922 m vertical relief) and one from Snowmass Mountain (835 m vertical relief). The four remaining laccoliths that were sampled include: Ragged Peak (1760 m vertical relief), Marcellina Mountain (632 m vertical relief), E. Beckwith Mountain (485 m vertical relief) and Mount Gunnison (732 m vertical relief). Lowest elevation samples for Gunnison, Capitol and Snowmass were collected near the chilled margin of the intrusions but the rest were collected from interior positions in the laccolith. Sample descriptions, photos and sample locations can be found in Appendix C.

2.2 Mineral Separation

Mineral separation for each dating method has similar techniques. The field samples are cleaned of any outside weathering and broken into smaller pieces so they can be crushed and pulverized in the jaw crusher and disc mill. The samples are then passed over the Wilfley table in order to concentrate apatite and zircon. The remaining fraction of each sample is dried and sieved into appropriate sizes between 20 – 115 mesh. The samples are washed in deionized water in an ultrasonic cleaner and passed through a Frantz magnetic separator. All minerals are further separated using heavy liquids and

then hand picked to ensure sample purity.

2.3 U/Pb

U/Pb ages were determined for three samples from the Snowmass stock using laser ablation-multicollector-inductively coupled plasma mass spectrometry (LA-MC-ICPMS) at the Arizona Laser-Chron Center (ALC) in order to ascertain intrusion history. The zircon mineral separates acquired during the main mineral separation process discussed above are mounted in a 1-inch-diameter epoxy plug (35 ± 10 zircons per sample) along with Sri-Lankan zircon standards (564 ± 4 Ma) and are polished to expose the interior portions of most grains (some grains may be smaller than average and therefore are not exposed). The zircons are imaged with cathodoluminescence (CL) for the purpose of laser pit placement in specific portion of each zircon. After loading the plugs, the zircons are ablated with a New Wave/Lambda Physik DUV193 Excimer laser (operating at a wavelength of 193 nm) using a spot diameter of 25-35 μm , yielding an average pit depth of $\sim 12\mu\text{m}$. The ablated material is removed from the ablation chamber with He carrier gas, mixed with Ar, and passed through the plasma source where U, Th, and Pb isotopes are measured simultaneously. All measurements are made in static mode using Faraday detectors and channeltron multipliers for different isotopes. A single analysis, which takes less than a minute, involves (1) a single 12-s integration on peaks with no laser firing to measure on-peak background intensities, (2) 12 s of laser ablation during which intensities are integrated once per second, and (3) ~ 30 s with no laser firing to allow the system to purge and prepare for the next sample.

Three corrections are applied to the data prior to age calculations. Depth-related

fractionation of $^{206}\text{Pb}/^{238}\text{U}$ and $^{208}\text{Pb}/^{232}\text{Th}$ occurring during the 9s data acquisition are accounted for by least squares projection back to the initial ratio and the uncertainty of this value is calculated as a standard deviation of this initial intercept. Accurate common Pb correction is essential for a robust data set and requires reliable ^{204}Pb measurements. Accuracy of this correction is determined by plotting the measured $^{206}\text{Pb}/^{204}\text{Pb}$ against the $^{206}\text{Pb}/^{204}\text{Pb}$ determined by ID-TIMS on zircons from the same sample. The ^{204}Pb measurements along with uncertainties determined from common Pb composition (Stacey & Kramers, 1975) are propagated through all age calculations. Fractionation of U, Th, and Pb occurs during laser ablation; therefore measured isotopic ratios for the unknowns are corrected by comparison with the Sri Lanka zircon standards that are analyzed once between every three to five unknowns. As an aside, U and Th concentrations are also determined by comparison with the Sri Lanka standard and are used as a means of understanding discordance patterns (e.g. high U zircons are more susceptible to Pb loss) and because U/Th is a useful indicator of whether metamorphic fluids were present during zircon crystallization (Gehrels et al., 2008).

Data reduction is done off-line with an Excel spreadsheet (“agecalc”) equipped with VBA macros that process age calculations, uncertainties and error correlations (Gehrels et al., 2008). Anomalously old ages, resulting from ablation of inherited zircon cores, are omitted from age calculations. The reported ages are calculated for a set of analyses using the weighted mean method from Ludwig (2003) following corrections for collector gains, on-peak backgrounds, depth-related fractionation, common Pb and elemental/isotopic fractionation. These age calculations are done with only internal errors (errors that arise from measurements of the isotopic ratios) assigned to each

analysis. Uncertainties are calculated from the weighted mean of each analysis but do not include systematic (external) errors. Systematic errors include uncertainties in the U decay constants, uncertainty in the age of the calibration standard used for fractionation correction, average uncertainty in fractionation correction, and average uncertainty that arises from the composition of common Pb. Instead the systematic errors are propagated separately and added quadratically to the uncertainty of the weighted mean yielding a final age uncertainty of 1 – 2% (2-sigma). The resulting ages and uncertainties are run through Isoplot 3.0 (Ludwig, 2003) and a TuffZirc age is given with two uncertainties (2-sigma) at 95% confidence. The two uncertainties are meant to provide extra information on whether the sample was vulnerable to positive (from xenocrysts or zircon cores) or negative (from Pb loss) age biases. For a more detailed explanations on the methods used at the ALC refer to Gehrels et al. (2008).

2.4 $^{40}\text{Ar}/^{39}\text{Ar}$

$^{40}\text{Ar}/^{39}\text{Ar}$ geochronology was used to determine the thermal history between 550°C and 175°C by analyzing one hornblende, eighteen biotites, and nine K-feldspar samples at the New Mexico Geochronology Research Laboratory (NMGRL). The samples were loaded into machined Al discs and irradiated in a known geometry with inter-laboratory standard Fish Canyon Tuff (FC-2) sanidine (28.02 Ma [Renne et al., 1998]). All discs were stacked and placed in an evacuated pyrex tube. The NM-222 package was irradiated at the Nuclear Science Center in College Station, TX for 8.92 hours. J factors were determined to a precision of $\pm 0.1\%$ by CO_2 laser fusion of 6 single crystal FC-2 sanidines from each of the 4 radial positions around the irradiation tray.

Correction factors for interfering nuclear reactions were determined using K-glass and CaF₂. Both J and corrections factors can be found in Appendix A.

Each sample was packaged in Cu foil and step heated in a double vacuum Mo resistance furnace. Reactive gases were removed with a SAES GP-50 getter in both the first and second stages of the extraction line. The gas was analyzed in a Mass Analyzer Products (MAP) 215-50 mass spectrometer operated in electron multiplier mode at a sensitivity of 7.22×10^{-17} moles/pA for the biotites and 7.77×10^{-17} moles/pA for the hornblende. Age calculations were facilitated by the Mass Spec v.7.75 written by A. Deino at the Berkeley Geochronology Center. All age errors reflect the propagation of errors associated with blanks and baselines, J error, interfering reactions, signal intensity vs. time regressions, and the mass spectrometer discrimination value (Appendix A). The mass spectrometer is centered on ⁴⁰Ar (“peak-up”) and numerous air standards are analyzed prior to, during and after running the unknowns in order to obtain a representative mean mass discrimination value. Blanks and backgrounds in the extraction line and mass spectrometer are also measured many times throughout data collection and are applied to the age calculation.

Age assignment criteria for a well-behaved plateau include 3 consecutive steps that contain 50% of the total ³⁹Ar overlapping at 2σ . The MSWD values should fall within the 95% confidence window for n-1 degrees of freedom. Age calculations follow the York (1969) method with all errors reported at 2σ .

2.5 Apatite Fission-Track

Apatite fission-track analysis, using the external detector method, was conducted

on thirty-three samples in order to constrain the thermal history in the 60 – 100°C range. The concentrated apatite separates obtained during mineral separation were poured onto quick-release paper, covered in epoxy and topped with a 1cm² glass slide. After the epoxy cured, the samples were polished with 400 grit paper, 6 µm diamond compound, and 0.3 µm alumina-polishing wheel. The slides were etched with a 5 molar solution of nitric acid for 25 seconds to reveal the fission tracks and examined under a petrographic microscope apatite and polish quality. A 1cm² sheet of muscovite covered the polished slides. The samples were packaged in stacks that included Corning CN-5 U-glass and Durango apatite standards, and irradiated at a nominal fluence of 1x10¹⁶ neutrons/cm² at the Texas A&M Nuclear Science Center. After cooling for a minimum of one month, small holes were drilled in the corner of each sample through the glass slide and muscovite detector as a reference point during counting. The muscovite detectors were etched in a solution of 48% HF for 13 minutes (unknowns) and 45 minutes (U-glasses). Then the grain mounts and corresponding muscovite detectors were mounted on a glass slide in epoxy and spontaneous and induced tracks were counted in 20 grains per sample. Zeta calibrations for each irradiation were determined by counting spontaneous and induced tracks in Durango apatite and CN-5 uranium-doped glass included in the irradiation packages. Counting and track length measurements were conducted on a Nikon petrographic microscope with a 100x objective. Track lengths were measured with a SumaSketch digitizing tablet (with a precision of ± 0.2 µm) attached to a PC running an in-house program written by S. Kelley. Data reduction was done using an Excel template also created by Kelley.

Interpretation of the AFT data is reliant on the age, the Chi-Square test, and the

spontaneous track length distributions. The ratio of the counted spontaneous track density and induced track density for a sample is proportional to the age and therefore the first step taken in the AFT process. The next step is to test if individual grain ρ_s/ρ_i ratios fit a standard normal distribution and ascertain if the apatites are from a single population or multiple populations. According to Galbraith (1981), if the Chi-Square of the population is greater than 5% then all the grains are from a single age population. By quantifying mean track lengths and their standard deviations for a variety of apatites from various geological environments, Gleadow et al. (1986) found that the distribution of confined track lengths can provide information for the following thermal histories: rapid cooling, basement terranes, and complex histories. Mean track lengths for a rapidly cooling sample (i.e. volcanic or shallow intrusive) range from 14.5 to 15 μm with a standard deviation of $\sim 1 \mu\text{m}$. Granitic basement terranes have a negatively skewed distribution due to slow, uninterrupted cooling, with a mean of 12 to 13 μm and standard deviations of 1.2 – 2 μm . Complex thermal histories correspond to complex multimodal distributions of confined tracks, which are in continuous production and are affected by variations in temperature over time.

2.6 (U-Th)/He

Apatite from 27 samples was analyzed for (U-Th)/He low temperature thermochronology to determine the time of cooling below $\sim 60^\circ\text{C}$. Samples were picked from apatite-concentrate separates with a Nikon high power stereoscope with polarizing lenses in order to pick inclusion-free grains. The process is as follows: First, the concentrated separate was poured onto a glass slide and acceptable grains were picked

and placed onto another clean glass slide. Then several drops of isopropyl alcohol were placed onto the slide and the grains were re-examined for inclusions, cracks, and overgrowths. Finally three aliquots per sample were picked (containing three grains per aliquot), and the grains were digitally imaged and measured for alpha-ejection age corrections before being loaded into 1 mm platinum tubes.

The samples were packaged and sent off to the University of Kansas Isotope Geochemistry Laboratory (IGL) for analysis. The samples were heated to 1070°C for 5 minutes each and analyzed for He on a Balzers Prisma QMS-200 quadrupole mass spectrometer using the isotope dilution method. Aliquots were then retrieved from the He extraction line and the U, Th, and Sm was analyzed. The grains were dissolved in a 30% HNO₃ solution at 90 °C for an hour and spiked in a solution of ²³⁰Th, ²³⁵U, and ¹⁴⁹Sm. The spiked aliquots were analyzed for U, Th, and Sm with a VG PlasmaQuad IIXS ICP-MS, fitted with a micro-concentric nebulizer and an auto-sampling device.

The University of Kansas reduced the data using in-house software programmed on Visual Basic and Excel macros. Uncertainties that need to be accounted for include He measurement error (0.3 – 0.5%); U, Th, and Sm measurement error (<1 – 2%); alpha-ejection calculation errors; and errors associated with non-uniform U and Th distribution. The latter two sources of error are difficult to quantify, therefore IGL typically assigns a percentage error to an aliquot analysis based on the standard deviation of the population derived from analyzing standards.

The effective uranium concentration (eU, a parameter that weights the decay of the two parents for their alpha productivity, computed as [U] + 0.235 x [Th]) and grain size of the apatites are also investigated due to their influence on apatite He diffusivity.

He diffusion from apatites is sensitive to the fraction of radiation damage in the apatite crystal, such that He retentivity changes through time during the build up and annealing of radiation damage (Shuster et al., 2006; Shuster and Farley, 2009). For slow cooling rates ($\leq 1^\circ\text{C}/\text{Ma}$), apatites of typical eU range may have several tens of degrees variation in closure temperature owing to different magnitudes of accumulated radiation damage (Flowers and Kelley, in press). In short, higher eU values have a greater chance of causing anomalously old AHe ages. He diffusion is also sensitive to grain size, which positively correlates with AHe dates according to Farley (2000) with the effect equating to a closure temperature variation of $\sim 10^\circ\text{C}$ for typical grain sizes and cooling rates.

2.7 Modeling

Two modeling programs were used during this project HEAT 3D and HeFTy. HEAT 3D (Wohletz, 2008) is a user interface that allows design of a computational mesh representing rock geometry, properties, and magma body emplacement in order to assess the thermal history in the vicinity of plutons during single and/or multiple intrusion events. The HeFTy forward and inverse model (Ketcham, 2005; Ketcham et al., 2007) evaluates thermal histories that are consistent with measured AFT ages and lengths, AHe ages, and known geologic constraints.

The HEAT program models both conductive and convective heat flow using a 2-D and 3-D design structure that calculates transient thermal regimes in and around magmatic intrusions (Wohletz, 2008). The model is capable of incorporating multiple intrusions into the computational mesh at any point during the simulation, making it a useful tool for understanding the cooling history in the field area. Additionally, the user

is able to assign rock and magma properties that include: density, porosity (fluid saturation), heat capacity, initial temperature, spatially and thermally varying thermal conductivities, and location.

A conductive HEAT model was constructed simulating the real time emplacement and cooling of the Mount Sopris pluton, Snowmass pluton, Ragged laccolith (Chair Mountain, Ragged Peak, and Ragged Mountain) and Crystal pluton. The 60 x 200 km mesh design with a 1 km grid size is made up of a single rock property for simplicity. The bedrock has a thermal conductivity of 3.3W/mK (based on measured values; Decker et al., 1988), a specific heat of 980 J/kgK, a bulk density of 2000 kg/m³, a surface temperature of 10°C and a geothermal gradient of 25-30°C/km. The plutons were individually added into the mesh at different times according to the emplacement ages found during this study. An intermediate composition was chosen for the Mt. Sopris, Snowmass and Ragged plutons, while a silicic composition was chosen for the Crystal pluton. The location and dimensions for each pluton were estimated from the geologic map and incorporated into the mesh. Pluton thickness was estimated using gravity data from a study done by Isaacson and Smithson (1976) and the surficial pluton dimension measured from the geologic map (Mount Sopris: 8 km, Snowmass: 15 km, Ragged: 2 km, and Crystal pluton: 20 km). Depth of emplacement was shallow for all the plutons, ranging from 2 – 4 km.

The HeFTy program creates a range of likely thermal histories for a particular sample, calculates the corresponding AFT and AHe ages and AFT lengths, and compares the results to the measured values. It poses candidate time-temperature paths using a constrained Monte Carlo scheme that allows the user to specify regions of time-

temperature space through which paths must pass. The program determines which of these paths pass certain statistical criteria, accepting some as having a “good” or “acceptable” fit and rejecting the rest. The Kolmogorov-Smirnov (K-S) test is used to determine the quality of the fit between measured and calculated fission-track length distributions (Ketchum, 2005).

Certain parameters need to be specified by the user for both the AFT and AHe models within HeFTy. The parameters set for the AFT model include: annealing model (Ketcham et al., 2007), c-axis projection (Ketcham et al., 2007, 5.0M), kinetic parameter (CI (wt%) = 0.05), and initial track length (15.94 μm). The parameters set for the AHe model include: diffusion calibration (Farley, 2000 [Durango apatite]), solution geometry (sphere), type of alpha correction used (none), and grain dimension for each sample (average taken from Table B.2).

After setting up the models, the user chooses an initial and final constraint for a simple thermal model and can specify additional geologic constraints for a more complex thermal history. The initial condition for the time-temperature history is a sufficiently high temperature to ensure that there is total annealing (i.e., no fission tracks present) and/or no retained He. The initial condition for this study is the emplacement age of the pluton and the assumed $^{40}\text{Ar}/^{39}\text{Ar}$ closure temperature for the dated mineral. The final constraint in time corresponds to the surface temperature at which the sample was collected, in this case $\sim 10^\circ\text{C}$. From this point on the user can make the model much more complex by introducing additional constraints such as corresponding age data (i.e., K-feldspar ages) or reheating events in the time temperature history.

Both a simple and a somewhat complex model were done for all six samples from

Ragged Mountain and just a simple model was done for the one sample from Snowmass Mountain. The simple models for four of the Ragged samples have an initial condition of ~28 Ma at 275°C with the previously mentioned final constraint of 10°C as a modern surface temperature. The two highest elevation samples needed an older initial condition in order to find solutions fitting the LTT data. Therefore, an age of ~37 Ma at 300°C was used. The simple model for 08Elk08 (Snowmass) has an initial constraint of ~34 Ma at 350°C and the same final constraint as Ragged. The complex models all incorporate a constraint box that invokes fast cooling to ambient temperatures after pluton emplacement and a reheating event around 12 Ma to investigate the effects of the nearby Crystal pluton intrusion. An additional K-feldspar age was incorporated in the thermal history model for 09Elk-R6a at ~17 Ma and 175°C.

CHAPTER 3

RESULTS

3.1 Emplacement History

3.1.1 U/Pb: Zircon

All the dating results are summarized in Table 3.1 and the raw U/Pb data can be found in Appendix A. The range of ages for the Snowmass stock, which is made up of two high elevation mountain peaks (Snowmass Mountain and Capitol Peak), is between 33.2 (+1.82/-0.81) – 34.6 (+0.51/-0.81) Ma (Table 3.1). Further U/Pb analyses were deemed unnecessary as a means of obtaining intrusion history since the ages fell within error of corresponding $^{40}\text{Ar}/^{39}\text{Ar}$ biotite ages, as discussed in a later section. Therefore, the biotite ages for the remaining plutons are used to define an estimate of emplacement age.

3.1.2 $^{40}\text{Ar}/^{39}\text{Ar}$: Hornblende

The dated hornblende is from a lower elevation sample (08Elk14) from Snowmass Mountain. The age spectrum is complex, with an oscillatory pattern that makes age determination unambiguous (Figure A.1). The spectrum complexity somewhat correlates with the K/Ca spectrum complexity and may signify the presence of inclusions within the coarse (297 – 500 μm) separate. All of the steps from the

Table 3.1: Summary Table. Errors are specified for each dating technique. Argon ages are reported as integrated ages.

Sample	Elevation (m)	Rock Type	Apatite (U-Th)/He Age (Ma) ± 6%	Apatite Fission-Track Age (Ma) ± 1s	⁴⁰ Ar/ ³⁹ Ar K-spar Age (Ma) ± 2s	⁴⁰ Ar/ ³⁹ Ar Biotite Age (Ma) ± 2s	⁴⁰ Ar/ ³⁹ Ar Hbl Age (Ma) ± 2s	U/Pb Zircon Age (Ma) ± 2s
Mt. Sopris								
09Elk-S1	3944	quartz monzonite	12.4 ± 0.32	30.0 ± 4.2	—	—	—	—
09Elk-S2	3777	quartz monzonite	12.4 ± 0.57	31.3 ± 4.0	Analyzed	34.59 ± 0.12	—	—
09Elk-S3	3649	quartz monzonite	10.1 ± 0.28	26.5 ± 4.9	33.2 ± 0.2**	—	—	—
09Elk-S4	3523	quartz monzonite	10.2 ± 0.28	30.0 ± 4.6	—	—	—	—
09Elk-S5	3107	quartz monzonite	9.9 ± 0.46	21.4 ± 3.7	—	—	—	—
09Elk-S7	1622	quartz monzonite	—	—	Analyzed	—	—	—
Capitol Peak								
08Elk01	4151	granodiorite	11.2 ± 0.52	23.2 ± 2.6	—	33.94 ± 0.09	—	33.20 (+1.82/-0.81)
08Elk02	3817	granodiorite	—	22.3 ± 4.7	—	—	—	—
08Elk03	3721	monzodiorite	—	—	—	33.90 ± 0.09	—	—
08Elk04	3762	monzodiorite	—	—	—	—	—	—
08Elk05	3543	monzodiorite	—	23.1 ± 3.9	33.19 ± 0.19*	—	—	—
08Elk06	3386	diorite	8.2 ± 0.31	23.8 ± 2.6	—	34.34 ± 0.09	—	34.60 (+0.51/-0.81)
08Elk07	3229	monzodiorite	—	—	28.6 ± 0.86*	—	—	—
Snowmass Mountain								
08Elk08	4295	granodiorite	14.8 ± 0.78	28.8 ± 3.7	33.06 ± 0.50*	33.73 ± 0.12	—	—
08Elk09	4201	granodiorite	15.0 ± 0.77	26.4 ± 3.4	—	33.98 ± 0.12	—	—
08Elk10	4107	granodiorite	12.9 ± 0.65	27.5 ± 3.3	—	33.93 ± 0.12	—	—
08Elk11	4020	granodiorite	12.5 ± 0.53	24.5 ± 3.2	—	33.71 ± 0.13	—	—
08Elk12	3827	granodiorite	10.6 ± 0.45	23.5 ± 2.8	—	33.57 ± 0.12	—	—
08Elk13	3691	granodiorite	12.3 ± 0.46	24.4 ± 2.7	32.64 ± 0.88*	33.79 ± 0.13	—	—
08Elk14	3598	diorite	5.8 ± 0.15	21.7 ± 2.9	—	33.92 ± 0.12	90.83 ± 0.50	33.78 (+0.82/-0.80)
08Elk15	3460	diorite	—	17.6 ± 8.1	—	33.89 ± 0.13	—	—
Ragged Mountain								
09Elk-R2	3641	porphyritic granodiorite	10.7 ± 0.38	31.1 ± 3.2	—	—	—	—
09Elk-R1	3410	porphyritic granodiorite	11.6 ± 0.40	22.0 ± 2.5	28.39 ± 0.14**	—	—	—
09Elk-R3	3280	porphyritic granodiorite	8.3 ± 0.34	30.2 ± 3.0	—	—	—	—
09Elk-R4	3071	porphyritic granodiorite	6.4 ± 0.22	27.1 ± 2.8	—	—	—	—
09Elk-R5	2900	porphyritic granodiorite	6.9 ± 0.30	27.1 ± 2.9	—	—	—	—
09Elk-R6a	1882	granodiorite	5.6 ± 0.22	15.4 ± 2.0	17.3 ± 2.4***	29.05 ± 0.74	—	—
Marcellina Mountain								
09Elk-M1	3458	diorite	—	25.7 ± 4.6	—	30.76 ± 0.11	—	—
09Elk-M2	3284	diorite	—	—	—	—	—	—
09Elk-M3	3156	diorite	—	—	—	30.90 ± 0.16	—	—
09Elk-M4	2826	diorite	—	22.4 ± 9.5	—	—	—	—
E. Beckwith Mountain								
09Elk-B1	3530	porphyritic granodiorite	29.4 ± 0.90	30.5 ± 3.8	—	—	—	—
09Elk-B2	3401	porphyritic granodiorite	15.1 ± 0.45	27.6 ± 3.2	—	29.62 ± 0.11	—	—
09Elk-B3	3220	porphyritic granodiorite	29.0 ± 1.10	30.0 ± 3.0	—	—	—	—
09Elk-B4	3045	porphyritic granodiorite	15.8 ± 0.45	30.0 ± 3.2	—	37.87 ± 0.13	—	—
Mt. Gunnison								
09Elk-G4	3881	porphyritic granodiorite	34.6 ± 1.21	33.8 ± 4.9	—	—	—	—
09Elk-G3	3698	porphyritic granodiorite	32.0 ± 1.03	32.5 ± 3.4	—	—	—	—
09Elk-G1	3503	porphyritic granodiorite	35.4 ± 1.27	30.1 ± 3.5	—	—	—	—
09Elk-G2	3328	porphyritic granodiorite	—	—	—	29.78 ± 0.17	—	—
09Elk-G5	3149	porphyritic granodiorite	—	29.0 ± 3.5	—	—	—	—

* = Minimum Age (~175°C); ** = Terminal Age (~250 - 300°C); *** = Minimum Age (closing at ~150°C when compared to LTT ages)
 Dates that are crossed out are unreliable due to excess argon or argon loss in the sample.

hornblende spectrum are older than the corresponding zircon and biotite ages, which implies the presence of extraneous ^{40}Ar in the sample. This contamination may involve Precambrian xenocrysts that were not fully degassed and/or phenocrysts that contain excess argon. In any case, the hornblende result will not be considered further in this study.

3.1.3 $^{40}\text{Ar}/^{39}\text{Ar}$: Biotite

Biotite ages range from ~35 – 30 Ma across the study area. Their spectra are variable but are generally characterized by a hump-shaped pattern with initial and final steps giving younger ages compared to the intermediate steps (cf. Heizler et al., 1988) (Figure 3.1). The first couple of steps of each sample have low radiogenic yields, low K/Ca ratios, and high errors. Additionally, these early steps usually contain less than 10% of the total ^{39}Ar . The remaining steps have sub-equal concentrations of ^{39}Ar with relatively old ages near the middle part of the spectra. In some cases this older single step prevents formation of a plateau while the majority of the other steps yield concordant ages. Lo and Onstott (1989) have interpreted this humped shape as a result of ^{39}Ar recoil into intercalated chlorite. However, they argue that the integrated age is accurate due to the fact that the recoiled ^{39}Ar remains within the biotite/chlorite mixture.

Possible impurities that could affect age results were mostly removed from the mineral separates during the picking process. However, chloritization was sometimes difficult to identify visually in all of the biotite samples and therefore must be considered since it is a common occurrence in biotites. As part of an investigation to determine if picking visually “pristine” biotites would help enhance the age analyses, two sets of

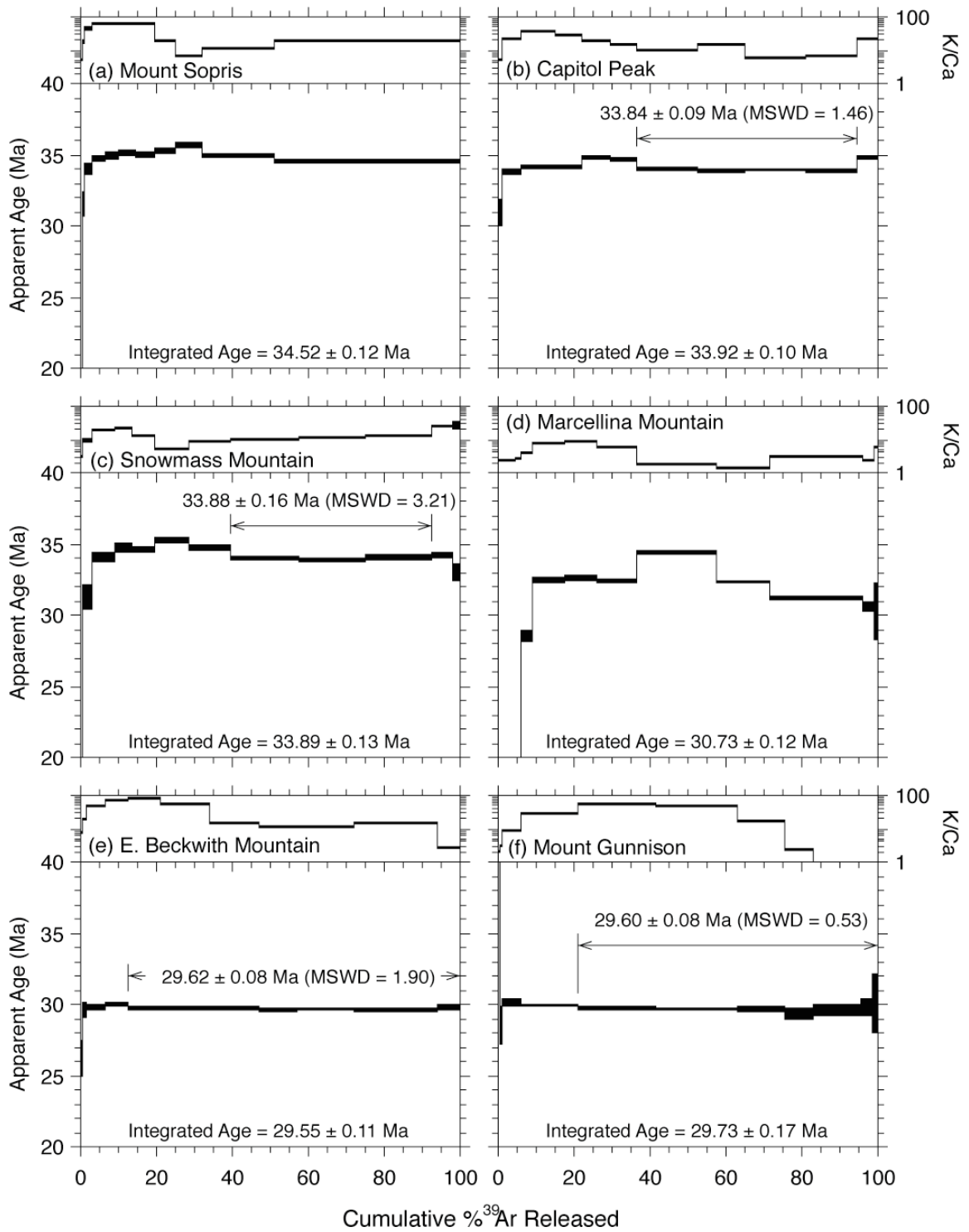


Figure 3.1: Representative $^{40}\text{Ar}/^{39}\text{Ar}$ biotite spectra from each mountain. Errors reported at 2σ .

biotite from sample 08Elk08 were picked and packaged separately. One set was visually pristine and the other was noticeably altered. Both biotite packages were step heated in the same manner and produced almost exactly the same age spectra (Figure A.2). The “pristine” biotite gave a total gas age of 33.73 ± 0.08 Ma and the “chloritized” biotite gave a total gas age of 33.71 ± 0.09 Ma. Apparent %K₂O for both samples was nearly identical, therefore even though the samples appeared visually different in chlorite content they in fact were not. Thus, this experiment demonstrated that picking “pristine” biotites alone will not prevent the presence of chloritization and therefore we can assume that chloritization might be present in all of the biotite samples that were dated. All age spectra and results are compiled in Appendix A.

Even with the added complications mentioned above, almost half of the biotite age spectra from these plutons yield a plateau age. A number of these plateaus consist of 6 – 8 steps with one or two of initial steps containing less than 50% of the total ³⁹Ar but the remaining steps exceeding 50%. There are three other spectra with plateaus that are comprised of only 3 to 4 steps but have higher percentages of the total ³⁹Ar released. The plateau ages, in 5 out of 7 spectra, are the same within error of the integrated ages and therefore the choice of one age over the other for these five spectra do not interfere with geologic interpretation. For consistency, integrated ages are reported for the biotite samples and can be found in Table 3.1.

The biotite ages from the Snowmass stock are equivalent to the zircon crystallization ages indicating fast cooling from ~900°C to ~350°C and therefore they may be used to estimate pluton emplacement ages as well as the other biotite ages found for the other plutons. One exception is 09Elk-G2, which has a biotite age (29.66 ± 0.08

Ma) that is younger than almost all the AFT and AHe ages for Mount Gunnison.

The biotite ages can be grouped into two broad suites with the older ages to the north and the younger ages in the south. Sopris, Capitol, and Snowmass all have ages of ~34 Ma, while Marcellina, E. Beckwith and Gunnison give biotite ages of ~30 Ma. Two of the plutons to the north, Capitol Peak and Snowmass Mountain, were dated more comprehensively than the rest and show a minute decrease in age as elevation decreases, but in general the ages are equal within error. Only one or two biotite dates were obtained from the remaining plutons for the purpose of constraining an emplacement age. Except for Mount Gunnison, the biotite ages for Mount Sopris, Marcellina Mountain and East Beckwith are consistent with their corresponding AFT and AHe ages in that they are older. The biotite age from Mount Gunnison is from a lower elevation sample in the traverse and is consistent with the AFT data from samples above and below it.

There are a few ages that will not be considered for this study due to excess argon (09Elk-B4) or argon loss (09Elk-R6a, M3) due to low potassium concentrations ($K_2O < 5\%$) that can cause a higher degree of ^{39}Ar recoil loss during irradiation.

3.1.4 $^{40}Ar/^{39}Ar$: K-Feldspar

The K-feldspars exhibit gradationally increasing spectra that record young ages during the early steps of gas release and ultimately rise to a terminal age. Sometimes the terminal age is older than the corresponding biotite and U/Pb ages. These older parts of the spectra are considered to reflect excess argon (Foster et al., 1990). Typically the youngest early gas release steps correspond to cooling through ~175°C (minimum age) and continuing to the oldest late release steps that corresponds to a T_c of ~300°C

(terminal age) (Lovera et al., 1989).

All the K-feldspar spectra have been plotted along with their corresponding biotites in order to help facilitate age assignment (Figure 3.2). From the seven samples, either a minimum age or a terminal age was interpreted from the spectra. All four spectra from Snowmass stock (Snowmass Mountain and Capitol Peak) were assigned a minimum age ranging from 28.6 – 33.2 Ma. A minimum age of 17.3 Ma at a closure temperature of 150°C was measured in the lowest Ragged Mountain sample (Figure 3.2g). The remaining two K-feldspar spectra from Mount Sopris and Ragged Mountain (Figures 3.2a and 3.2f) provided enough concordant steps to determine a plateau age. The terminal age from Mt. Sopris (33.2 Ma, 09Elk-S3) is younger than the biotite age from a higher elevation sample (09Elk-S2; ~128 m elevation difference). The highest elevation Ragged sample (09Elk-R1) yields an age of 28.39 Ma, representing the time of closure at ~250 – 300°C and is equal to the AFT age within error. There is no upper bound age to compare this sample of Ragged with since the biotite age spectrum did not provide a valid age. However, this K-spar spectrum behaves similarly to the other K-spar spectra that do not show signs of excess argon and therefore its terminal age is considered accurate. Since there is no usable biotite age for Ragged Mountain and the terminal K-spar age from 09Elk-R1 has a very similar closure temperature as biotite, it will be used as an estimated emplacement age for the pluton.

Two K-feldspar spectra, out of the nine analyzed, were not assigned ages due to low precision and low %K₂O from either alteration or plagioclase contamination (09Elk-S2) or because of a complicated hump-shaped spectra (09Elk-S7). All K-feldspar ages are reported in Table 3.1 with individual sample data tables located in Appendix A.

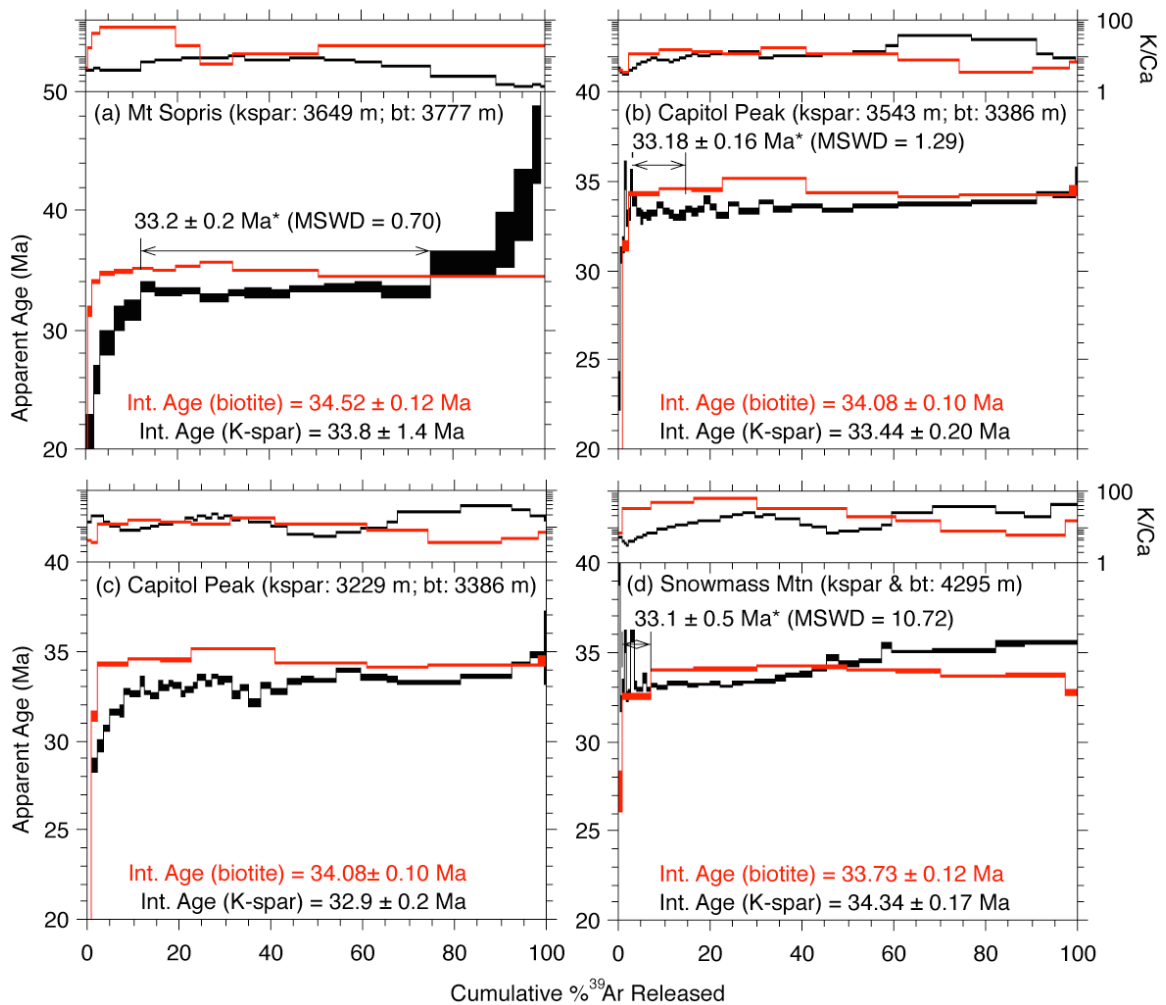


Figure 3.2: $^{40}\text{Ar}/^{39}\text{Ar}$ K-feldspar spectra with corresponding biotite where applicable. (a) 09Elk-S3 (3649 m) from Mt. Sopris plotted with the biotite spectra for 09Elk-S2 (3777 m). (b) 08Elk5 (3543 m) from Capitol Peak plotted with the biotite spectra for 08Elk6 (3386 m). (c) 08Elk7 (3229 m) from Capitol Peak plotted with the biotite spectra for 08Elk6 (3386 m). (d) 08Elk8 (4295 m) from Snowmass Mountain plotted with the biotite spectra from the same sample. Errors reported at 2σ .

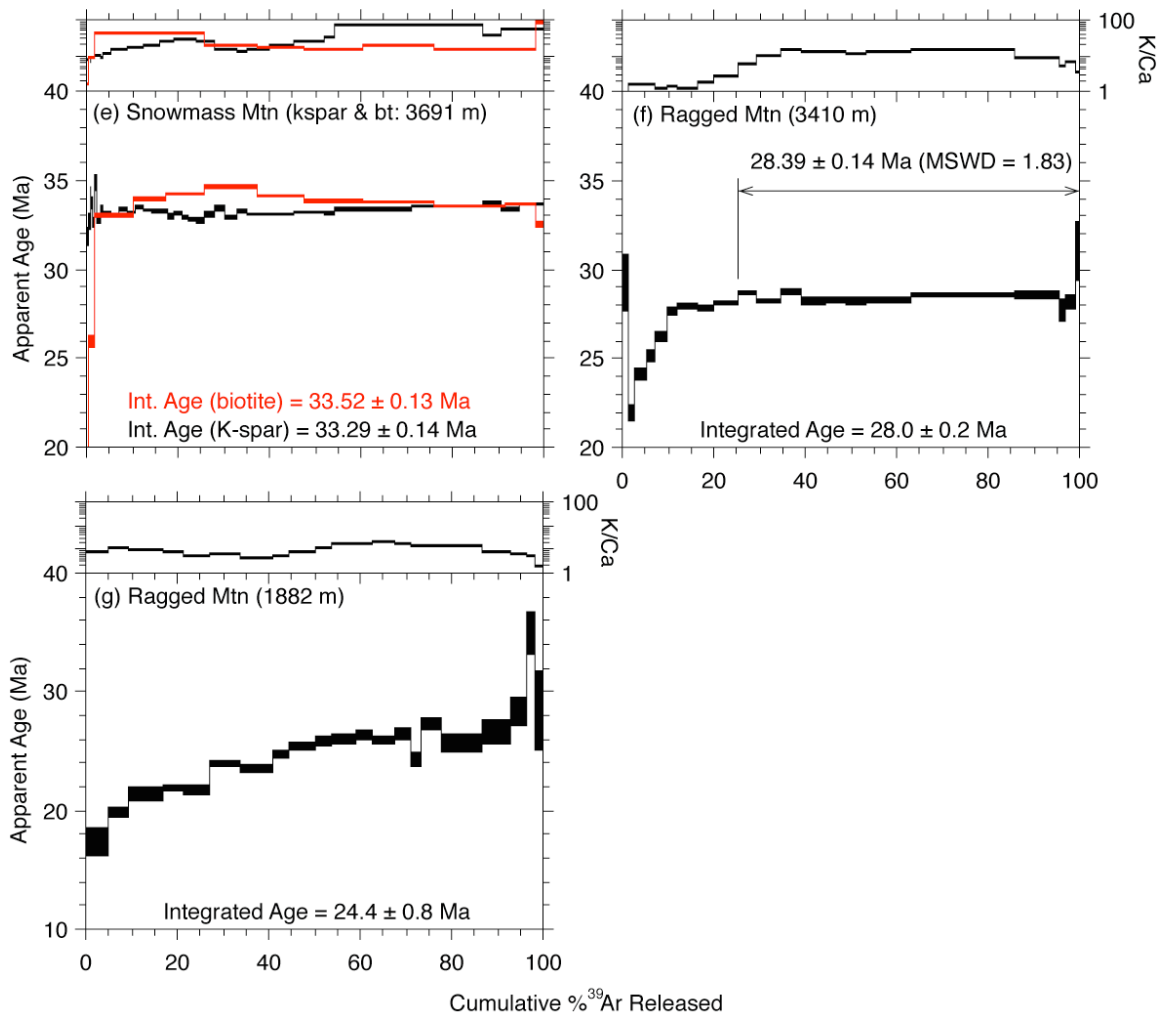


Figure 3.2 (continued): $^{40}\text{Ar}/^{39}\text{Ar}$ K-feldspar spectra with corresponding biotite where applicable. (e) 08Elk13 (3691 m) from Snowmass Mountain plotted with the biotite spectra from the same sample. (f) 09Elk-R1 (3410 m) from Ragged Mountain (no available biotite age for this pluton). (g) 09Elk-R6a (1882 m) from Ragged Mountain (no available biotite age for this pluton). Errors reported at 2σ .

3.2 Cooling History

3.2.1 Apatite Low Temperature Thermochronology

3.2.1.1 Qualitative Observations

The AFT data pass the Chi-Square test ($P [\chi^2] > 5\%$; Galbraith, 1981), indicative of a single age population. The mean track lengths for the Snowmass stock range from 12.3 – 13.8 μm , with standard deviations of 1.4 – 5.2 μm . The mean track lengths for Ragged Mountain pluton range from 12.8 – 14.1 μm , with standard deviations of 2.0 – 3.2 μm . The mean track lengths fit the profile for granitic basement terranes from Gleadow et al. (1986), indicating cooling of the plutons through the closure temperature at depth instead of a fast cooling scenario that produces track lengths that range from 14.5 – 15 μm . The raw AFT and AHe data can be found in Appendix B.

Some characteristics of the quality, size, color and shape of the apatites used in AHe and AFT analysis were noted during the picking and counting process. The apatites are generally classified as fluorapatites based upon visual inspection of etch pit size (1.5 – 1.9 μm ; Donelick (1991)) and geologic environment. In general, the apatites are full of curvilinear defects that complicated the AFT counting process. Only the apatites from Beckwith were free of these defects. Apatites from Snowmass (08Elk13 and 08Elk15) and Sopris (09Elk-S3) were smaller than average compared to all the other samples. The apatites from Capitol, especially from high on the traverse, were measurably elongated compared to the other samples. Apatites from 09Elk-G5, the lowest sample in the Gunnison transect, were brown in color. The middle samples from East Beckwith, 09Elk-B2 and 09Elk-B3, have apatites that are much larger and produce a blue-green sheen, due to thickness, under transmitted light. These differences may reflect episodic

variation in the chemistry of the magma as the laccoliths were emplaced.

Plots of AHe date versus eU, AHe date versus grain size (r), and r versus eU (Figure 3.3) are evaluated to assess the affect of radiation damage on the AHe ages. A typical eU for apatites with an average spherical radius of 60 μm is 28 ppm (Flowers et al., 2009). All the eU values from this study are less than 30 ppm, however the radii are also smaller than average, ranging from 37 – 55 μm . A weak positive correlation between date and eU is observed for a majority of the plutons (Figure 3.3a); however, data from Snowmass are somewhat negatively skewed, and data from Beckwith and Gunnison are poorly correlated. The two southernmost plutons, Gunnison and Beckwith, have some of the highest eU values, while Sopris, the northernmost pluton, has the lowest values, indicating a possible enrichment in U and Th of the magma feeding the plutons toward the south. A slight positive correlation is observed between date and grain size for the younger samples but not the older ones (Figures 3.3b and 3.3c). There is also no correlation between grain size and eU (Figure 3.3d).

In general, the AFT and AHe data for each pluton are younger than their corresponding argon and U/Pb dates, except for some complexity in the data from Mount Gunnison and East Beckwith Mountain. Two out of three of the AHe dates for Gunnison are slightly older than the AFT and biotite data, but still agree within error. The lower elevation sample 09Elk-G1 (35.4 ± 1.27 Ma) is not only older than the AFT and biotite dates but also the higher elevation AHe dates. Since there is no evidence of faulting or the presence of a secondary intrusion, then the higher eU values may be the cause of the older ages.

Radiation damage to the apatites can cause retentivity of He, which in turn causes

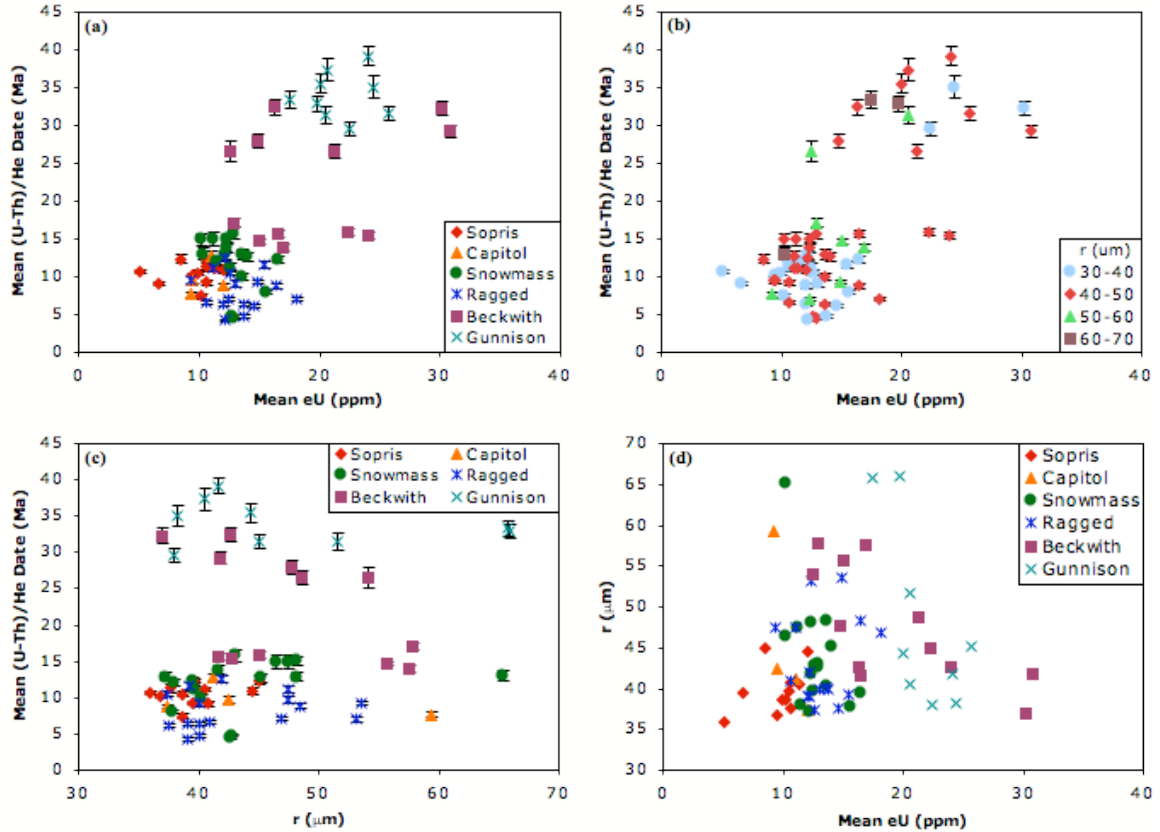


Figure 3.3. AHe age, eU, and grain size comparisons. (a) Age vs. eU. (b) Age vs. eU with respect to grain size. (c) Age vs. grain size (r). (d) Grain size vs. eU

a change in the closure temperature (T_c) for the mineral. The change in T_c is variable and dependent on cooling rate and eU. The eU values for Gunnison are not particularly high (~17 – 26 ppm) and the cooling rate is reasonably fast (~100 – 300 °C/Ma) leading to a rise in T_c by about 5°C resulting in a T_c of ~65°C. This small change may be enough to affect the dates by 1 – 2 Ma and needs to be taken into consideration when interpreting the cooling history for Gunnison.

The AHe dates from Beckwith also display some complexity by forming a step pattern (listed by decreasing elevation: 29.4, 15.1, 29.0, 15.8 Ma). The most reasonable explanation is a sample mix up in the lab, the presence of a fault or two, or the presence of zones of 15 Ma alterations due to hydrothermal fluids associated with a Miocene

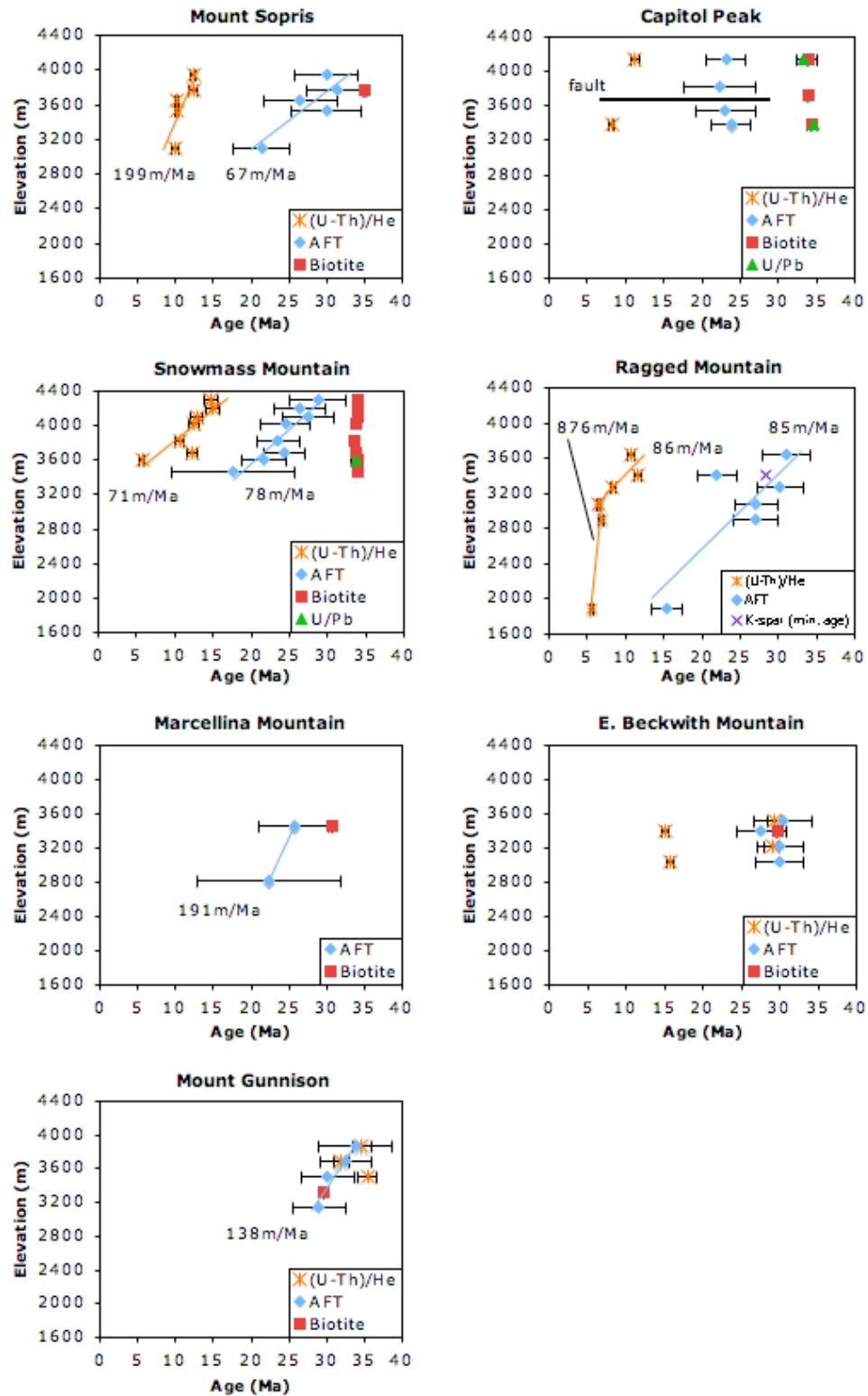


Figure 3.4: Age vs. elevation plots for each traverse. The K-Feldspar age is a minimum age.

thermal event. Faulting was not evident either in the field or on a geologic map. The hand samples were inspected for alteration using a hand lens. In general, the mafic minerals appeared relatively fresh and only minor alteration of feldspar to clay was present in the fine-grained matrix of sample 09Elk-B3 (See Table C.1 for additional sample descriptions). Thus it is most likely that the samples were mixed up in the lab, however the dates will not be discarded since they still provide useful information.

The AFT and AHe ages for each traverse were plotted on age vs. elevation diagrams (Figure 3.4) to evaluate changes in cooling rates through time and space. U/Pb and biotite dates are plotted along with the low temperature thermochronology data to constrain the time of pluton emplacement. The slope of the age-elevation data for Mount Sopris goes from gradual to steep indicating a slower cooling rate of the pluton after emplacement with an increase in rate occurring at about 12 Ma. Capitol Peak and Snowmass Mountain are both in the same pluton, but the cooling history from each area is different. Snowmass Mountain cools at a steady rate of $4^{\circ}\text{C}/\text{Ma}$ producing a geothermal gradient of $43.75^{\circ}\text{C}/\text{km}$. In contrast, Capitol Peak appears to cool quite rapidly ($11^{\circ}\text{C}/\text{Ma}$). This difference in cooling rate is due to the presence of a fault at Capitol Peak that was observed in the saddle just east of Capitol Lake with a strike of 55°E and a plane dip of 85°N (Figure C.8). The fault cut through the traverse resulting in the higher elevation samples being located on the hanging wall and the lower elevation samples on the footwall. The cooling history of Ragged Mountain is comparable to Mount Sopris, but the acceleration in cooling rate occurs much later (~ 6.5 Ma) in the AHe data. Although the data from Marcellina Mountain are sparse, the apparent cooling rate is relatively high ($47^{\circ}\text{C}/\text{Ma}$). Note that the complex AHe data for East Beckwith

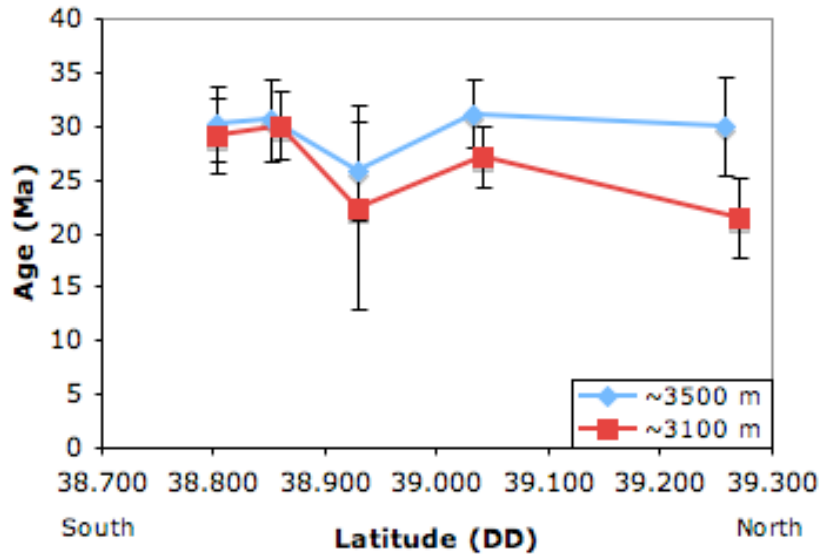


Figure 3.5: Similar elevation age plot of the field area. The data points represent the different plutons (left to right: Gunnison, Beckwith, Marcellina, Ragged, and Sopris).

mentioned in the previous paragraph remain on the plot and can be interpreted differently depending on which interpretation the reader chooses to believe. If the samples were indeed mislabeled, then East Beckwith Mountain rapidly cooled at two distinct times, at ca. 28 Ma and 15 Ma. The AFT and AHe data from Mount Gunnison plot on top of each other indicating rapid cooling of the pluton. The AHe dates are a little older than the AFT dates but are still within error of those values. Generally, the plutons toward the north cooled more slowly than those to the south.

AFT data from five of the plutons in the field area was compared at similar elevations (one at ~3500 m and another at ~3100 m) in order to determine if there was a regional tilt in cooling surface across the field area. The resulting plot (Figure 3.5) shows cooling occurring at the same time to the north and the south. However, cooling seems to be delayed for ~5 Ma in the middle of the field area (around Marcellina Mountain).

The variable cooling rates (Table B.4) are likely due to several distinct geologic

processes, including rapid cooling following shallow pluton emplacement (e.g., Mt. Gunnison, Marcellina), thermal overprinting by emplacement of Miocene intrusions (Crystal and Redwell plutons affecting Ragged and East Beckwith, respectively), disruption and tilting by faulting (Capitol), or exhumation after latest Eocene to Oligocene magmatism ceased (Snowmass). The relative importance of each of these processes is explored more thoroughly in the next section.

3.2.1.2 Quantitative Observations

Simple and complex models were constructed for samples from Ragged Mountain in HeFTy to determine how well thermal histories that involve (1) only exhumation or (2) a thermal pulse at 12 Ma fit the observed data. Both models generate good fits to the data. The simple model (Figure 3.6) provides the most unbiased version of possible thermal histories for a sample. Obviously, this model does not constrain the thermal history above 110°C very well. In general, based on the average cooling history (blue line) the samples cooled monotonically at rates of 6 to 13°C/Ma. The short track lengths for 09Elk-R6 and best fit model for 09Elk-R5 suggests that the rocks in the low elevation portion of the profile may have lingered in the AFT PAZ prior to 10 Ma.

The more complex models for Ragged Mountain (Figure 3.7) incorporate a reheating event ~12 Ma due to the intrusion of the nearby Crystal pluton (~ 1 to 8 km away). All the samples record the reheating event, but the lowest elevation samples seem to be the most affected. The HeFTy models were developed based on the results from the HEAT 3D program. Time-temperature calculations at points equivalent to the position of 09Elk-R6a and 09Elk-R1 relative to the 11 km wide, 20 km high Crystal pluton

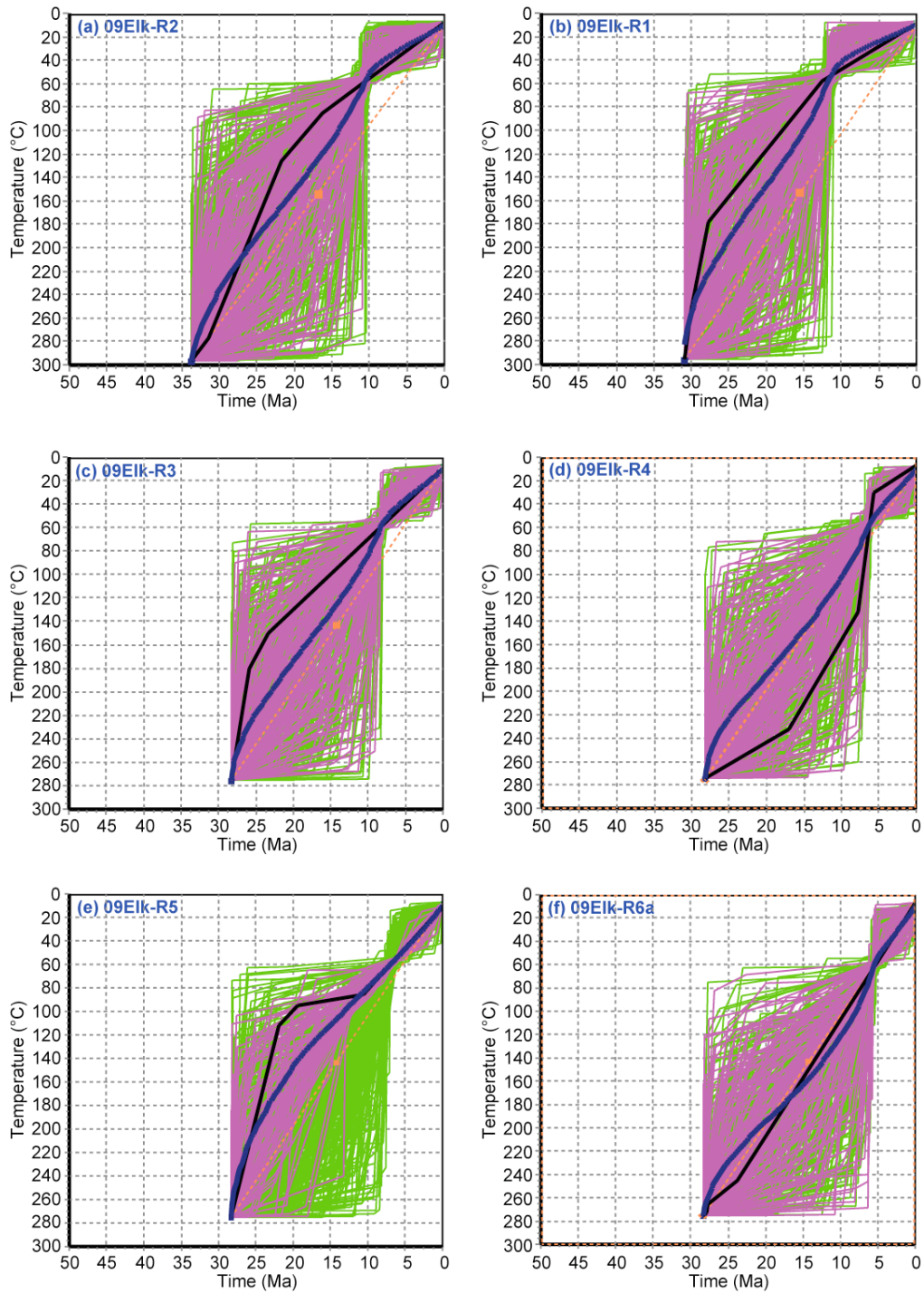


Figure 3.6: Simple thermal history models for Ragged Mountain using the HeFTy inverse modeling program (Ketcham, 2007). The surface temperature is set $\sim 10^{\circ}\text{C}$. The initial condition for (a) and (b) ranges from 31 – 34 Ma and $\sim 300^{\circ}\text{C}$. The initial condition for (c) – (f) is 28.3 Ma and $\sim 275^{\circ}\text{C}$. (a) 3641m, (b) 3410 m, (c) 3280 m, (d) 3071 m, (e) 2900 m, and (f) 1882 m. Green lines (acceptable path), pink lines (good path), black line (best-fit model), blue line (weighted mean path), and the orange dotted line (constraint path).

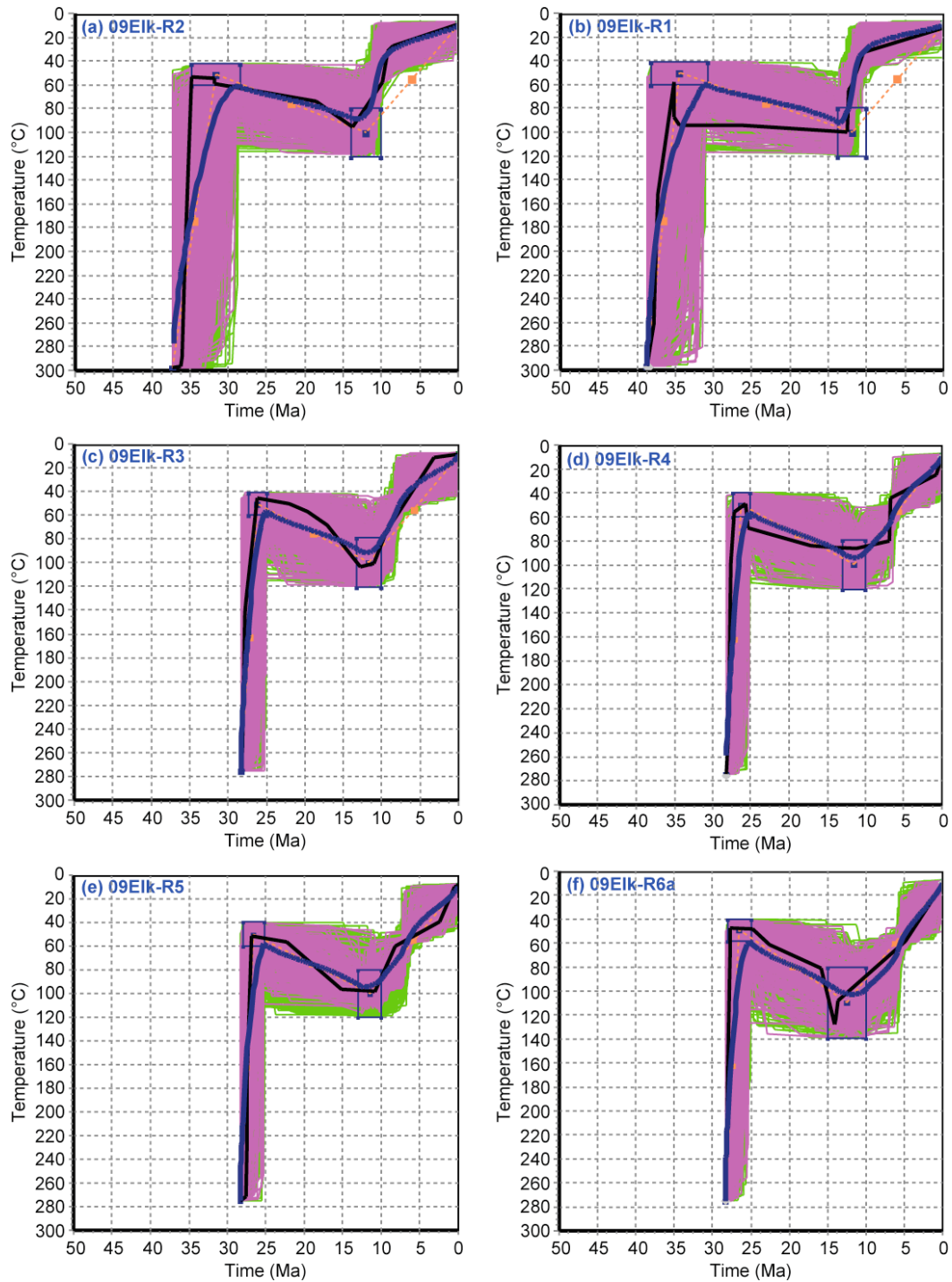


Figure 3.7: Thermal history models for Ragged Mountain exploring a reheating event ~ 12 Ma using HeFTy (Ketcham, 2007). The surface temperature is set $\sim 10^\circ\text{C}$. The initial condition for (a) and (b) is ~ 38 Ma and $\sim 300^\circ\text{C}$. The initial condition for (c) – (f) is 28.3 Ma and $\sim 275^\circ\text{C}$. (a) 3641m, (b) 3410 m, (c) 3280 m, (d) 3071 m, (e) 2900 m, and (f) 1882 m. Green lines (acceptable path), pink lines (good path), black line (best-fit model), blue line (weighted mean path), the orange dotted line (constraint path) and blue boxes (constraint boxes).

indicate that the more distant (8 km away), but low elevation R6a sample was less affected by the pluton than the close-by (1 km) higher elevation sample R1; the temperatures were about 50°C higher for R1 compared to R6a, which is greater than the temperature differential recorded by the AFT data.

Another thermal model was created using the HEAT program (Wohletz, 2008) in order to constrain how fast plutons like Sopris, Snowmass and Ragged individually cooled over time and how emplacement of multiple intrusions affected that cooling. The dimensions and relative position of the plutons are illustrated in Figure 3.8 and the timing of pluton emplacement is constrained by the geochronology data. The Sopris pluton almost reaches ambient temperatures when Snowmass pluton intruded ~1 Ma after the emplacement of Sopris. As Snowmass begins to cool, its heat radiates out in all directions but moves more freely through the Sopris pluton, increasing the temperature to ~120°C at the center of the pluton (~9.6 km away from the Snowmass pluton). Three million years after the emplacement of Snowmass, the Ragged laccolith intrudes into the bedrock. The laccolith is a lot thinner than the other plutons and therefore cools much faster (~0.7 Ma) and doesn't affect the nearby plutons. However, Snowmass is still cooling and keeps Ragged's temperatures slightly elevated. The geothermal gradient also remains elevated in the region due to the intrusions. By the time Crystal pluton intrudes at 12 Ma, the surrounding plutons are at ambient temperatures. Cooling of the Crystal pluton not only increases temperatures in the Ragged laccolith to ~110 - 160°C but it also increases temperatures at the deeper part of the Snowmass pluton to 90°C.

The highest elevation sample on Snowmass, which is the only sample to yield numerous track length measurements, was also evaluated using HeFTy. The best fit

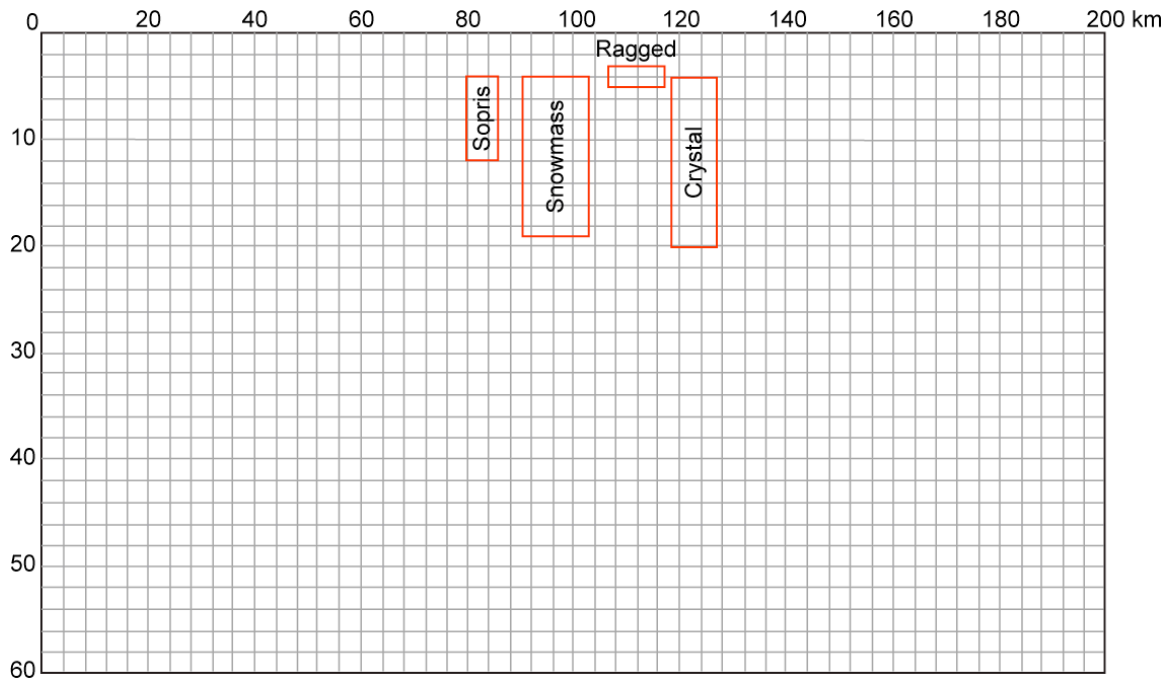


Figure 3.8: Design mesh for the multiple intrusions HEAT model. Each pluton was intruded according to their emplacement ages.

model for the Snowmass sample (Figure 3.9) indicates constant cooling ($13^{\circ}\text{C}/\text{Ma}$) after emplacement until ~ 17 Ma where the sample instantly cools $\sim 70^{\circ}\text{C}$. Unfortunately, the affect of the Crystal pluton on the lowest elevation samples on Snowmass cannot be determined because <10 confined tracks were found in each of these samples.

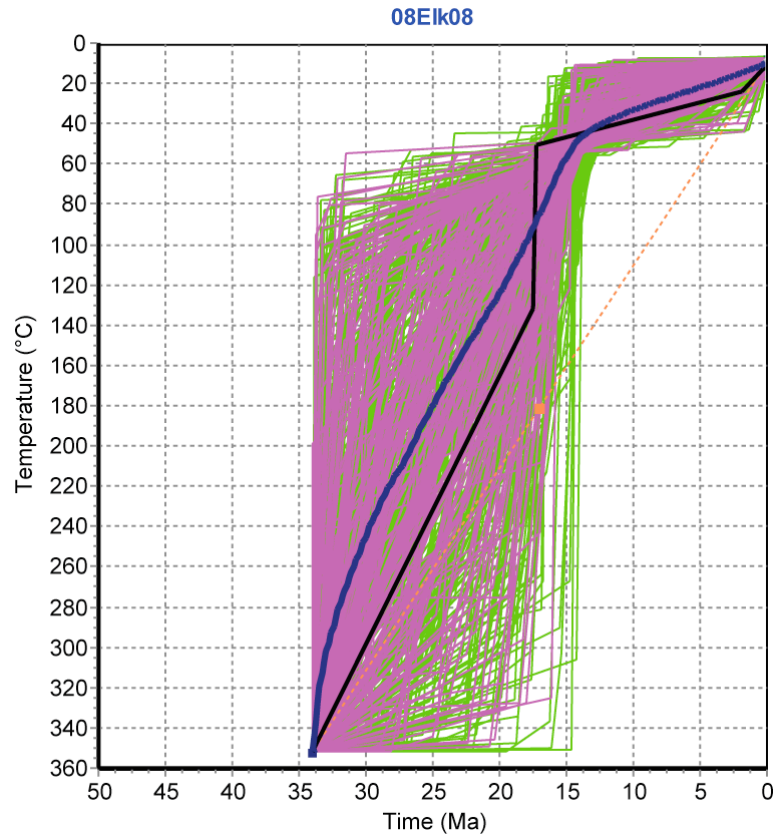


Figure 3.9: Simple thermal history model for 08Elk08 (4295 m, Snowmass Mountain) using the HeFTy inverse modeling program (Ketcham, 2007). The surface temperature is set $\sim 10^{\circ}\text{C}$. The initial condition is 33.7 Ma and 350°C . Green lines (acceptable path), pink lines (good path), black line (best-fit model), blue line (weighted mean path), and the orange dotted line (constraint path).

CHAPTER 4

DISCUSSION

4.1 Emplacement History

The plutons analyzed during this study were emplaced during the middle Cenozoic (late Eocene – Oligocene) and are part of a history of igneous emplacements that occurred in the region. Emplacement ages in the Elk and West Elk Mountains are generally younging toward the middle of both ranges (Figure 4.1). Mount Sopris, the northernmost peak in the Elk Range, has a biotite emplacement age of 34.93 ± 0.28 Ma. Mount Gunnison, the southernmost sampled mountain in the West Elks, has an AFT age of 33.8 ± 4.9 Ma. Ragged Mountain, the most centrally located pluton in the field area, has a K-feldspar age of 28.39 ± 0.14 Ma.

Two laccoliths from this study were previously dated: Snowmass Mountain and Mount Sopris (Table 1.1). The K-Ar date for Snowmass is 34.1 ± 1.4 Ma (Obradovich, 1969) and is in agreement with the $^{40}\text{Ar}/^{39}\text{Ar}$ biotite ages from this study (33.82 ± 0.08 Ma). The K-Ar age for Mount Sopris is 34.2 ± 0.8 Ma (Cunningham et al., 1994) and agrees with the Ar/Ar biotite age mentioned above. Zircon FT dating (34.3 ± 4.1 Ma) was done on the same K-Ar sample from Sopris and is concordant with the higher temperature methods and the AFT dates from this study.

In addition to the middle Cenozoic intrusions, there are periods of emplacement in the Elk and West Elk Mountains during the Late Cretaceous (72 - 67 Ma) and the

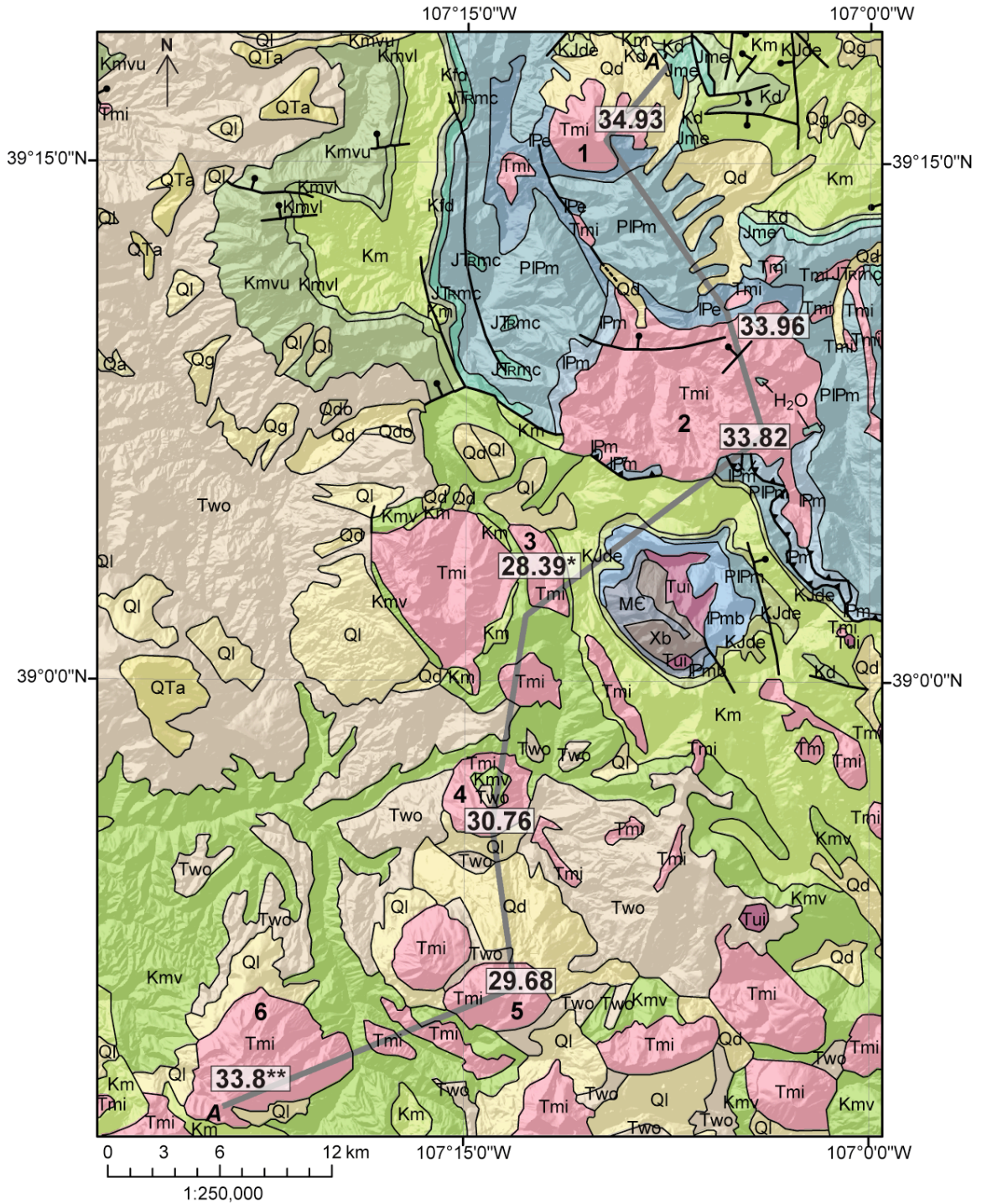


Figure 4.1: Geologic map of the field area. The intrusion ages are $^{40}\text{Ar}/^{39}\text{Ar}$ biotite ages except for the $^{40}\text{Ar}/^{39}\text{Ar}$ K-feldspar age for Ragged Mountain (*) and the AFT age for Mount Gunnison (**). The legend for the map is on next page. Base geology map from Tweto and Schoenfeld (1979).

EXPLANATION


Q	Quaternary deposits
Two	Tertiary Wasatch Fm. & Ohio Creek Fm.
Tui	Upper Tertiary intrusives
Tmi	Middle Tertiary intrusions
Kmv	Cretaceous Mesaverde Fm.
Km	Cretaceous Mancos shale
Kd	Cretaceous Dakota Ss.
Kfd	Cretaceous Frontier Ss. & Mowry shale
KJde	Cretaceous Entrada, Morrison, & Dakota
Jme	Jurassic Morrison Fm. & Entrada Ss.
JTrmc	Jurassic/Triassic Morrison, Entrada & Chinle Fm.
PIPm	Penn.-Perm. Maroon Fm.
IPm	Penn. Minturn Fm.
IPmb	Penn. Minturn & Belden Fm.
IPe	Penn. Eagle Valley Fm.
IPee	Penn. Evaporitic facies
ME	M: Leadville, Gilman; D: Dyer, Parting; O: Fremont, Harding, Manitou; C: Dotsero, Peerless & Sawatch
Xb	Proterozoic biotite gneiss, schist, & migmatite


DATED PLUTONS

1	Mount Sopris
2	Snowmass Stock
3	Ragged Mountain
4	Marcellina Mountain
4	East Beckwith Mountain
6	Mount Gunnison

SYMBOLS

—— Contact

 Fault -- Dotted where concealed. Bar and ball on downthrown side.

 Low-angle thrust fault -- Sawteeth on upper plate.

34.93 Pluton intrusion ages (Ma)

Figure 4.1 (continued): Legend for geologic map of field area.

Miocene (12 Ma). Previous K-Ar and FT dating in the area (Table 1.1) shows late Cretaceous intrusions occurred in the northern part of the Elk Mountains, near Aspen, as porphyries and aplites (Figure 4.3). Middle Miocene intrusions are located at Treasure Mountain (12 Ma) and in Redwell Basin (16-18 Ma) near the intersection of the Elk and West Elk Mountains.

The episodic plutonism seen in the Elk and West Elk Mountains can also be seen regionally within the boundary of the Colorado Mineral Belt. The Laramide age plutons are scattered along the entire extent of the CMB with the majority located in the Front Range and the southern portion of the Gore Range and the rest occurring in the Sawatch Range (i.e. Twin Lakes Batholith) and the southwest corner of Colorado (La Plata Mountains and Sleeping Ute Mountain). The middle Cenozoic intrusions (35 – 15 Ma) also occur within the CMB. Most of these plutons occur in the Elk, West Elk and Sawatch Ranges with a few others in the Front Range and the San Juan Mountains. Laramide and middle Cenozoic plutons that do not fall within the maximum boundaries of the CMB (Tweto and Sims, 1963) are located in the northern Park Range or the Sangre de Cristo Mountains (i.e. Spanish Peaks, Great Plains alkalic province).

Four distinct pulses of emplacement and a period of inactivity between 54 – 44 Ma are recorded in the geochronology data from the Elk, West Elk and Sawatch Ranges (Figures 4.2 and 4.3). The first episode of magmatism started in the Aspen-mining district, located between the Elk Mountains and the Sawatch Range, between 73 and 67 Ma. Magmatism continued to the east in the Twin Lakes Batholith from 63 – 56 Ma. Then there was a period of quiescence in the Twin Lakes area with the second episode of plutonism occurring from 43 – 39 Ma. The third episode began when plutonism stepped

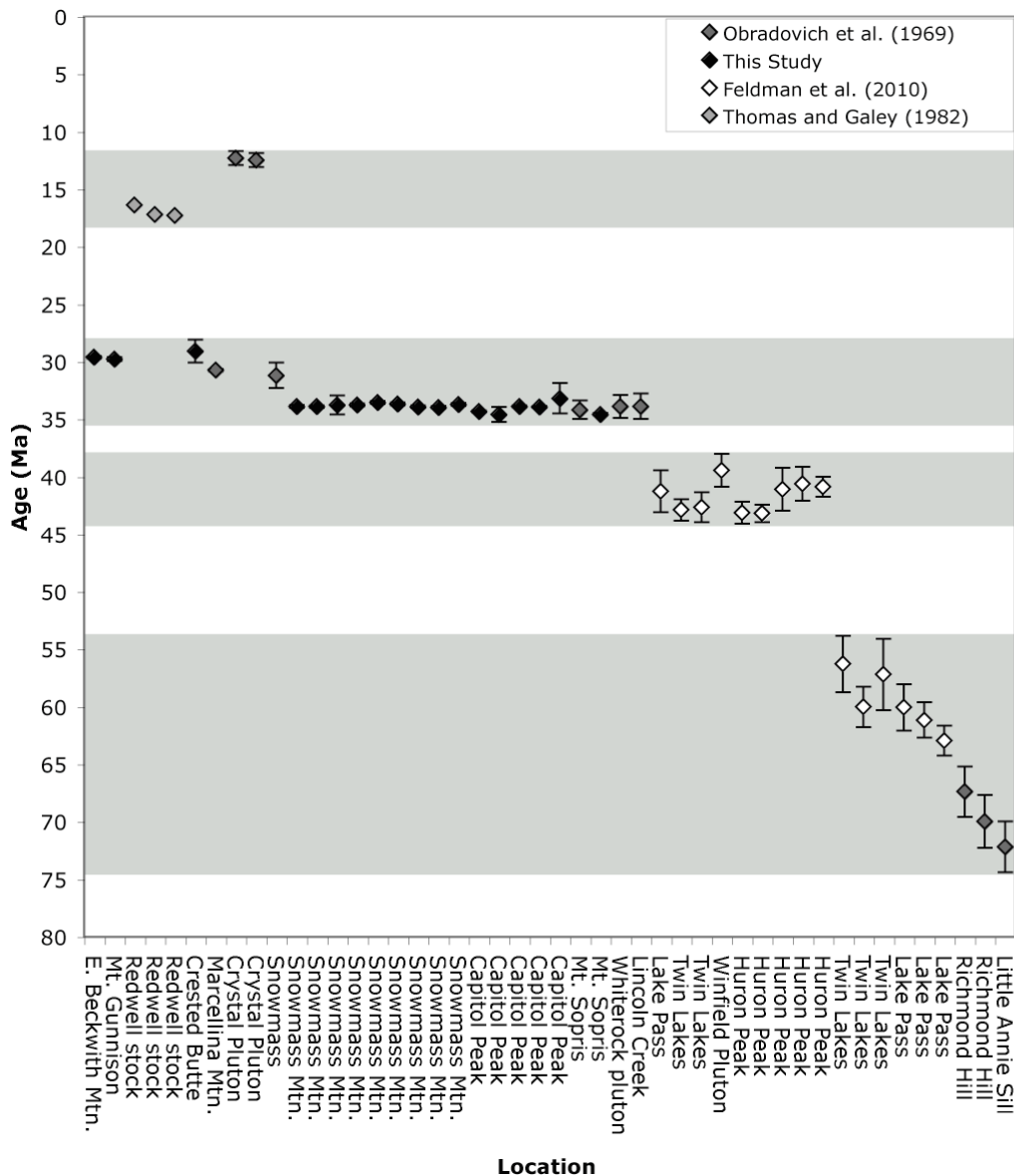


Figure 4.2: Regional plutonic history. The gray bars highlight different periods of magmatism in the region. Dating Techniques: K-Ar (Obradovich and Thomas and Gayle), U/Pb (Feldman), $^{40}\text{Ar}/^{39}\text{Ar}$ biotite (this study).

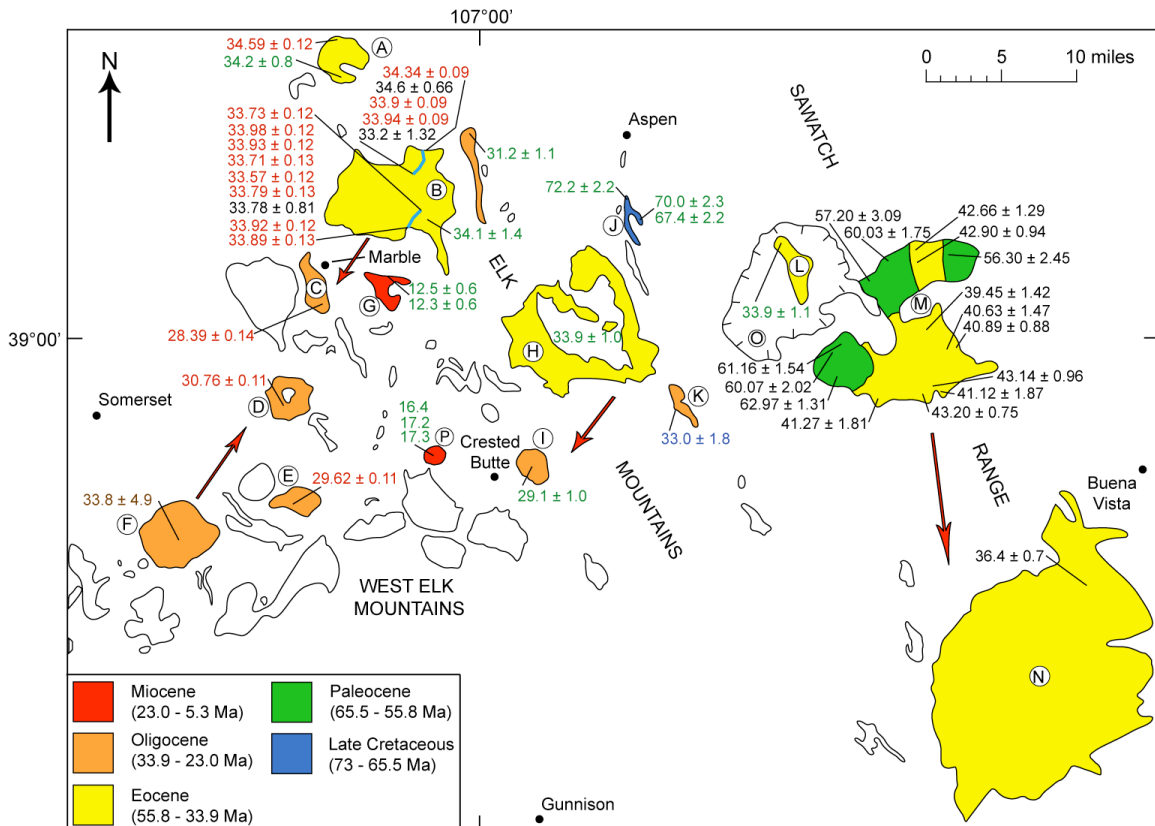


Figure 4.3: Regional plutonic trends. Plutons from the Elk, West Elk and Sawatch Range were mapped along with their intrusive age data. The dates are color-coded by dating technique (U/Pb: black; Ar/Ar: red; K-Ar: green; ZFT: blue; and AFT: brown). The letters on the map correspond to their location name: A. Mount Sopris; B. Snowmass pluton; C. Ragged Mountain; D. Marcellina Mountains; E. East Beckwith Mountain; F. Mount Gunnison; G. Treasure Mountain dome; H. Whiterock pluton; I. Crested Butte pluton; J. Little Annie sill and Richmond Hill; K. Italian Mountain complex; L. Lincoln Creek stock; M. Twin Lakes batholith; N. Mount Princeton batholith; O. Grizzly Peak caldera; P. Redwell stock. Directional arrows indicate younging patterns. Map after Obradovich et al. (1969).

westward to the Grizzly Peak Caldera, where the Lincoln Creek stock has a K/Ar age of 33.9 Ma (Obradovich, 1969). Plutonism of similar age was also happening in the Elk and West Elk Mountains beginning in the northern Elk Mountains and southern West Elk Mountains ~34 – 33 Ma and then migrating towards the intersection of the two ranges around the Ragged Wilderness ~28.4 Ma. The final episode of magmatism was a localized event ~12 Ma creating the Crystal pluton and Redwell intrusion 16-18 Ma.

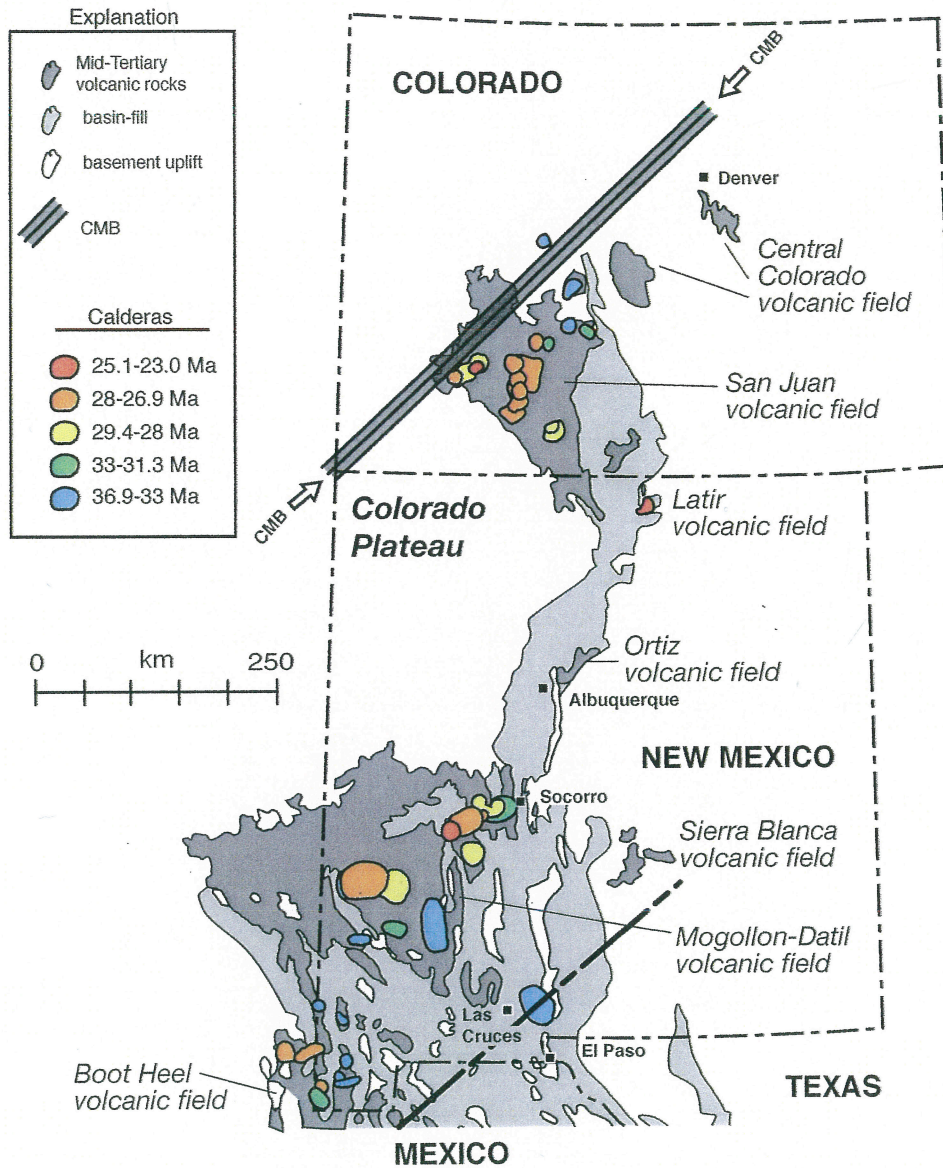


Figure 4.4: Map showing the CMB and middle Cenozoic volcanic fields and calderas (Chapin, in press). Dark gray = middle Cenozoic volcanic fields; light gray = basin fill of Rio Grande rift and Basin and Range province.

There is a west, southwest younging pattern in the plutonism beginning around 39 Ma that mirrors a similar younging trend in the regional volcanism (Chapin, in press). During rollback of the flat slab, episodic, regional volcanism became progressively younger to the west, southwest (Figure 4.4; Chapin, in press). Chapin (in press) believes that the ignimbrite flare-up volcanism and the CMB magmatism and mineralization were both controlled by slab rollback.

Lipman et al. (1969) also suggests that there is a link between the volcanism in the San Juan volcanic field (SJVF) and the plutons in the Elk Mountains. They conjecture that there was volcanic activity occurring in the Elk region during the same period of time that the initial eruptions were happening in the SJVF (38 - 26 Ma). However, any evidence of these eruptions was erased, most likely by erosion, leaving behind the plutonic remnants.

4.2 Cooling History

Discordance between emplacement age and cooling through 110°C is variable across the study area. Ragged Mountain, East Beckwith and Mount Gunnison cooled through 110°C shortly after emplacement (<1 Ma), while Mount Sopris, the Snowmass stock and Marcellina Mountain took 5 – 10 Ma. The variation in cooling appears to reflect variation of emplacement depth.

Most of the AFT and AHe data decrease in age with decreasing elevation (Figure 3.4), which is interpreted to record exhumation through 110°C and 60°C respectively. The majority of the AFT and AHe data are discordant signifying slow and possibly variable cooling of the pluton. However, Beckwith and Gunnison have concordant LTT

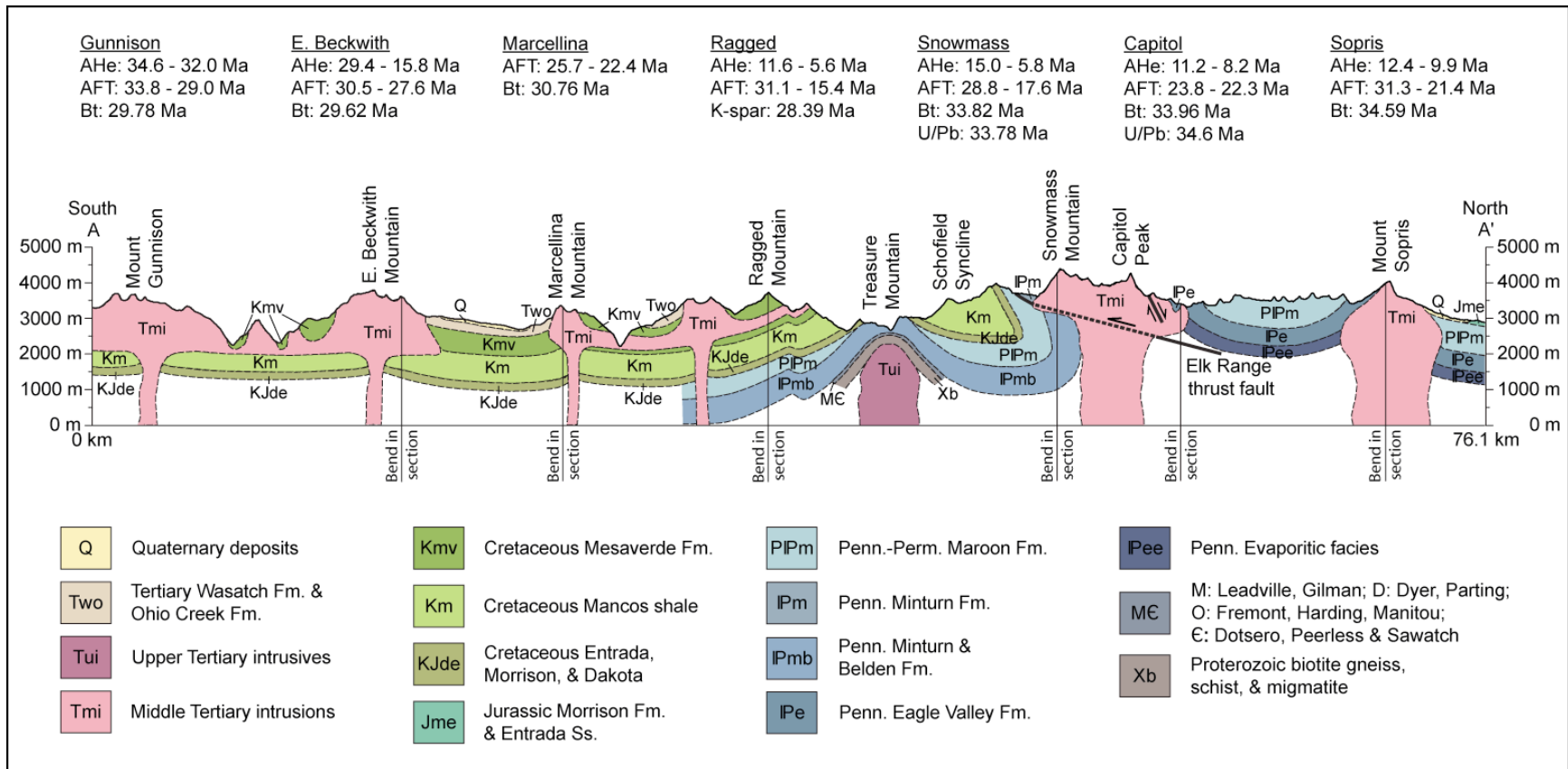


Figure 4.5: Generalized cross section of the study area. The geochronology for each mountain is listed at the top of the figure. Geology interpreted from Gaskill and Godwin (1966a), Gaskill and Godwin (1966b), Godwin (1968), Mutschler (1970), Streufert (1999), and Tweto and Schoenfeld (1979).

data signifying rapid cooling through $\sim 60^{\circ}\text{C}$ right after emplacement.

According to Flowers et al. (2009), the presence or absence of an eU correlation in an apatite suite can also be used to constrain cooling rates. The presence of a positive correlation between date and eU signifies slow cooling because apatites with higher eU accumulate more radiation damage and in turn develop a higher effective closure temperature, which results in older dates. At fast cooling rates, the apatites yield uniform dates regardless of eU because there is insufficient time for their He diffusivities to diverge during rapid cooling. Both of these cases are seen in the data from this study. The northernmost plutons reveal a weak positive correlation between eU and date signifying slow cooling. The absence of an eU correlation in apatites from Mount Gunnison confirms fast cooling in the south.

In order to fully understand these cooling trends, a generalized cross-section was drawn along a transect line connecting each sampled pluton (Figure 4.5). Thick Pennsylvanian/Permian strata of the Maroon Formation are exposed in the Elk Range northeast of the ERTF, while the younger Cretaceous strata of the Mesa Verde Formation and the Mancos Shale are exposed in the West Elk Mountains. A correlation can be seen between the age and thickness of the strata and the rate of cooling of the plutons. The plutons experiencing slower cooling intruded into the Pennsylvanian/Permian strata, while the faster cooling plutons were more shallowly emplaced in the Cretaceous strata of the southern West Elk Mountains.

Accelerated cooling is preserved by AHe data from Mount Sopris, Capitol Peak and Ragged Mountain. After a pause in cooling, both Mount Sopris and Capitol Peak plutons started to record cooling that is likely related to exhumation around 12.3 Ma until

about 8.2 Ma. Around 6.5 Ma the cooling rate for the Ragged Mountain pluton increased ($5.1^{\circ}\text{C}/\text{Ma}$), recording an AHe age of 5.6 Ma for the lowest elevation sample. Based on the thermal and HeFTy modeling, the Crystal pluton clearly affected the lower elevation samples collected from Ragged Mountain, partially annealing the AFT system and totally resetting the AHe system. The apparent change in cooling rate may be due to the onset of exhumation in the area, combined with continued isotherm relaxation following emplacement of Crystal pluton intrusion into Treasure Mountain.

4.3 Regional Thermochronology

Regional AFT and AHe data were separately mapped and overlain on top of two different tomographic interpretations of Colorado in order to identify any correlations that may exist between modern day seismic velocities in the mantle and episodes of cooling and/or exhumation recorded in the data. The two tomographic images come from different authors using different data sets and methodologies for handling the data. In addition, these authors analyzed different depth slices using different color schemes. One of the images is at 100 km (Figure 4.8a; McCarthy et al., 2010) and the other is a mean of 60 – 100 km (Figure 4.8b; Schmandt and Humphreys, 2010). The tomography reveals three notable, low velocity mantle anomalies in Colorado; one is located under the San Juan Mountains, another is located under the Front Range just west of the Denver Basin and the third one is in the south central part of the state extending into New Mexico (Jemez Anomaly). The first two anomalies (San Juan Anomaly and Aspen Anomaly) are the most relevant to this study since they fall within or right next to the bounds of the CMB.

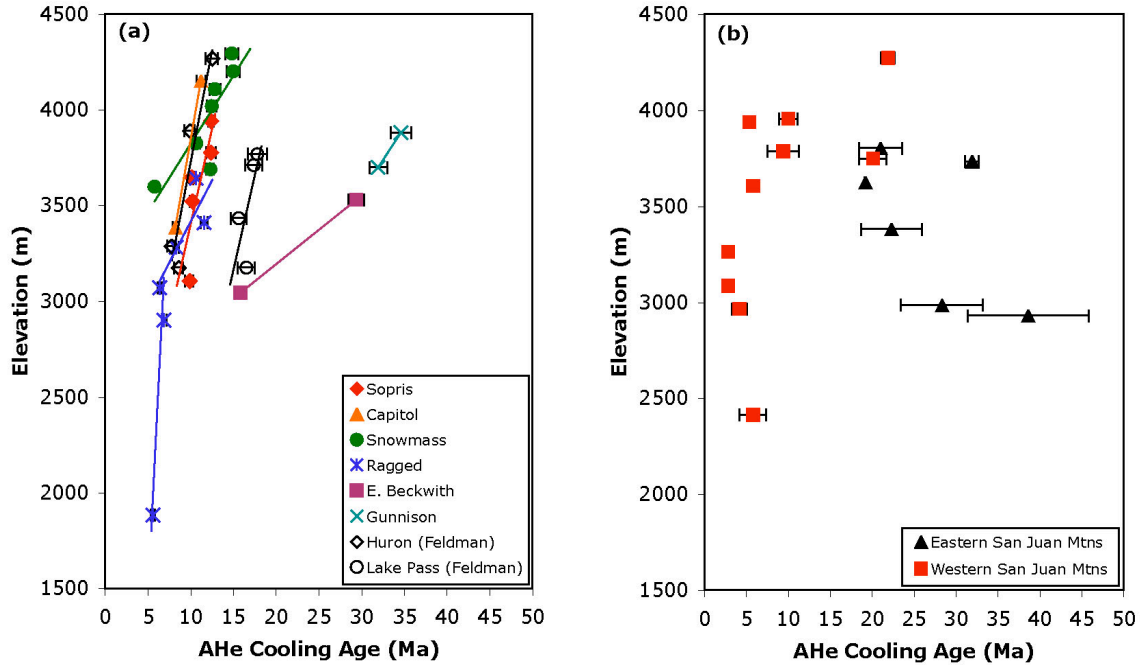


Figure 4.6: AHe age vs. elevation plots. (a) Data from this study and two additional AHe age transects from the Twin Lakes area (Feldman, 2010). (b) McKeon (2009).

The low temperature late Eocene – Oligocene data from this study is compared to a recent AHe thermochronology study done by McKeon (2009) on plutons in the San Juan volcanic field. The AHe data from McKeon’s study shows two distinct periods of cooling that span from 38 – 19 Ma and 10 – 2 Ma (Figure 4.6) that are also separated geographically with the older period of cooling occurring in the eastern San Juan Mountains and the younger period occurring in the western region (Figure 4.7). One pluton in the western region fits into the older episode of cooling (Mount Wilson, ~21 Ma). Either the AHe age from Mt. Wilson is recording the true cooling age, meaning it cooled before the surrounding plutons of Mount Sneffels and Bear Peak. More likely, the AFT and AHe data from Mount Sneffels and Bear Peak were reset by a thermal event that occurred 5 - 15 Ma after the formation of the Silverton caldera (~27.5 Ma), which caused mineralization in the area that was recorded in the plutons (Lipman et al., 1976).

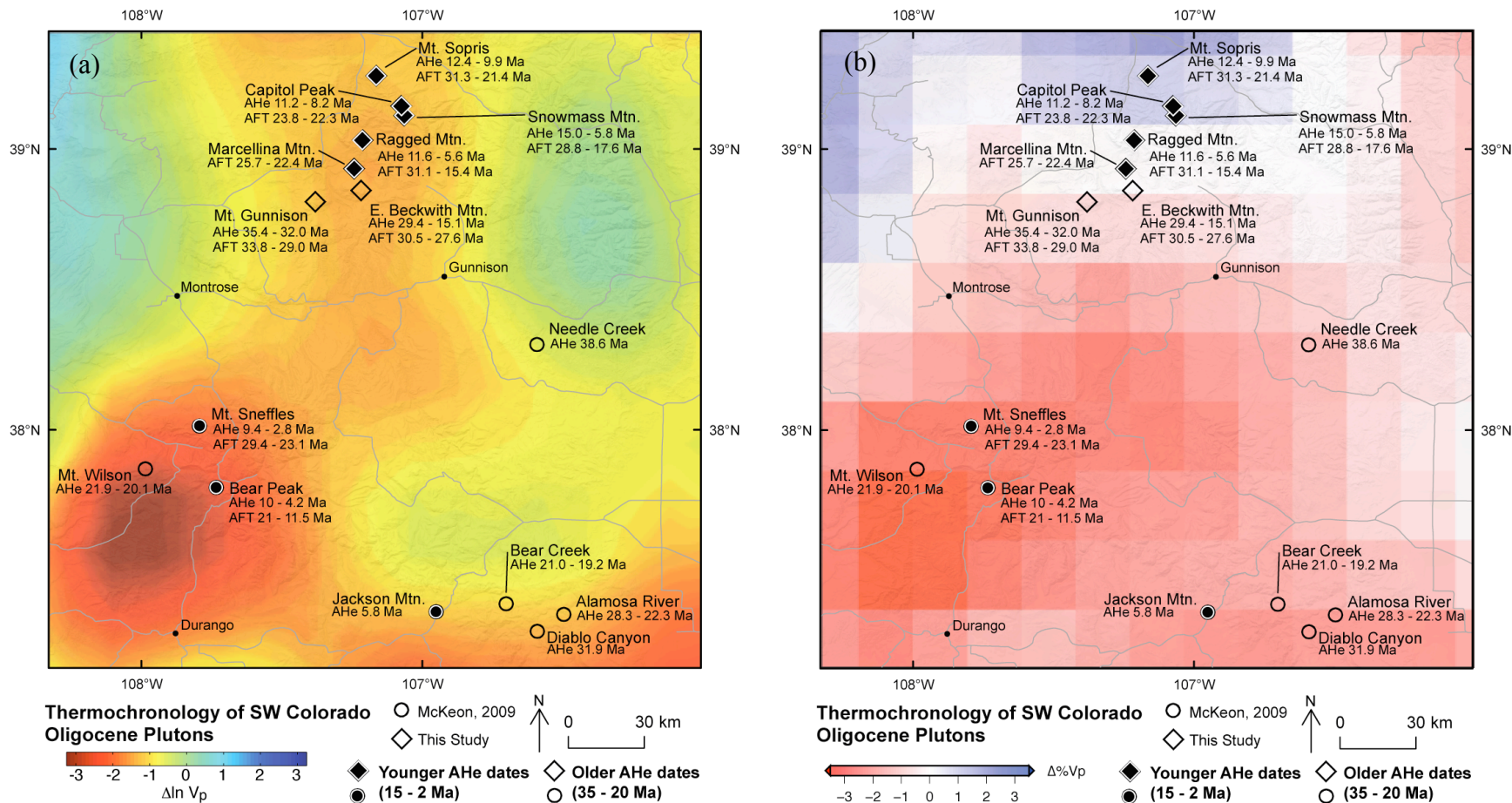


Figure 4.7: Thermochronology map of Oligocene plutons in the Elk, West Elk and San Juan Mountains. Both AFT and AHe data from this study and McKeon (2009) are mapped. (a) Tomography depth slice is at 100 km by McCarthy et al. (2010). (b) Tomography depth slice is a mean of 60 – 100 km by Schmandt and Humphreys (2010). Figure keyed to Table C.3.

Burbank (1941) proposed that northwest-trending fractures formed in this area during the Silverton caldera collapse and emplacement of part of the granitic Sneffels stock. These fractures were reopened and mineralized about 17 and 10.5 Ma ago and perhaps at other times as well. It is possible that McKeon (2009) dated some of these zones of mineralization and therefore is constraining the post-mineralization cooling history for Mount Sneffels and Bear Peak.

The AHe data in the Elk and West Elk Mountains can also be separated into two geographically and temporally distinct periods of cooling. The plutons in the southern part of the field area (West Elk Mountains) cooled between 34 – 15 Ma and the remaining northern plutons (Elk Mountains) cooled between 15 – 5 Ma (Figure 4.6). A regional pattern of cooling through the 60 – 70°C range includes an older episode in the West Elk Mountains and the eastern SJVF and a younger episode in the Elk Mountains and the western SJVF (Figure 4.7). The younger AHe dates, even those from areas with complicated middle Miocene mineralization and intrusive histories, may record regional scale late Miocene to Pliocene exhumation. AHe data from Mount Sopris, Capitol Peak and Ragged Mountain, when coupled with AHe data from the San Juan Mountains, record an exhumation history from 12 – 5 Ma that is perhaps related to the development of low velocity zones in the upper mantle currently observed beneath southwestern Colorado.

The Laramide AFT data (75 – 35 Ma) is mostly concentrated along the Front Range, with some additional point clusters in the southern part of the White River uplift, the Twin Lakes batholith and the Black Canyon of the Gunnison (Figure 4.8). The middle Cenozoic AFT ages follow along the trend of the CMB with the southernmost ages

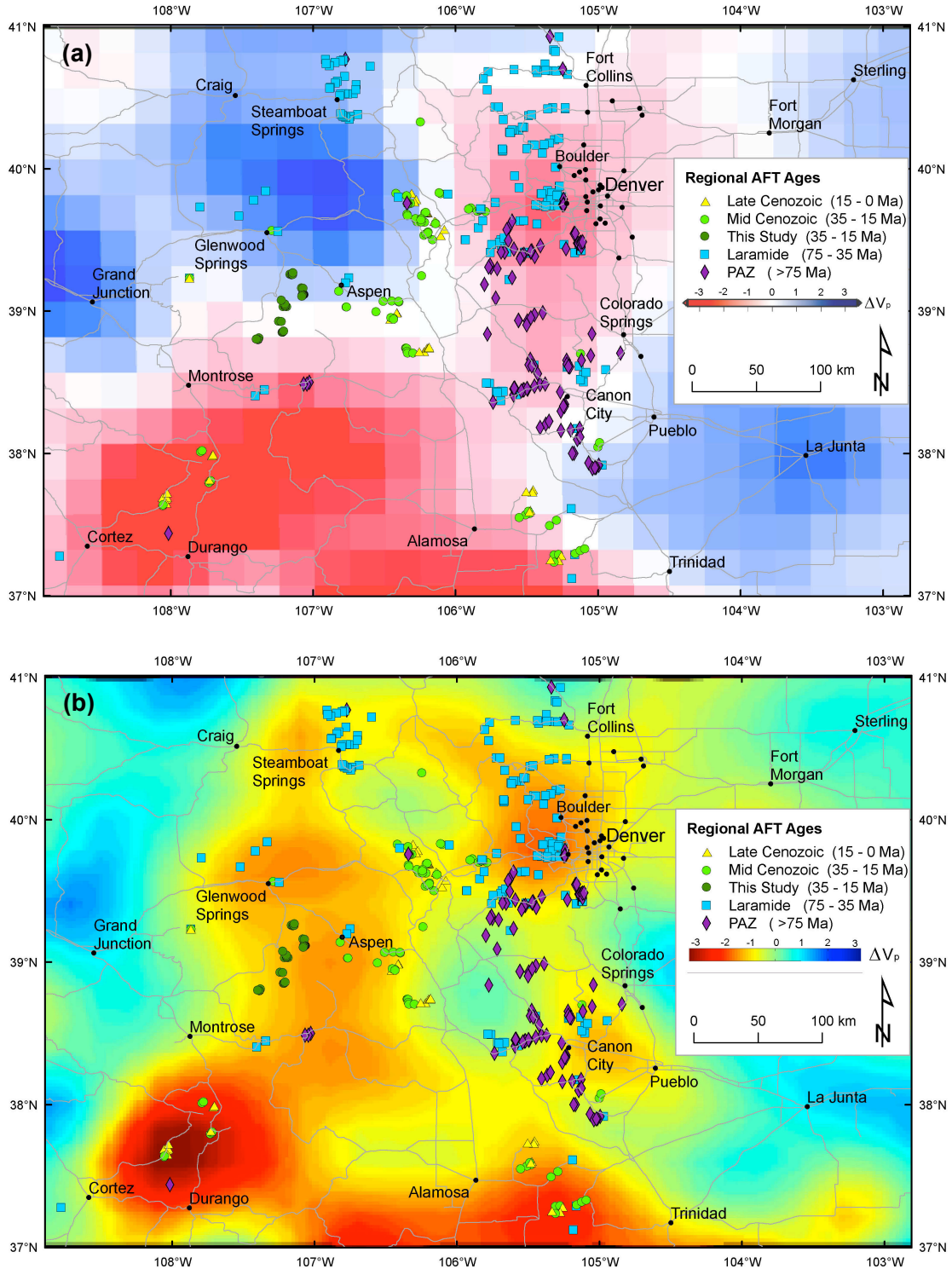


Figure 4.8: Regional AFT data with tomography map. (a) Tomography depth slice is at 100 km by McCarthy et al. (2010). (b) Tomography depth slice is a mean of 60 – 100 km by Schmandt and Humphreys (2010). Figure keyed to Table C.2.

occurring in the San Juan Mountains and the northernmost ages occurring in the Gore Range. The late Cenozoic AFT data follows a similar pattern as the middle Cenozoic ages but the data is constrained to the edges of the CMB. There are a number of AFT ages that are older than 75 Ma and located along the Front Range (purple diamond). These relatively old apatite ages are due to an extended stay in the partial annealing zone (PAZ) marking the Late Cretaceous 110°C isotherm (Kelley and Chapin, 2004).

The AFT data from this study fall within a transition zone in Figure 4.8a or in a zone of semi-low velocity in Figure 4.8b. Many of the AFT ages around the margin of the broad seismic velocity anomaly beneath SW Colorado, including those from this study, record middle to late Cenozoic cooling, with the exception of the data from the Laramide highland preserved along the Black Canyon of the Gunnison River. The AFT data above the San Juan Anomaly are also middle – late Cenozoic in age. Thus, the AFT ages in SW Colorado appear to record regional scale latest Eocene to middle Miocene cooling. In part, this trend is due to the fact that many samples from southwestern Colorado come from latest Eocene to Oligocene plutons, and consequently capture only that part of the cooling history. The timing of cooling derived from AFT samples in older Mesozoic, Paleozoic and Proterozoic rocks roughly coincides with the ignimbrite flare-up and might be related to relaxation of isotherms and exhumation associated with modification of the density structure of the crust and mantle caused by the voluminous eruptions in the San Juan and Elk volcanic fields (Roy et al., 2004; Farmer et al., 2008). The AFT data from surface samples in southwestern Colorado provide little information about the anomalous state of the current mantle, but these data might provide insights into past mantle conditions.

Thermochronology data and river incision rates from the CREST Project, along with AHe data from Sopris indicate acceleration in regional exhumation and uplift around (6 – 12 Ma) that is thought to be driven by mantle flow. An increase in exhumation rates from regional values of 40 – 85 m/Ma to 150 – 800 m/Ma begin around ~12 Ma (67 m/Ma to 199 m/Ma (Mt Sopris); 85 m/Ma to 876 m/Ma (Ragged Mountain)). Comparable cooling rates in the same time frame have been observed nearby in the MWX well in the Piceance Basin near Rifle, Colorado (~200 m/Ma; Kelley and Blackwell, 1990), and in a well at the south end of the Monument uplift in Utah (150 m/Ma; Hoffman et al., 2010). The extremely high rate from Ragged Mountain may be enhanced by isotherm relaxation following intrusion of the Crystal pluton ~12 Ma (Karlstrom et al., in review). River incision rates of ~50 to 150 m/Ma record the regional uplift driven by mantle flow over the last several million years. This amounts to 25 – 50% of the post-late Cretaceous uplift of the Colorado Plateau and Colorado Rocky Mountain regions that has occurred in the last 10 Ma.

CONCLUSION

The geo and thermochronologic study of the Elk and West Elk Mountains along with previous low temperature thermochronology studies of the region and newly modeled tomography gathered by the CREST project provided great insight into the Cenozoic history of southwest Colorado. The region experienced episodic magmatism beginning during the Laramide (~75 Ma) in the form of plutonism that occurred across the entire CMB. There were additional pulses from 65 – 56 Ma in the Twin Lakes Batholith (TLB) (Feldman, 2010) and the Front Range. After a period of magmatic quiescence, plutonism reinitiated in the TLB from 43 – 41 Ma (Feldman, 2010). Magmatism then stepped west to the Elk Range starting at ~35 Ma, then generally migrated southward, mirroring the southwestward younging of calderas in the SJVF. This time transgression in magmatism is most likely due to the subduction and rollback of the Farallon flat slab. Small volume 12 to 18 Ma mineralized granitic plutons emplaced in the area between the Elk and West Elk Mountains may be early indicators of the development of low-velocity, hot mantle beneath southwestern Colorado.

The AFT and AHe data from the Elk and West Elk plutons also provide key information about the cooling history of the area. Since the northern plutons in the field area were emplaced at greater depths than the southern plutons, cooling began in the south and at much greater rates. These southern plutons have similar cooling histories to those in the eastern SJVF (McKeon, 2009), while the plutons to the north have similar

histories to those in the western SJVF. There were also two episodes of cooling recorded in the data from this study: a more pronounced middle Cenozoic period from 25 – 15 Ma that can be seen in every pluton and a younger, Late Cenozoic period from 12 – 5 Ma that records exhumation at Mount Sopris, Capitol Peak, and Ragged Mountain. Additional thermochronology (exhumation rates of 150 – 800 m/Ma) and river incision rates (50 – 150 m/Ma over the last 10 million years) from the Crest project (Karlstrom et al., in review) also indicate onset of rapid regional exhumation and uplift around 6 – 12 Ma. The middle Cenozoic ages are perhaps recording the effects of changes in the thermal and density structure of the crust and mantle due to the voluminous magmatism during the ignimbrite flare-up. The late Cenozoic exhumation recorded in the AHe data is perhaps driven by the mantle convection created by anomalous low velocity mantle beneath southwestern Colorado.

APPENDIX A
GEOCHRONOLOGY DATA

Appendix A contains the raw data for the U/Pb zircon analysis and the data tables and incremental age spectra for the $^{40}\text{Ar}/^{39}\text{Ar}$ analyses. Table A.1 is a summary table of the U/Pb data collected at the Arizona LaserChron Center. Figure A.1 and Table A.2 pertain to the hornblende analysis; Figure A.2 pertains to a biotite – chloritized biotite experiment on sample 08Elk8; Figures A.3, A.4, A.5 and Table A.3 pertain to the biotite analyses; and Figure A.6 and Table A.4 pertain to the K-feldspar analyses.

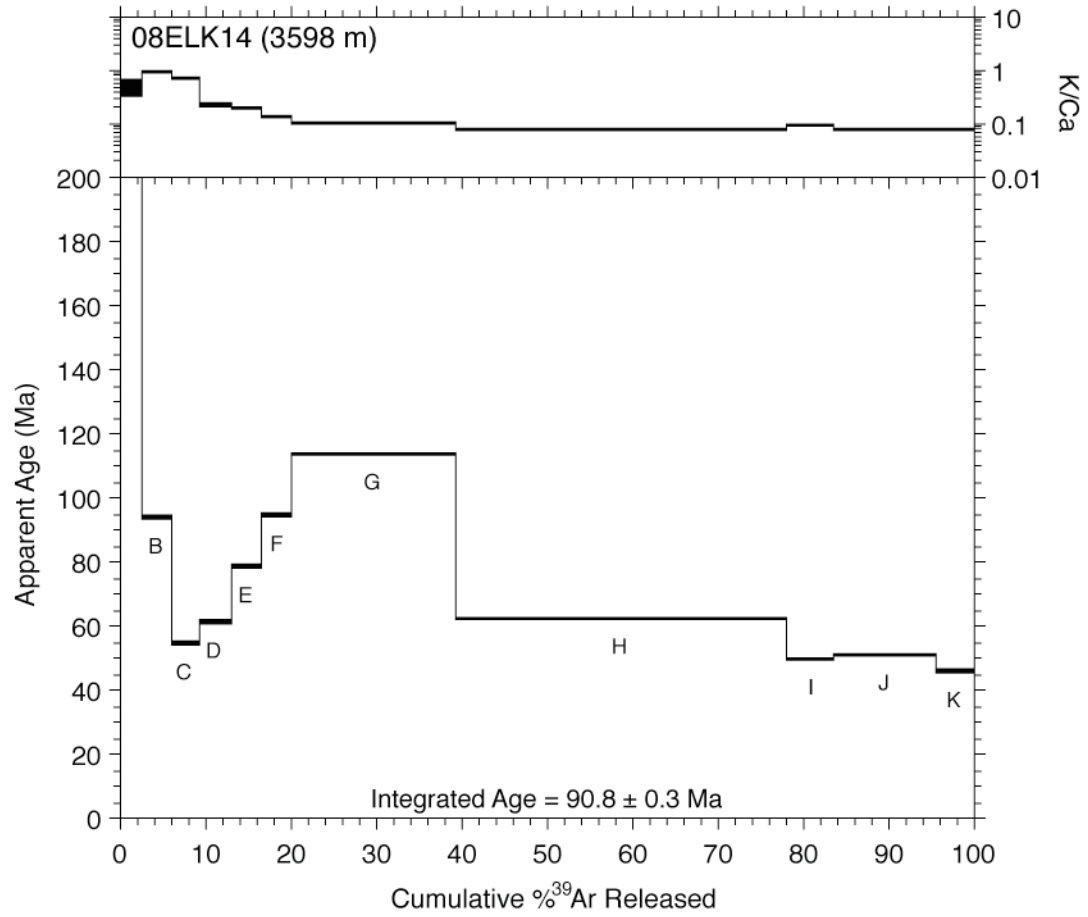


Figure A.1: $^{40}\text{Ar}/^{39}\text{Ar}$ hornblende spectrum for Snowmass Mountain.

Table A.2: Hornblende $^{40}\text{Ar}/^{39}\text{Ar}$ analytical data.

ID	Power (Watts)	$^{40}\text{Ar}/^{39}\text{Ar}$	$^{37}\text{Ar}/^{39}\text{Ar}$	$^{36}\text{Ar}/^{39}\text{Ar}$ ($\times 10^{-3}$)	$^{39}\text{Ar}_k$ ($\times 10^{-15}$ mol)	K/Ca	$^{40}\text{Ar}^*$ (%)	^{39}Ar (%)	Age (Ma)	$\pm 1\sigma$ (Ma)
08ELK14 , Hornblende, 17.96 mg, $J=0.0010059\pm 0.12\%$, $D=1.004\pm 0.001$, NM-222L, Lab#=58854-01										
A	900	805.7	1.062	1193.7	1.42	0.48	56.2	83.9	677.8	4.6
B	1000	70.04	0.5178	57.84	1.84	0.99	75.7	88.0	93.72	0.85
C	1050	40.78	0.7292	35.59	1.83	0.70	74.4	90.5	54.24	0.60
D	1080	40.74	2.268	23.16	2.08	0.22	83.7	92.1	60.90	0.60
E	1090	50.35	2.602	22.56	1.87	0.20	87.2	93.7	78.08	0.64
F	1100	58.55	3.959	18.80	1.91	0.13	91.1	95.0	94.51	0.62
G	1120	69.80	4.916	19.69	10.4	0.10	92.2	96.4	113.58	0.28
H	1180	37.07	6.406	9.917	21.0	0.080	93.5	97.1	62.12	0.14
I	1220	30.81	5.301	12.97	2.93	0.096	89.0	98.0	49.25	0.45
J	1260	30.46	6.678	9.986	6.48	0.076	92.1	98.7	50.45	0.25
K	1650	30.38	6.722	18.76	2.38	0.076	83.6	100.0	45.70	0.54
Integrated age $\pm 1\sigma$		n = 11		$\text{K}_2\text{O} = 1.15\%$	Age = 90.83 ± 0.25					

Notes:

Isotopic ratios corrected for blank, radioactive decay, and mass discrimination, not corrected for interfering reactions.
 Errors quoted for individual analyses include analytical error only, without interfering reaction or J uncertainties.
 Integrated age calculated by summing isotopic measurements of all steps.
 Integrated age error calculated by quadratically combining errors of isotopic measurements of all steps.
 Plateau age is inverse-variance-weighted mean of selected steps.
 Plateau age error is inverse-variance-weighted mean error (Taylor, 1982) times root MSWD where $\text{MSWD} > 1$.
 Plateau error is weighted error of Taylor (1982).
 Decay constants and isotopic abundances after Steiger and Jäger (1977).
 Weight percent K_2O calculated from ^{39}Ar signal, sample weight, and instrument sensitivity.
 Ages calculated relative to FC-2 Fish Canyon Tuff sanidine interlaboratory standard at 28.02 Ma (Renne et al., 1998).
 Decay Constant ($\text{LambdaK}(\text{total})$) = $5.543\text{e-}10/\text{a}$

Correction factors:

$$\begin{aligned}
 (^{39}\text{Ar}/^{37}\text{Ar})_{\text{Ca}} &= 0.0007 \pm 5\text{e-}05 \\
 (^{36}\text{Ar}/^{37}\text{Ar})_{\text{Ca}} &= 0.00028 \pm 2\text{e-}05 \\
 (^{38}\text{Ar}/^{39}\text{Ar})_k &= 0.013 \\
 (^{40}\text{Ar}/^{39}\text{Ar})_k &= 0.01 \pm 0.002
 \end{aligned}$$

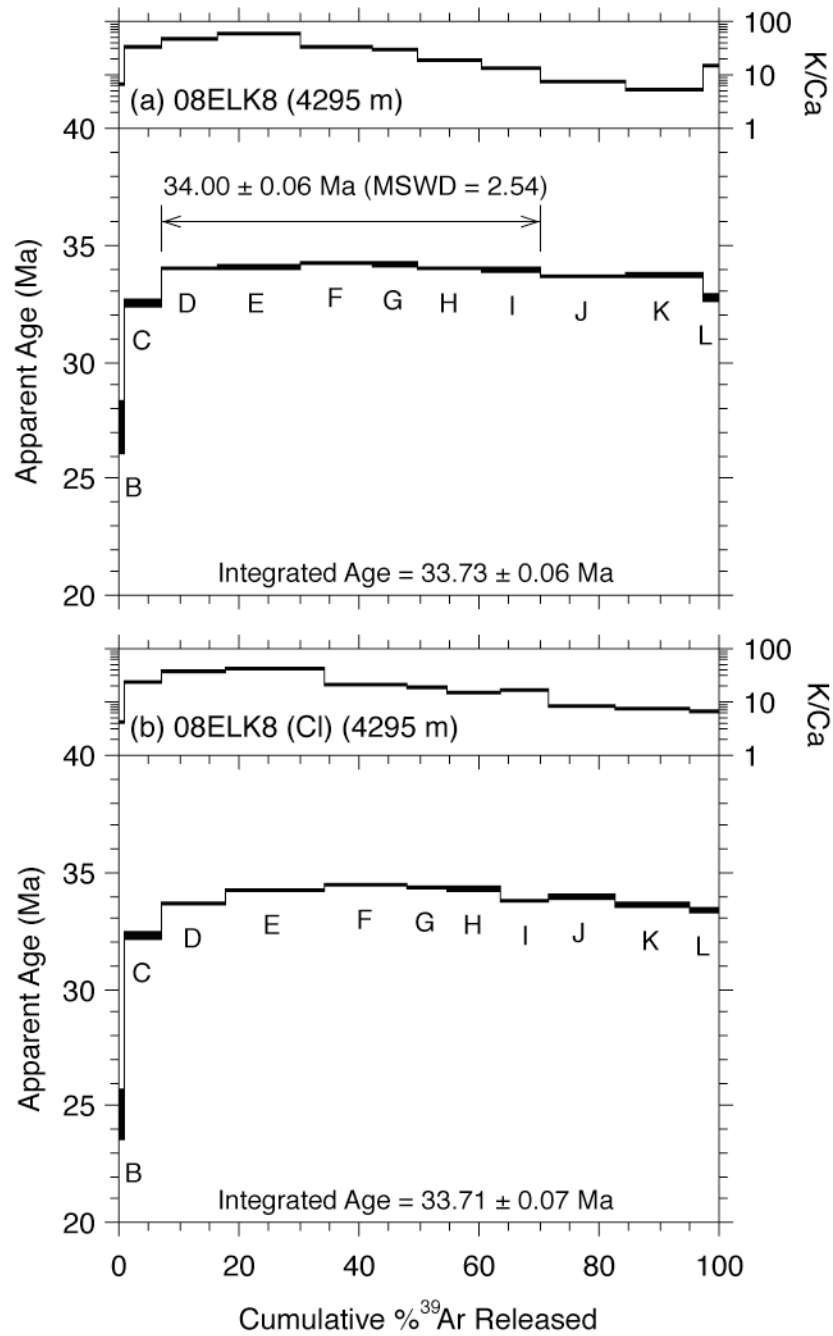


Figure A.2: $^{40}\text{Ar}/^{39}\text{Ar}$ biotite spectra for Snowmass Mountain for the biotite-chloritized biotite experiment on sample 08Elk08. (a) Visibly pristine biotite sample. (b) Visibly altered biotite sample.

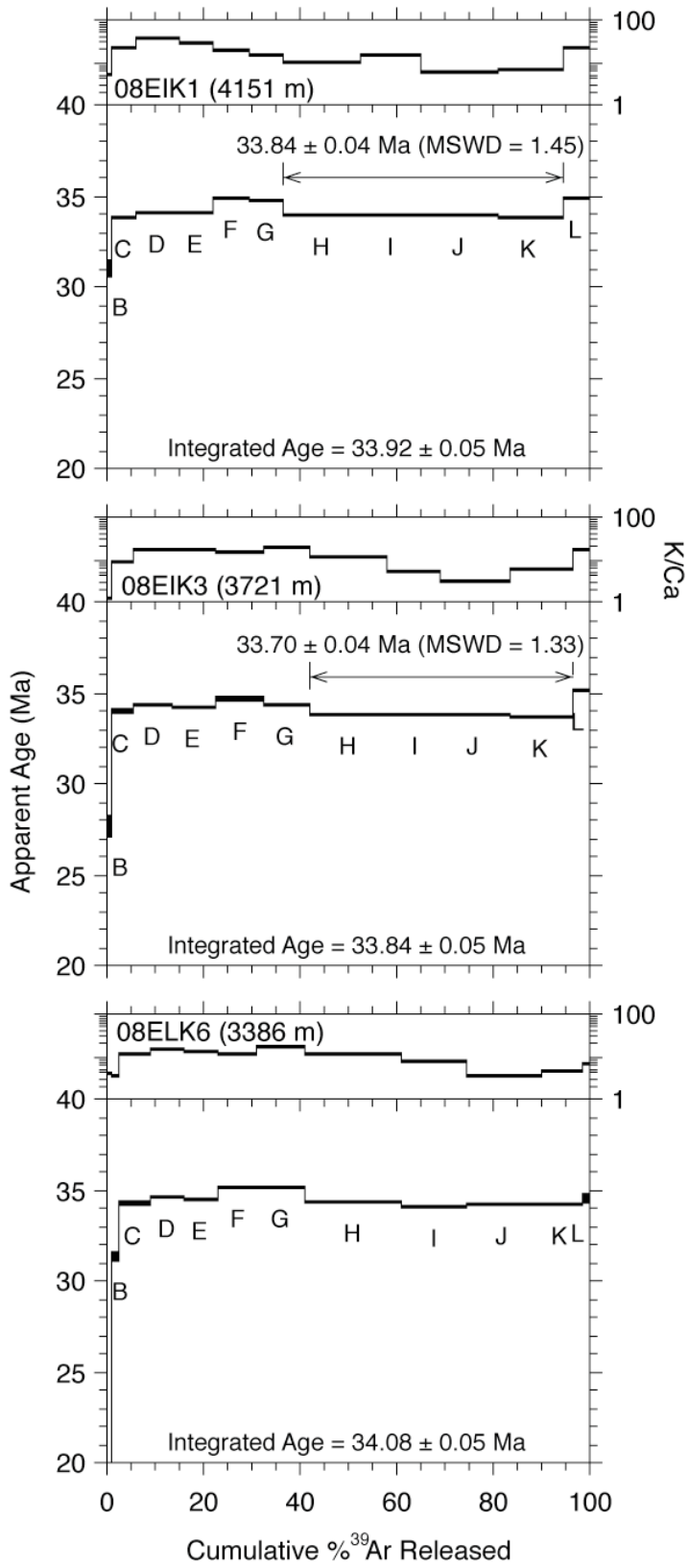


Figure A.3: $^{40}\text{Ar}/^{39}\text{Ar}$ biotite spectra for Capitol Peak.

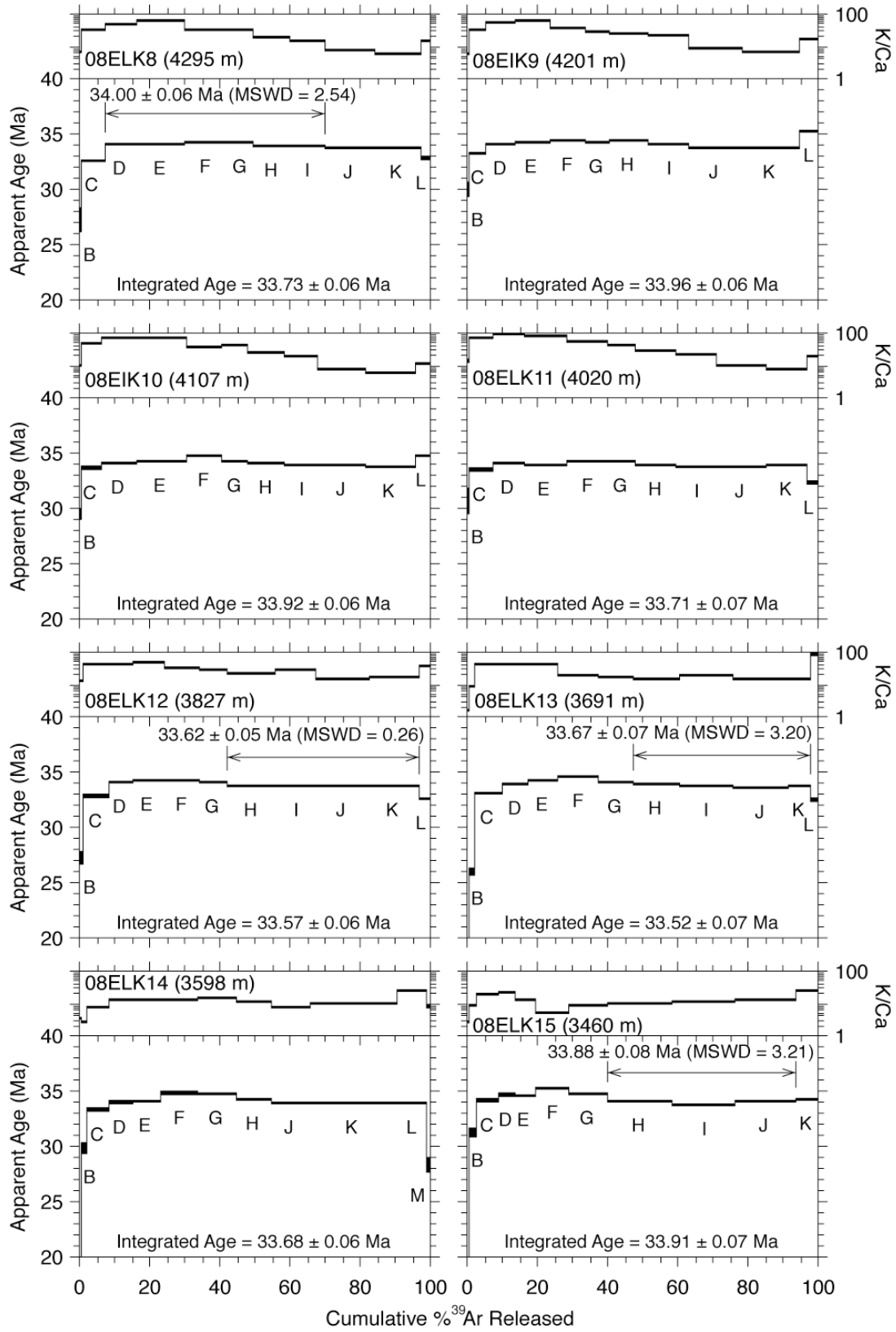


Figure A.4: $^{40}\text{Ar}/^{39}\text{Ar}$ biotite spectra for Snowmass Mountain.

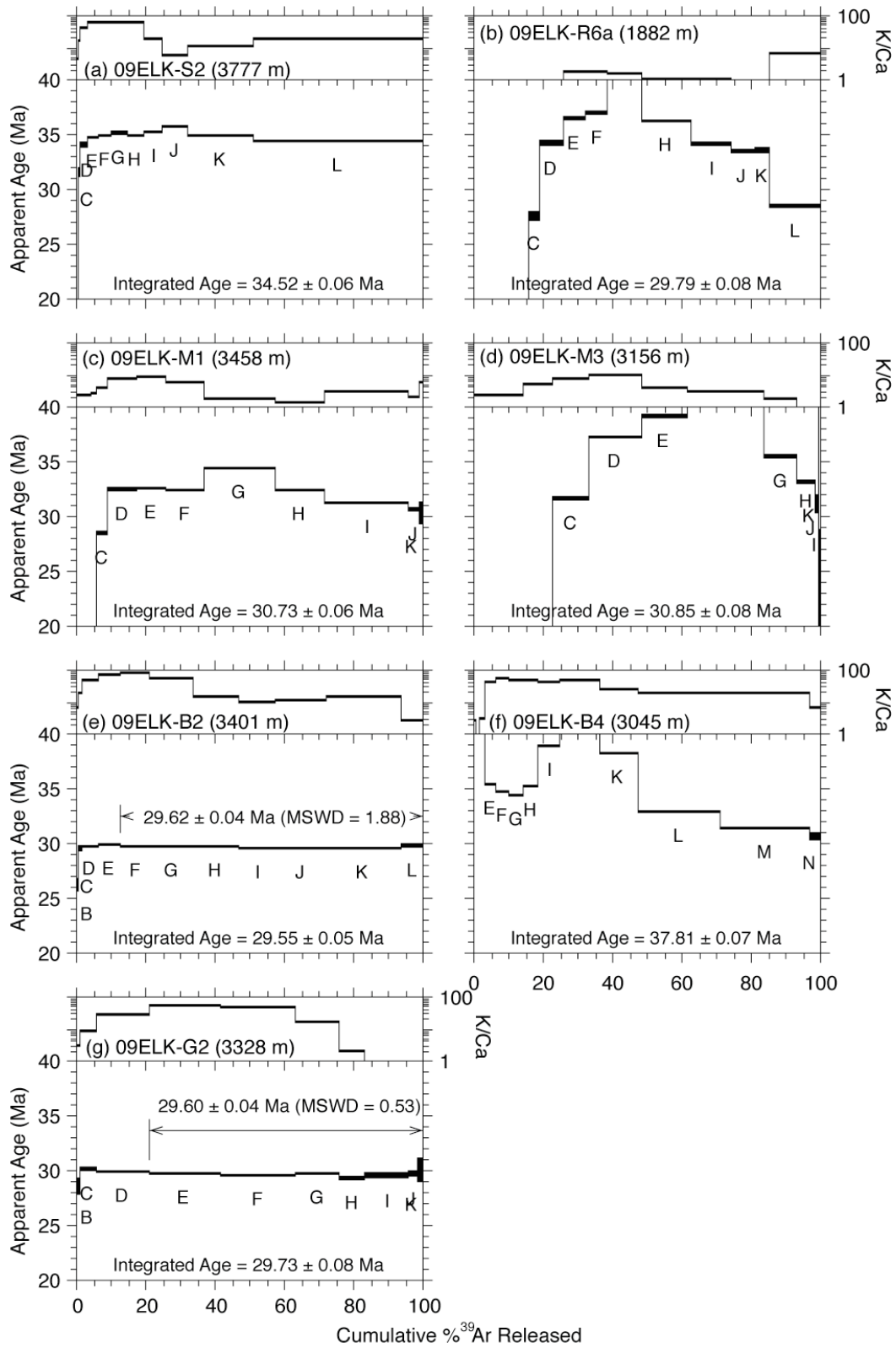


Figure A.5: $^{40}\text{Ar}/^{39}\text{Ar}$ biotite spectra from Mount Sopris (a), Ragged Mountain (b), Marcellina Mountain (c-d), E. Beckwith Mountain (e-f), and Mount Gunnison (g).

Table A.3: Biotite $^{40}\text{Ar}/^{39}\text{Ar}$ analytical data.

ID	Power (Watts)	$^{40}\text{Ar}/^{39}\text{Ar}$	$^{37}\text{Ar}/^{39}\text{Ar}$	$^{36}\text{Ar}/^{39}\text{Ar}$ ($\times 10^{-3}$)	$^{39}\text{Ar}_K$ ($\times 10^{-15}$ mol)	K/Ca	$^{40}\text{Ar}^*$ (%)	^{39}Ar (%)	Age (Ma)	$\pm 1\sigma$ (Ma)
09ELK-S2 , Biotite, 11.5 mg, J=0.0015976 \pm 0.07%, D=1.005 \pm 0.001, NM-2331, Lab#=59581-01										
X A	600	35.70	0.1742	111.9	0.849	2.9	7.4	0.2	7.6	1.4
X B	680	19.22	0.1076	48.36	2.25	4.7	25.7	0.8	14.15	0.59
X C	740	20.81	0.0305	33.12	2.89	16.7	52.9	1.5	31.46	0.44
X D	800	15.45	0.0121	12.00	7.90	42.1	77.0	3.4	33.97	0.20
X E	840	13.90	0.0085	5.906	12.6	59.8	87.4	6.6	34.66	0.11
X F	880	13.91	0.0083	5.737	14.8	61.5	87.8	10.3	34.85	0.11
X G	930	13.90	0.0084	5.421	18.5	60.6	88.5	14.8	35.09	0.10
X H	980	13.45	0.0084	4.126	19.5	60.8	90.9	19.7	34.895	0.087
X I	1040	14.28	0.0255	6.524	21.5	20.0	86.5	25.0	35.230	0.088
X J	1100	14.63	0.0818	7.231	29.4	6.2	85.4	32.3	35.642	0.097
X K	1200	13.28	0.0453	3.584	75.6	11.3	92.0	51.1	34.869	0.061
X L	1600	13.27	0.0250	4.077	197.0	20.4	90.9	100.0	34.430	0.054
Integrated age $\pm 1\sigma$			n = 12	$\text{K}_2\text{O} = 8.42\%$					Age = 34.520 \pm 0.06	
08EIK1 , Biotite, 10.08 mg, J=0.0011685 \pm 0.08%, D=1.004 \pm 0.001, NM-224L, Lab#=59015-01										
X A	650	51.79	0.1344	159.2	0.867	3.8	9.2	0.3	10.0	1.6
X B	750	25.96	0.1003	37.84	1.98	5.1	57.0	1.1	30.90	0.48
X C	850	19.06	0.0248	9.838	13.7	20.6	84.7	6.4	33.71	0.12
X D	920	17.02	0.0136	2.458	22.9	37.4	95.7	15.3	34.001	0.070
X E	1000	16.79	0.0188	1.637	18.0	27.1	97.1	22.3	34.025	0.068
X F	1075	17.39	0.0283	2.490	19.0	18.0	95.8	29.6	34.748	0.076
X G	1110	16.97	0.0344	1.319	18.2	14.8	97.7	36.7	34.601	0.077
H	1180	16.54	0.0518	0.9988	41.4	9.8	98.2	52.7	33.923	0.059
I	1210	16.43	0.0357	0.7996	32.6	14.3	98.6	65.3	33.802	0.062
J	1250	16.40	0.0919	0.6160	40.5	5.6	98.9	81.0	33.860	0.060
K	1300	16.31	0.0808	0.5006	36.0	6.3	99.1	95.0	33.758	0.059
X L	1680	17.13	0.0249	1.604	12.9	20.5	97.2	100.0	34.750	0.080
Integrated age $\pm 1\sigma$			n = 12	$\text{K}_2\text{O} = 8.41\%$					Age = 33.924 \pm 0.052	
Plateau $\pm 1\sigma$ steps H-K			n = 4	MSWD = 1.45					Age = 33.836 \pm 0.045	
08EIK3 , Biotite, 10.3 mg, J=0.0011686 \pm 0.08%, D=1.004 \pm 0.001, NM-224L, Lab#=59016-01										
X A	650	108.1	0.2551	354.6	0.936	2.0	3.1	0.4	7.0	1.4
X B	750	27.36	0.4138	47.99	2.22	1.2	48.3	1.2	27.63	0.56
X C	850	19.05	0.0606	9.406	12.0	8.4	85.4	5.7	33.97	0.12
X D	920	17.16	0.0313	2.498	21.1	16.3	95.7	13.8	34.286	0.071
X E	1000	16.83	0.0303	1.651	23.3	16.8	97.1	22.6	34.121	0.072
X F	1075	17.21	0.0355	2.161	26.5	14.4	96.3	32.7	34.590	0.076
X G	1110	16.78	0.0285	1.276	25.3	17.9	97.8	42.3	34.238	0.083
H	1180	16.51	0.0449	1.100	41.3	11.4	98.1	58.0	33.786	0.059
I	1210	16.37	0.0979	0.8052	29.9	5.2	98.6	69.4	33.688	0.063
J	1250	16.28	0.1654	0.5054	38.1	3.1	99.2	83.9	33.708	0.060
K	1300	16.21	0.0819	0.3735	34.3	6.2	99.4	97.0	33.619	0.060
X L	1680	17.44	0.0323	2.177	8.01	15.8	96.3	100.0	35.05	0.12
Integrated age $\pm 1\sigma$			n = 12	$\text{K}_2\text{O} = 8.39\%$					Age = 33.836 \pm 0.054	
Plateau $\pm 1\sigma$ steps H-K			n = 11	MSWD = 1.33					Age = 33.702 \pm 0.045	
08ELK6 , Biotite, 8.22 mg, J=0.0011544 \pm 0.07%, D=1.004 \pm 0.001, NM-224K, Lab#=59014-01										
X A	650	29.47	0.1269	86.74	1.99	4.0	13.0	1.0	7.97	0.63
X B	750	20.36	0.1443	17.63	3.10	3.5	74.5	2.6	31.29	0.29
X C	850	17.90	0.0435	4.434	13.1	11.7	92.7	9.3	34.220	0.097
X D	920	17.15	0.0357	1.351	14.0	14.3	97.7	16.4	34.529	0.088
X E	1000	17.05	0.0417	1.180	13.1	12.2	98.0	23.1	34.444	0.078
X F	1075	17.56	0.0430	1.870	16.5	11.9	96.9	31.5	35.073	0.072
X G	1110	17.35	0.0303	1.184	19.3	16.8	98.0	41.3	35.044	0.072
H	1180	16.89	0.0425	0.8234	39.1	12.0	98.6	61.1	34.335	0.062
I	1210	16.67	0.0673	0.6004	26.5	7.6	99.0	74.6	34.020	0.066
J	1250	16.67	0.1444	0.4255	31.1	3.5	99.3	90.4	34.140	0.064
K	1300	16.67	0.1113	0.4200	15.9	4.6	99.3	98.5	34.132	0.070

Table A.3 (continued)

ID	Power (Watts)	⁴⁰ Ar/ ³⁹ Ar	³⁷ Ar/ ³⁹ Ar	³⁶ Ar/ ³⁹ Ar (x 10 ⁻³)	³⁹ Ar _K (x 10 ⁻¹⁵ mol)	K/Ca	⁴⁰ Ar* (%)	³⁹ Ar (%)	Age (Ma)	±1σ (Ma)
X L	1680	20.33	0.0800	12.34	2.91	6.4	82.1	100.0	34.41	0.27
Integrated age ± 1σ			n = 12	K ₂ O = 7.96%	Age = 34.079 ± 0.051					
Plateau ± 1σ		steps H-K	n = 4	MSWD = 4.20	Age = 34.163 ± 0.071					
08ELK8 , Biotite, 7.07 mg, J=0.0010379±0.09%, D=1.0014±0.001, NM-222L, Lab#=58848-01										
X A	650	311.0	0.2677	979.4	0.315	1.9	7.0	0.2	40.0	5.0
X B	750	69.17	0.0753	184.6	1.37	6.8	21.1	0.9	27.2	1.1
X C	850	24.28	0.0166	22.92	11.7	30.8	72.1	7.5	32.49	0.15
D	920	19.35	0.0106	3.526	16.5	48.3	94.6	16.8	33.954	0.087
E	1000	18.87	0.0089	1.804	24.0	57.5	97.2	30.3	34.014	0.071
F	1075	19.09	0.0152	2.295	21.4	33.7	96.5	42.4	34.159	0.074
G	1110	18.79	0.0168	1.311	13.5	30.3	97.9	49.9	34.131	0.078
H	1180	18.71	0.0281	1.451	18.8	18.1	97.7	60.5	33.913	0.069
I	1210	18.56	0.0371	1.008	17.3	13.7	98.4	70.2	33.876	0.068
X J	1250	18.41	0.0712	0.9699	25.5	7.2	98.5	84.6	33.635	0.070
X K	1300	18.42	0.0923	0.9757	23.0	5.5	98.5	97.5	33.658	0.075
X L	1680	20.08	0.0344	8.338	4.47	14.8	87.7	100.0	32.70	0.19
Integrated age ± 1σ			n = 12	K ₂ O = 9.30%	Age = 33.735 ± 0.061					
Plateau ± 1σ		steps D-I	n = 6	MSWD = 2.54	Age = 34.002 ± 0.056					
08ELK8 , Chlorite Biotite, 9.77 mg, J=0.0010336±0.09%, D=1.0014±0.001, NM-222L, Lab#=58849-01										
X A	650	467.4	0.3505	1556.5	0.827	1.5	1.6	0.3	13.8	4.9
X B	750	99.85	0.1206	293.1	1.94	4.2	13.3	1.2	24.6	1.1
X C	850	30.07	0.0228	42.77	15.3	22.3	58.0	7.5	32.22	0.20
X D	920	19.38	0.0145	3.982	24.8	35.1	93.9	17.8	33.631	0.083
X E	1000	18.94	0.0129	1.474	40.0	39.5	97.7	34.5	34.190	0.059
X F	1075	19.28	0.0258	2.164	33.3	19.8	96.7	48.3	34.441	0.068
X G	1110	18.96	0.0265	1.366	15.9	19.2	97.9	54.9	34.286	0.077
X H	1180	19.05	0.0348	1.750	20.9	14.6	97.3	63.6	34.230	0.066
X I	1210	18.65	0.0306	1.328	19.3	16.7	97.9	71.7	33.732	0.072
X J	1250	18.60	0.0617	0.8763	27.4	8.3	98.6	83.1	33.884	0.076
X K	1300	18.40	0.0695	0.8460	29.3	7.3	98.7	95.2	33.542	0.063
X L	1680	19.02	0.0785	3.368	11.4	6.5	94.8	100.0	33.323	0.087
Integrated age ± 1σ			n = 12	K ₂ O = 9.14%	Age = 33.713 ± 0.071					
08ELK9 , Biotite, 10.12 mg, J=0.001168±0.11%, D=1.004±0.001, NM-224L, Lab#=59019-01										
X A	650	185.7	0.2166	604.3	0.400	2.4	3.8	0.2	15.0	3.6
X B	750	36.52	0.0942	75.18	1.49	5.4	39.2	0.7	29.88	0.70
X C	850	19.29	0.0171	11.52	12.3	29.9	82.4	5.5	33.15	0.11
X D	920	16.86	0.0095	1.930	21.9	53.8	96.6	14.0	33.977	0.066
X E	1000	16.62	0.0080	0.8770	25.9	63.8	98.4	24.0	34.121	0.068
X F	1075	16.82	0.0145	1.167	25.5	35.1	98.0	33.8	34.363	0.065
X G	1110	16.65	0.0188	0.8706	18.5	27.1	98.5	41.0	34.205	0.076
X H	1180	16.67	0.0219	0.7540	28.0	23.2	98.7	51.8	34.303	0.071
X I	1210	16.48	0.0242	0.6605	30.5	21.1	98.8	63.6	33.986	0.061
X J	1250	16.32	0.0583	0.5173	39.0	8.8	99.1	78.7	33.745	0.057
X K	1300	16.25	0.0730	0.4519	41.6	7.0	99.2	94.8	33.639	0.059
X L	1680	17.42	0.0292	1.894	13.5	17.5	96.8	100.0	35.166	0.084
Integrated age ± 1σ			n = 12	K ₂ O = 8.40%	Age = 33.963 ± 0.058					
08ELK10 , Biotite, 10.49 mg, J=0.0011676±0.13%, D=1.004±0.001, NM-224L, Lab#=59020-01										
X A	650	90.39	0.2666	297.6	0.775	1.9	2.7	0.3	5.2	1.9
X B	750	28.70	0.0510	49.37	1.98	10.0	49.2	1.0	29.46	0.48
X C	850	18.95	0.0114	9.698	16.1	44.9	84.9	6.8	33.56	0.10
X D	920	16.75	0.0072	1.498	26.6	70.8	97.4	16.5	34.016	0.065
X E	1000	16.62	0.0071	0.8112	39.9	72.0	98.6	30.9	34.160	0.061
X F	1075	16.99	0.0148	1.266	26.9	34.5	97.8	40.7	34.642	0.074
X G	1110	16.64	0.0127	0.8000	21.1	40.1	98.6	48.3	34.210	0.069
X H	1180	16.59	0.0194	0.8611	28.8	26.2	98.5	58.8	34.060	0.068

Table A.3 (continued)

ID	Power (Watts)	$^{40}\text{Ar}/^{39}\text{Ar}$	$^{37}\text{Ar}/^{39}\text{Ar}$	$^{36}\text{Ar}/^{39}\text{Ar}$ ($\times 10^{-3}$)	$^{39}\text{Ar}_K$ ($\times 10^{-15}$ mol)	K/Ca	$^{40}\text{Ar}^*$ (%)	^{39}Ar (%)	Age (Ma)	$\pm 1\sigma$ (Ma)
X I	1210	16.45	0.0259	0.6560	26.5	19.7	98.8	68.4	33.902	0.069
X J	1250	16.35	0.0686	0.5563	37.0	7.4	99.0	81.8	33.777	0.062
X K	1300	16.28	0.0884	0.3540	39.9	5.8	99.4	96.3	33.746	0.055
X L	1680	17.14	0.0465	1.786	10.3	11.0	96.9	100.0	34.644	0.098
Integrated age $\pm 1\sigma$		n = 12	$\text{K}_2\text{O} = 8.65\%$	Age = 33.919 ± 0.062						
08ELK11 , Biotite, 7 mg, $J=0.0010098\pm 0.12\%$, $D=1.0014\pm 0.001$, NM-222L, Lab#=58853-01										
X A	650	190.0	0.1329	628.4	0.341	3.8	2.3	0.2	7.8	3.2
X B	750	82.72	0.0379	222.7	1.48	13.5	20.5	1.0	30.6	1.1
X C	850	30.61	0.0079	40.96	12.4	64.6	60.5	7.7	33.41	0.20
X D	920	19.93	0.0061	3.796	16.0	84.3	94.4	16.4	33.944	0.078
X E	1000	19.13	0.0064	1.304	23.1	80.0	98.0	28.9	33.839	0.069
X F	1075	19.48	0.0094	1.917	21.3	54.4	97.1	40.5	34.130	0.078
X G	1110	19.40	0.0121	1.594	13.9	42.3	97.6	48.0	34.167	0.077
X H	1180	19.35	0.0188	2.101	22.0	27.1	96.8	59.9	33.803	0.069
X I	1210	19.20	0.0224	1.814	20.9	22.8	97.2	71.2	33.697	0.064
X J	1250	19.10	0.0534	1.577	26.6	9.6	97.6	85.6	33.645	0.074
X K	1300	19.05	0.0695	1.151	21.6	7.3	98.2	97.4	33.787	0.065
X L	1680	19.53	0.0268	5.557	4.86	19.0	91.6	100.0	32.30	0.17
Integrated age $\pm 1\sigma$		n = 12	$\text{K}_2\text{O} = 10.03\%$	Age = 33.708 ± 0.067						
08ELK12 , Biotite, 7.45 mg, $J=0.001018\pm 0.11\%$, $D=1.0014\pm 0.001$, NM-222L, Lab#=58851-01										
X A	650	116.4	0.1484	363.8	0.520	3.4	7.6	0.3	16.2	2.3
X B	750	41.31	0.0404	89.30	2.20	12.6	36.1	1.4	27.21	0.60
X C	850	22.44	0.0122	15.06	14.0	42.0	80.2	8.9	32.73	0.10
X D	920	19.73	0.0121	3.607	13.0	42.3	94.6	15.8	33.965	0.099
X E	1000	19.39	0.0109	2.086	16.4	46.6	96.8	24.5	34.150	0.080
X F	1075	19.71	0.0163	3.056	19.0	31.3	95.4	34.6	34.213	0.076
X G	1110	19.24	0.0193	1.806	14.2	26.5	97.2	42.2	34.030	0.077
H	1180	18.91	0.0245	1.493	25.6	20.8	97.7	55.8	33.615	0.072
I	1210	18.83	0.0192	1.237	22.0	26.6	98.1	67.5	33.602	0.066
J	1250	18.84	0.0328	1.137	29.3	15.5	98.2	83.1	33.680	0.074
K	1300	18.74	0.0315	0.9091	26.8	16.2	98.6	97.3	33.605	0.065
X L	1680	19.43	0.0144	5.345	5.02	35.5	91.9	100.0	32.49	0.16
Integrated age $\pm 1\sigma$		n = 12	$\text{K}_2\text{O} = 9.52\%$	Age = 33.567 ± 0.061						
Plateau $\pm 1\sigma$ steps H-K		n = 4	MSWD = 0.26	Age = 33.623 ± 0.05						
08ELK13 , Biotite, 10.7 mg, $J=0.0010171\pm 0.14\%$, $D=1.0014\pm 0.001$, NM-222M, Lab#=58864-01										
X A	650	70.30	0.3183	220.6	1.90	1.6	7.3	0.6	9.40	0.96
X B	750	35.39	0.0627	71.64	4.60	8.1	40.2	2.1	25.91	0.36
X C	850	20.93	0.0118	9.431	25.4	43.1	86.7	10.4	32.981	0.086
X D	920	19.88	0.0121	4.205	21.6	42.2	93.8	17.4	33.872	0.081
X E	1000	19.55	0.0119	2.578	26.9	42.7	96.1	26.2	34.147	0.078
X F	1075	20.14	0.0271	3.800	34.6	18.8	94.4	37.5	34.575	0.069
X G	1110	19.13	0.0290	1.343	31.0	17.6	97.9	47.6	34.059	0.065
H	1180	18.88	0.0351	1.021	40.1	14.5	98.4	60.7	33.772	0.062
I	1210	18.76	0.0268	0.6744	47.1	19.1	98.9	76.0	33.739	0.060
J	1250	18.62	0.0346	0.5905	48.8	14.7	99.1	92.0	33.531	0.064
K	1300	18.70	0.0366	0.7464	19.6	13.9	98.8	98.4	33.609	0.069
X L	1680	19.84	0.0060	6.729	4.99	85.0	90.0	100.0	32.46	0.18
Integrated age $\pm 1\sigma$		n = 12	$\text{K}_2\text{O} = 10.82\%$	Age = 33.524 ± 0.066						
Plateau $\pm 1\sigma$ steps H-K		n = 4	MSWD = 3.20	Age = 33.669 ± 0.073						

Table A.3 (continued)

ID	Power (Watts)	$^{40}\text{Ar}/^{39}\text{Ar}$	$^{37}\text{Ar}/^{39}\text{Ar}$	$^{36}\text{Ar}/^{39}\text{Ar}$ ($\times 10^{-3}$)	$^{39}\text{Ar}_K$ ($\times 10^{-15}$ mol)	K/Ca	$^{40}\text{Ar}^*$ (%)	^{39}Ar (%)	Age (Ma)	$\pm 1\sigma$ (Ma)
08ELK14 , Biotite, 5.45 mg, J=0.001013 \pm 0.10%, D=1.0014 \pm 0.001, NM-222M, Lab#=58865-01										
X A	650	82.14	0.1618	268.0	1.09	3.2	3.6	0.9	5.4	1.4
X B	750	32.85	0.1870	55.70	1.59	2.7	49.9	2.1	29.74	0.51
X C	850	22.01	0.0632	12.52	8.31	8.1	83.2	8.8	33.17	0.16
X D	920	20.33	0.0405	5.432	8.41	12.6	92.1	15.5	33.91	0.11
X E	1000	20.33	0.0404	5.350	10.1	12.6	92.2	23.6	33.95	0.10
X F	1075	20.77	0.0399	5.335	13.3	12.8	92.4	34.1	34.745	0.092
X G	1110	19.72	0.0346	1.803	13.3	14.8	97.3	44.8	34.734	0.082
X H	1180	19.23	0.0447	1.374	13.0	11.4	97.9	55.2	34.094	0.081
X J	1210	18.89	0.0673	0.8176	13.6	7.6	98.8	66.0	33.766	0.082
X K	1250	18.86	0.0528	0.5593	31.2	9.7	99.1	90.9	33.849	0.067
X L	1300	18.83	0.0199	0.5860	10.4	25.6	99.1	99.2	33.777	0.094
X M	1680	23.98	0.0661	28.42	0.945	7.7	65.0	100.0	28.27	0.71
Integrated age $\pm 1\sigma$		n = 12		K ₂ O = 8.72%		Age = 33.675 \pm 0.064				
08ELK15 , Biotite, 6.15 mg, J=0.001024 \pm 0.08%, D=1.0014 \pm 0.001, NM-222M, Lab#=58866-01										
X A	650	108.8	0.1857	348.8	1.37	2.7	5.3	1.0	10.6	1.5
X B	750	34.20	0.0577	58.09	2.91	8.8	49.8	3.1	31.22	0.44
X C	850	24.19	0.0261	18.95	8.40	19.5	76.9	9.1	34.03	0.16
X D	920	22.01	0.0248	10.41	6.63	20.6	86.0	13.9	34.64	0.15
X E	1000	21.08	0.0389	7.480	7.92	13.1	89.5	19.6	34.53	0.12
X F	1075	21.99	0.0959	9.382	13.0	5.3	87.4	28.9	35.177	0.095
X G	1110	19.75	0.0581	2.807	15.2	8.8	95.8	39.9	34.634	0.085
X H	1180	18.95	0.0517	1.404	25.0	9.9	97.8	57.9	33.932	0.071
X I	1210	18.68	0.0457	0.8372	24.2	11.2	98.7	75.3	33.750	0.068
X J	1250	18.71	0.0414	0.4695	24.1	12.3	99.3	92.6	33.991	0.074
X K	1300	18.86	0.0214	0.6314	8.13	23.9	99.0	98.5	34.18	0.10
X L	1680	21.76	0.0205	12.75	2.15	24.8	82.7	100.0	32.93	0.32
Integrated age $\pm 1\sigma$		n = 12		K ₂ O=8.47%		Age = 33.891 \pm 0.066				
Plateau $\pm 1\sigma$ steps H-J		n = 3		MSWD = 3.21		Age = 33.884 \pm 0.078				
09ELK-R6a , Biotite, 5.89 mg, J=0.0016383 \pm 0.07%, D=1.005 \pm 0.001, NM-233C, Lab#=59551-01										
X A	650	5.208	0.5182	15.09	12.0	0.98	15.0	12.1	2.31	0.14
X B	740	18.52	1.294	41.63	4.10	0.39	34.1	16.2	18.60	0.48
X C	800	12.69	1.379	11.67	3.15	0.37	73.7	19.4	27.44	0.40
X D	880	13.02	0.7694	4.777	6.71	0.66	89.6	26.1	34.17	0.23
X E	930	12.87	0.2897	1.485	6.32	1.8	96.8	32.4	36.43	0.21
X F	980	13.65	0.2960	3.554	5.95	1.7	92.5	38.4	36.92	0.21
X G	1040	14.82	0.3184	3.565	10.4	1.6	93.1	48.9	40.28	0.15
X H	1100	13.11	0.4647	2.684	13.9	1.1	94.2	62.8	36.13	0.12
X I	1150	12.19	0.4890	1.932	11.4	1.0	95.6	74.2	34.13	0.13
X J	1200	11.99	1.349	2.317	7.13	0.38	95.2	81.4	33.43	0.17
X K	1250	12.50	0.8056	3.717	3.99	0.63	91.7	85.4	33.57	0.26
X L	1600	14.90	0.0793	17.68	14.5	6.4	65.0	100.0	28.38	0.18
Integrated age $\pm 1\sigma$		n = 12		K ₂ O = 3.96%		Age = 29.792 \pm 0.081				
09ELK-M1 , Biotite, 13.4 mg, J=0.0016054 \pm 0.05%, D=1.005 \pm 0.001, NM-233I, Lab#=59585-01										
X A	650	9.663	0.2282	28.81	14.1	2.2	12.0	4.7	3.35	0.19
X B	700	14.26	0.1937	27.96	4.28	2.6	42.1	6.1	17.30	0.34
X C	800	14.29	0.1299	14.89	9.03	3.9	69.3	9.1	28.42	0.20
X D	900	13.38	0.0694	7.071	25.8	7.3	84.4	17.6	32.406	0.095

Table A.3 (continued)

ID	Power (Watts)	⁴⁰ Ar/ ³⁹ Ar	³⁷ Ar/ ³⁹ Ar	³⁶ Ar/ ³⁹ Ar (x 10 ⁻³)	³⁹ Ar _K (x 10 ⁻¹⁵ mol)	K/Ca	⁴⁰ Ar* (%)	³⁹ Ar (%)	Age (Ma)	±1σ (Ma)
X E	950	11.91	0.0598	1.893	25.3	8.5	95.3	26.0	32.558	0.081
X F	1000	12.16	0.0891	2.954	32.6	5.7	92.9	36.9	32.391	0.068
X G	1100	13.04	0.3002	3.747	62.1	1.7	91.7	57.5	34.288	0.064
X H	1150	11.87	0.3593	2.197	42.9	1.4	94.8	71.8	32.271	0.061
X I	1200	11.19	0.1570	1.153	73.6	3.2	97.1	96.2	31.158	0.049
X J	1250	11.55	0.2342	3.147	9.03	2.2	92.1	99.2	30.52	0.16
X K	1600	57.38	0.0922	158.6	2.30	5.5	18.3	100.0	30.2	1.0
Integrated age ± 1σ			n = 11	K ₂ O = 5.38%	Age = 30.728 ± 0.057					
09ELK-M3 , Biotite, 8.4 mg, J=0.0015999±0.06%, D=1.005±0.001, NM-233I, Lab#=59586-01										
X A	650	6.187	0.2268	19.22	17.4	2.2	8.3	14.5	1.49	0.15
X B	750	11.84	0.1048	22.37	10.2	4.9	44.2	22.9	15.04	0.21
X C	850	12.95	0.0679	6.435	12.5	7.5	85.3	33.3	31.60	0.15
X D	920	13.71	0.0499	2.265	18.2	10.2	95.1	48.5	37.229	0.095
X E	1000	15.09	0.1312	4.720	16.1	3.9	90.8	62.0	39.10	0.11
X F	1100	16.67	0.1618	4.399	26.2	3.2	92.3	83.8	43.837	0.100
X G	1150	13.04	0.2771	2.257	11.6	1.8	95.1	93.5	35.40	0.15
X H	1200	12.46	0.6271	3.249	6.19	0.81	92.7	98.7	33.04	0.19
X I	1250	16.19	0.6998	18.28	1.13	0.73	67.0	99.6	31.02	0.84
X J	1300	42.54	0.6111	101.5	0.223	0.83	29.6	99.8	36.0	4.5
X K	1600	338.4	0.8342	1121.8	0.265	0.61	2.1	100.0	20.0	8.7
Integrated age ± 1σ			n = 11	K ₂ O = 3.43%	Age = 30.854 ± 0.082					
09ELK-B2 , Biotite, 11.7 mg, J=0.0016065±0.09%, D=1.005±0.001, NM-233I, Lab#=59583-02										
X A	650	23.50	0.0848	69.17	1.18	6.0	13.0	0.3	8.84	0.98
X B	740	20.19	0.0739	37.51	1.83	6.9	45.1	0.7	26.19	0.63
X C	800	15.74	0.0286	18.52	4.64	17.9	65.2	1.8	29.50	0.27
X D	880	12.65	0.0110	7.827	20.3	46.5	81.7	6.7	29.700	0.098
X E	930	11.25	0.0071	2.856	25.6	72.0	92.5	12.7	29.890	0.070
F	980	10.73	0.0061	1.315	35.0	84.1	96.4	21.1	29.694	0.055
G	1040	10.67	0.0090	1.122	55.2	56.9	96.9	34.2	29.678	0.047
H	1100	10.77	0.0364	1.514	55.3	14.0	95.9	47.3	29.658	0.051
I	1150	11.06	0.0485	2.642	42.3	10.5	93.0	57.4	29.530	0.058
J	1200	11.36	0.0474	3.601	62.3	10.8	90.7	72.2	29.589	0.059
K	1250	11.27	0.0367	3.353	92.5	13.9	91.2	94.2	29.519	0.050
X L	1600	14.71	0.1887	14.82	24.4	2.7	70.3	100.0	29.72	0.12
Integrated age ± 1σ			n = 12	K ₂ O = 8.59%	Age = 29.556 ± 0.053					
Plateau ± 1σ steps F-K			n = 6	MSWD = 2.11	Age = 29.615 ± 0.042					
09ELK-B4 , Biotite, 9.5 mg, J=0.0016088±0.09%, D=1.005±0.001, NM-233I, Lab#=59584-01										
X A	600	68.03	0.1922	61.67	2.22	2.7	73.2	0.7	139.10	0.87
X B	680	100.2	3.019	79.12	1.55	0.17	76.9	1.1	211.4	1.2
X C	740	90.75	5.013	55.43	2.08	0.10	82.4	1.8	205.6	1.0
X D	800	17.19	0.1607	9.283	5.70	3.2	84.1	3.5	41.47	0.21
X E	840	13.49	0.0123	4.036	9.91	41.3	91.2	6.5	35.30	0.12
X F	880	12.79	0.0099	2.388	12.7	51.5	94.5	10.3	34.704	0.099
X G	930	12.51	0.0108	1.872	13.8	47.4	95.6	14.4	34.352	0.094
X H	980	12.74	0.0115	1.708	13.9	44.5	96.0	18.6	35.137	0.095
X I	1040	14.33	0.0123	2.743	21.2	41.5	94.3	25.0	38.802	0.076
X J	1100	16.19	0.0111	3.179	38.6	46.1	94.2	36.5	43.692	0.078
X K	1150	14.03	0.0193	2.492	36.0	26.5	94.8	47.4	38.142	0.081

Table A.3 (continued)

ID	Power (Watts)	⁴⁰ Ar/ ³⁹ Ar	³⁷ Ar/ ³⁹ Ar	³⁶ Ar/ ³⁹ Ar (x 10 ⁻³)	³⁹ Ar _K (x 10 ⁻¹⁵ mol)	K/Ca	⁴⁰ Ar* (%)	³⁹ Ar (%)	Age (Ma)	±1σ (Ma)
X L	1200	11.80	0.0264	1.175	80.3	19.3	97.1	71.5	32.928	0.047
X M	1250	11.19	0.0274	0.9722	85.1	18.6	97.5	97.1	31.346	0.044
X N	1600	25.74	0.0751	51.17	9.75	6.8	41.3	100.0	30.55	0.33
Integrated age ± 1σ		n = 14	K ₂ O = 8.36%		Age = 37.812 ± 0.066					
09ELK-G2 , Biotite, 7.3 mg, J=0.001601±0.07%, D=1.005±0.001, NM-233I, Lab#=59582-02										
X A	650	69.46	0.2733	178.5	1.00	1.9	24.1	0.5	47.7	1.6
X B	750	17.03	0.1745	24.00	1.32	2.9	58.4	1.2	28.49	0.69
C	880	12.19	0.0627	5.657	9.56	8.1	86.3	6.0	30.12	0.13
D	980	11.02	0.0191	1.975	29.8	26.7	94.7	21.2	29.867	0.059
E	1040	10.82	0.0093	1.603	40.1	54.7	95.6	41.6	29.626	0.055
F	1100	10.99	0.0107	2.182	43.0	47.6	94.1	63.5	29.603	0.056
G	1150	11.97	0.0307	5.513	24.4	16.6	86.4	75.9	29.605	0.082
H	1200	18.64	0.2346	28.55	14.5	2.2	54.8	83.3	29.28	0.20
I	1250	22.31	1.028	40.89	25.0	0.50	46.2	96.0	29.54	0.21
X J	1300	19.29	1.281	30.56	5.23	0.40	53.7	98.6	29.69	0.29
X K	1600	62.51	0.7200	176.3	2.71	0.71	16.7	100.0	30.0	1.0
Integrated age ± 1σ		n = 11	K ₂ O = 6.46%		Age = 29.733 ± 0.084					
Plateau ± 1σ		steps C-I	n = 7	MSWD = 4.86		Age = 29.690 ± 0.067				

Notes:

Isotopic ratios corrected for blank, radioactive decay, and mass discrimination, not corrected for interfering reactions.

Errors quoted for individual analyses include analytical error only, without interfering reaction or J uncertainties.

Integrated age calculated by summing isotopic measurements of all steps.

Integrated age error calculated by quadratically combining errors of isotopic measurements of all steps.

Plateau age is inverse-variance-weighted mean of selected steps.

Plateau age error is inverse-variance-weighted mean error (Taylor, 1982) times root MSWD where MSWD>1.

Plateau error is weighted error of Taylor (1982).

Decay constants and isotopic abundances after Steiger and Jäger (1977).

X symbol preceding sample ID denotes analyses excluded from plateau age calculations.

Weight percent K₂O calculated from ³⁹Ar signal, sample weight, and instrument sensitivity.

Ages calculated relative to FC-2 Fish Canyon Tuff sanidine interlaboratory standard at 28.02 Ma (Renne et al., 1998).

Decay Constant (LambdaK (total)) = 5.543e-10/a

Correction factors:

$$(^{39}\text{Ar}/^{37}\text{Ar})_{\text{Ca}} = 0.0007 \pm 5\text{e-}05$$

$$(^{36}\text{Ar}/^{37}\text{Ar})_{\text{Ca}} = 0.00028 \pm 2\text{e-}05$$

$$(^{38}\text{Ar}/^{39}\text{Ar})_{\text{K}} = 0.013$$

$$(^{40}\text{Ar}/^{39}\text{Ar})_{\text{K}} = 0.01 \pm 0.002$$

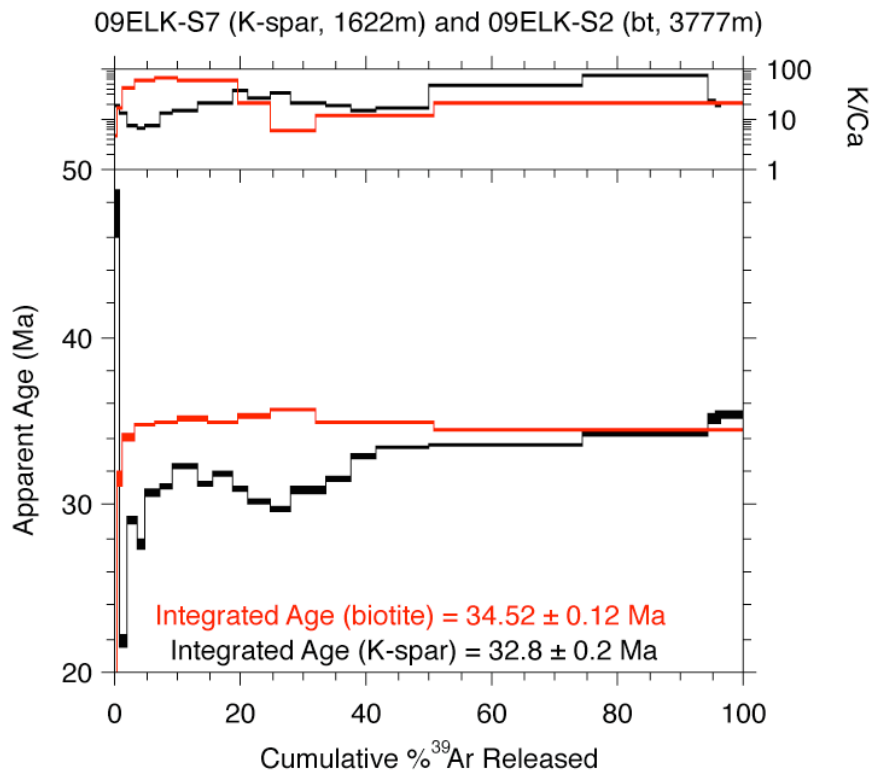
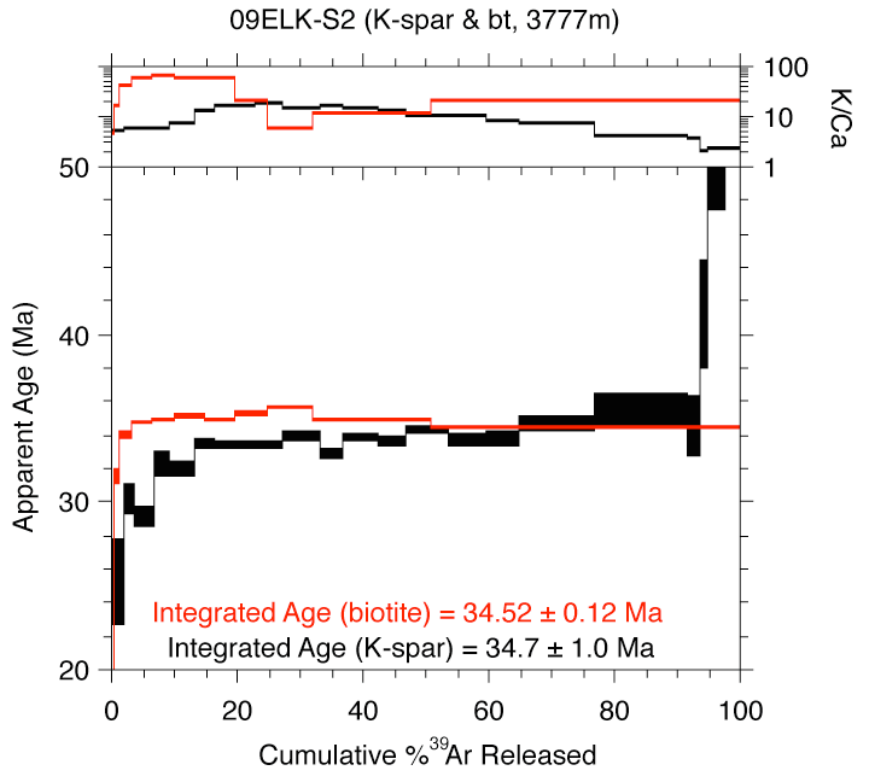


Figure A.6: $^{40}\text{Ar}/^{39}\text{Ar}$ K-Feldspar spectra that was too complicated to provide good age data.

Table A.4: $^{40}\text{Ar}/^{39}\text{Ar}$ K-Feldspar analytical data.

ID	Power (Watts)	$^{40}\text{Ar}/^{39}\text{Ar}$	$^{37}\text{Ar}/^{39}\text{Ar}$	$^{36}\text{Ar}/^{39}\text{Ar}$ (x 10^{-3})	$^{39}\text{Ar}_k$ (x 10^{-15} mol)	K/Ca	$^{40}\text{Ar}^*$ (%)	^{39}Ar (%)	Age (Ma)	$\pm 1\sigma$ (Ma)
09ELK-S2 , K-Feldspar, 7.26 mg, J=0.0016155±0.08%, D=1.005±0.001, NM-233H, Lab#=59624-01										
X G	550	179.9	0.0971	579.5	2.62	5.3	4.8	2.1	25.2	2.6
X H	550	56.74	0.0924	156.8	2.17	5.5	18.3	3.9	30.08	0.93
X I	625	38.81	0.0908	97.29	3.77	5.6	25.9	6.9	29.08	0.61
X J	625	26.25	0.0865	51.06	2.94	5.9	42.5	9.3	32.24	0.73
X K	700	29.19	0.0681	61.41	4.98	7.5	37.8	13.3	31.90	0.43
X L	700	17.87	0.0386	21.26	4.13	13.2	64.8	16.6	33.43	0.27
X M	800	19.23	0.0317	25.99	7.96	16.1	60.1	23.0	33.34	0.24
X N	800	14.03	0.0287	8.438	5.33	17.8	82.2	27.3	33.31	0.22
X O	900	21.82	0.0337	34.05	7.60	15.1	53.9	33.4	33.93	0.30
X P	900	15.97	0.0301	15.56	4.48	17.0	71.2	37.0	32.82	0.26
X Q	1000	18.83	0.0363	24.09	6.98	14.0	62.2	42.7	33.80	0.25
X R	1000	18.67	0.0407	23.85	5.42	12.5	62.3	47.0	33.55	0.27
X S	1075	22.59	0.0469	36.32	8.65	10.9	52.5	54.0	34.21	0.26
X T	1075	26.81	0.0502	51.21	7.15	10.2	43.6	59.7	33.71	0.39
X U	1120	31.71	0.0586	67.72	6.57	8.7	36.9	65.0	33.76	0.44
X V	1160	41.19	0.0679	98.80	14.9	7.5	29.1	77.0	34.60	0.46
X W	1200	93.91	0.1172	276.2	18.5	4.4	13.1	91.9	35.4	1.0
X X	1250	116.6	0.1318	354.3	2.54	3.9	10.2	94.0	34.5	1.8
X Y	1300	199.8	0.2377	627.8	1.13	2.1	7.1	94.9	41.1	3.2
X Z	1350	202.3	0.2156	625.8	3.81	2.4	8.6	98.0	49.9	2.5
X AA	1650	247.1	0.2300	766.2	2.53	2.2	8.4	100.0	59.3	3.0
Integrated age $\pm 1\sigma$			n = 21	K ₂ O = 4.07%					Age = 34.66 \pm 0.51	
09ELK-S3 , K-Feldspar, 10.2 mg, J=0.0016174±0.07%, D=1.005±0.001, NM-233H, Lab#=59625-01										
X A	550	249.0	0.1345	819.9	2.77	3.8	2.7	1.9	19.6	3.3
X B	550	73.56	0.1137	218.9	2.37	4.5	12.1	3.5	25.7	1.2
X C	625	71.78	0.1358	209.2	4.17	3.8	13.9	6.4	28.83	0.96
X D	625	54.33	0.1268	147.7	3.17	4.0	19.7	8.5	30.89	1.00
X E	700	55.49	0.1226	150.9	5.28	4.2	19.7	12.1	31.58	0.81
F	700	27.37	0.0792	53.34	4.53	6.4	42.4	15.2	33.54	0.39
G	800	31.38	0.0695	67.41	8.83	7.3	36.5	21.2	33.11	0.39
H	800	17.04	0.0564	18.77	5.94	9.0	67.5	25.3	33.20	0.29
I	900	29.25	0.0618	60.78	8.87	8.3	38.6	31.3	32.63	0.35
J	900	17.55	0.0535	20.80	5.49	9.5	65.0	35.1	32.97	0.27
K	1000	26.31	0.0650	50.37	8.05	7.9	43.4	40.6	33.01	0.37
L	1000	22.83	0.0692	38.73	6.25	7.4	49.9	44.9	32.92	0.32
M	1075	26.63	0.0619	51.05	11.0	8.2	43.4	52.4	33.37	0.30
N	1075	28.78	0.0651	58.13	9.40	7.8	40.3	58.8	33.53	0.34
O	1120	33.66	0.0801	74.64	8.41	6.4	34.5	64.6	33.55	0.39
P	1160	46.60	0.1055	118.9	15.5	4.8	24.6	75.1	33.17	0.52
X Q	1200	99.52	0.1885	295.4	20.8	2.7	12.3	89.4	35.4	1.1
X R	1250	189.1	0.3412	595.9	6.33	1.5	6.9	93.7	37.5	2.3
X S	1300	253.1	0.3728	809.1	5.99	1.4	5.5	97.8	40.4	3.0
X T	1350	221.4	0.3293	696.1	1.97	1.5	7.1	99.1	45.4	3.3
X U	1650	307.3	0.3590	972.7	1.29	1.4	6.5	100.0	57.2	4.7
Integrated age $\pm 1\sigma$			n = 21	K ₂ O = 3.41%					Age = 33.75 \pm 0.69	
Plateau $\pm 1\sigma$ steps F-P			n = 11	MSWD = 0.70					Age = 33.17 \pm 0.11	
09ELK-S7 , K-Feldspar, 10.37 mg, J=0.0016201±0.09%, D=1.005±0.001, NM-233H, Lab#=59626-01										
X A	550	118.1	0.0282	344.0	5.23	18.1	13.9	1.1	47.3	1.4
X B	550	18.55	0.0371	37.35	4.23	13.7	40.5	2.0	21.79	0.37
X C	625	21.26	0.0697	38.07	7.89	7.3	47.1	3.7	29.00	0.27
X D	625	14.94	0.0740	18.37	6.36	6.9	63.7	5.1	27.58	0.25
X E	700	17.84	0.0687	24.50	11.0	7.4	59.4	7.4	30.70	0.21
X F	700	13.14	0.0376	8.241	8.97	13.6	81.5	9.4	31.00	0.15
X G	800	15.46	0.0345	14.57	18.2	14.8	72.2	13.3	32.29	0.15
X H	800	12.24	0.0240	5.023	11.1	21.2	87.9	15.6	31.14	0.13

Table A.4 (continued)

ID	Power (Watts)	⁴⁰ Ar/ ³⁹ Ar	³⁷ Ar/ ³⁹ Ar	³⁶ Ar/ ³⁹ Ar (x 10 ⁻³)	³⁹ Ar _K (x 10 ⁻¹⁵ mol)	K/Ca	⁴⁰ Ar* (%)	³⁹ Ar (%)	Age (Ma)	±1σ (Ma)
X I	900	16.33	0.0235	18.14	16.4	21.7	67.2	19.1	31.75	0.16
X J	900	13.12	0.0145	8.335	10.4	35.2	81.2	21.4	30.87	0.14
X K	1000	18.93	0.0196	28.82	17.4	26.0	55.0	25.1	30.15	0.19
X L	1000	16.19	0.0159	20.05	13.6	32.0	63.4	28.0	29.73	0.17
X M	1075	20.82	0.0238	34.47	26.0	21.4	51.1	33.6	30.79	0.20
X N	1075	17.00	0.0270	20.75	19.5	18.9	63.9	37.8	31.47	0.15
X O	1120	17.66	0.0333	21.38	19.4	15.3	64.2	42.0	32.84	0.16
X P	1160	16.75	0.0293	17.66	39.3	17.4	68.8	50.4	33.37	0.12
X Q	1200	15.68	0.0110	13.91	112.5	46.4	73.8	74.5	33.471	0.095
X R	1250	16.56	0.0068	16.08	93.7	75.4	71.3	94.6	34.17	0.10
X S	1300	19.08	0.0223	23.46	6.11	22.9	63.7	95.9	35.13	0.30
X T	1350	21.04	0.0294	30.13	3.53	17.4	57.7	96.6	35.10	0.36
X U	1650	23.50	0.0234	38.18	15.6	21.8	52.0	100.0	35.35	0.24
Integrated age ± 1σ		n = 21		K ₂ O = 10.66%	Age = 32.77 ± 0.12					
08EIK5 , K-Feldspar, 12.24 mg, J=0.0011686±0.08%, D=1.004±0.001, NM-224L, Lab#=59017-01										
X B	540	358.1	0.1120	1192.3	1.43	4.6	1.6	0.4	12.2	4.0
X C	540	51.23	0.1149	135.9	0.990	4.4	21.6	0.6	23.2	1.1
X D	590	43.73	0.1303	99.49	1.05	3.9	32.8	0.9	30.0	1.1
X E	590	27.53	0.1565	43.29	1.58	3.3	53.6	1.3	30.81	0.49
X F	590	25.88	0.1599	36.77	1.77	3.2	58.0	1.7	31.38	0.51
X G	640	36.97	0.1733	68.01	1.16	2.9	45.7	2.0	35.24	0.78
X H	640	24.08	0.1664	28.26	1.87	3.1	65.4	2.4	32.87	0.48
X I	640	21.69	0.1376	19.85	2.50	3.7	73.0	3.1	33.07	0.31
X J	690	39.30	0.1394	76.43	1.65	3.7	42.6	3.5	34.91	0.65
K	690	19.96	0.1141	12.78	2.74	4.5	81.1	4.1	33.80	0.28
L	690	19.35	0.0925	11.70	3.64	5.5	82.2	5.0	33.20	0.24
M	740	24.57	0.0788	29.81	2.19	6.5	64.2	5.6	32.93	0.39
N	740	18.40	0.0736	8.764	3.49	6.9	86.0	6.5	33.02	0.19
O	790	23.44	0.0703	25.83	3.97	7.3	67.4	7.4	33.02	0.28
P	790	18.39	0.0630	8.508	5.15	8.1	86.4	8.7	33.16	0.18
Q	840	22.90	0.0696	23.08	4.77	7.3	70.2	9.9	33.58	0.20
R	840	19.08	0.0648	10.67	5.49	7.9	83.5	11.3	33.25	0.17
S	890	23.33	0.0732	25.37	4.85	7.0	67.9	12.5	33.07	0.26
T	890	19.25	0.0679	11.76	5.37	7.5	82.0	13.8	32.94	0.17
U	940	26.22	0.0619	35.17	4.67	8.2	60.4	14.9	33.06	0.30
X V	940	19.13	0.0552	10.60	4.98	9.2	83.6	16.2	33.40	0.17
X W	990	24.91	0.0480	30.56	4.91	10.6	63.8	17.4	33.16	0.26
X X	990	19.95	0.0522	13.41	5.30	9.8	80.2	18.7	33.39	0.18
X Y	1040	26.39	0.0499	34.46	5.42	10.2	61.4	20.0	33.84	0.24
X Z	1040	21.22	0.0475	17.57	6.87	10.7	75.5	21.7	33.46	0.16
X AA	1090	25.57	0.0430	32.99	9.39	11.9	61.9	24.1	33.05	0.19
X AB	1090	21.48	0.0426	18.13	8.92	12.0	75.1	26.3	33.65	0.16
X AC	1140	24.90	0.0420	30.41	18.4	12.2	63.9	30.8	33.23	0.15
X AD	1140	21.48	0.0610	17.93	12.5	8.4	75.3	33.9	33.78	0.15
X AE	1190	22.36	0.0545	21.61	16.6	9.4	71.5	38.0	33.37	0.12
X AF	1190	21.69	0.0546	19.02	27.2	9.3	74.1	44.8	33.55	0.11
X AG	1190	20.89	0.0471	16.66	27.4	10.8	76.4	51.6	33.35	0.11
X AH	1190	20.66	0.0402	15.50	27.3	12.7	77.8	58.3	33.58	0.11
X AI	1240	20.11	0.0256	13.70	11.2	20.0	79.9	61.1	33.53	0.13
X AJ	1290	20.09	0.0137	13.47	64.4	37.1	80.2	77.0	33.626	0.083
X AK	1340	20.93	0.0181	16.05	57.2	28.1	77.3	91.2	33.787	0.094
X AL	1390	21.39	0.0482	16.92	14.4	10.6	76.6	94.8	34.22	0.12
X AM	1560	21.46	0.0600	17.26	19.7	8.5	76.2	99.6	34.16	0.13
X AN	1750	35.69	0.0793	63.98	1.45	6.4	47.0	100.0	35.04	0.63
Integrated age ± 1σ		n = 39		K ₂ O = 10.84%	Age = 33.444 ± 0.097					
Plateau ± 1σ		steps K-U		n = 11	MSWD = 1.29	Age = 33.181 ± 0.080				

Table A.4 (continued)

ID	Power (Watts)	⁴⁰ Ar/ ³⁹ Ar	³⁷ Ar/ ³⁹ Ar	³⁶ Ar/ ³⁹ Ar (x 10 ⁻³)	³⁹ Ar _K (x 10 ⁻¹⁵ mol)	K/Ca	⁴⁰ Ar* (%)	³⁹ Ar (%)	Age (Ma)	±1σ (Ma)
09EIK7 , K-Feldspar, 12.1 mg, J=0.0011685±0.09%, D=1.004±0.001, NM-224L, Lab#=59018-01										
X B	540	262.8	0.0401	865.8	4.26	12.7	2.6	1.1	14.6	2.4
X C	540	34.68	0.0272	71.12	4.64	18.7	39.4	2.3	28.55	0.43
X D	590	28.20	0.0292	47.36	5.18	17.5	50.4	3.6	29.67	0.34
X E	590	21.72	0.0414	23.88	6.84	12.3	67.5	5.3	30.63	0.21
X F	590	21.59	0.0516	21.92	7.27	9.9	70.0	7.2	31.56	0.18
X G	640	29.09	0.0686	47.28	4.06	7.4	52.0	8.2	31.59	0.30
X H	640	19.85	0.0681	14.21	5.83	7.5	78.9	9.7	32.68	0.18
X I	640	19.50	0.0642	13.29	7.35	8.0	79.9	11.6	32.53	0.16
X J	690	28.04	0.0624	40.97	3.94	8.2	56.8	12.6	33.28	0.30
X K	690	18.90	0.0562	11.08	5.73	9.1	82.7	14.0	32.63	0.16
X L	690	18.88	0.0499	11.27	6.80	10.2	82.4	15.7	32.47	0.16
X M	740	22.76	0.0469	23.49	3.51	10.9	69.5	16.6	33.02	0.25
X N	740	18.31	0.0449	8.569	4.89	11.4	86.2	17.9	32.94	0.16
X O	790	20.18	0.0467	14.56	4.59	10.9	78.7	19.0	33.15	0.21
X P	790	17.83	0.0403	6.773	5.49	12.7	88.8	20.4	33.05	0.16
X Q	840	18.65	0.0398	10.37	4.80	12.8	83.6	21.7	32.54	0.19
X R	840	17.44	0.0312	5.870	5.79	16.4	90.1	23.1	32.80	0.16
X S	890	18.61	0.0331	9.511	4.93	15.4	84.9	24.4	32.99	0.19
X T	890	17.43	0.0264	4.698	6.11	19.3	92.0	25.9	33.48	0.14
X U	940	19.63	0.0309	12.72	5.15	16.5	80.8	27.3	33.12	0.21
X V	940	17.75	0.0226	5.742	6.08	22.5	90.4	28.8	33.52	0.15
X W	990	20.86	0.0300	16.63	5.23	17.0	76.4	30.1	33.29	0.22
X X	990	19.06	0.0262	10.47	6.32	19.5	83.8	31.7	33.34	0.15
X Y	1040	25.33	0.0363	33.00	6.62	14.1	61.5	33.4	32.54	0.24
X Z	1040	21.90	0.0292	20.78	7.96	17.5	72.0	35.4	32.91	0.17
X AA	1090	27.71	0.0399	41.78	9.82	12.8	55.4	37.9	32.09	0.23
X AB	1090	22.54	0.0396	22.76	9.73	12.9	70.2	40.4	33.03	0.17
X AC	1140	27.96	0.0531	41.62	14.0	9.6	56.0	44.0	32.70	0.20
X AD	1140	21.76	0.0828	19.80	11.1	6.2	73.1	46.8	33.23	0.14
X AE	1190	24.71	0.0874	29.53	11.1	5.8	64.7	49.6	33.38	0.19
X AF	1190	22.34	0.1018	21.68	19.6	5.0	71.4	54.6	33.28	0.13
X AG	1190	21.71	0.0813	18.59	20.6	6.3	74.7	59.9	33.87	0.12
X AH	1190	21.83	0.0571	19.60	22.8	8.9	73.5	65.7	33.49	0.13
X AI	1240	22.41	0.0418	21.73	9.06	12.2	71.4	68.0	33.38	0.18
X AJ	1290	23.09	0.0193	24.43	53.0	26.4	68.7	81.5	33.15	0.12
X AK	1340	24.72	0.0143	29.30	44.8	35.7	65.0	92.8	33.53	0.13
X AL	1390	24.74	0.0189	28.23	15.3	27.1	66.3	96.7	34.21	0.16
X AM	1560	25.04	0.0261	28.35	12.4	19.5	66.5	99.9	34.76	0.17
X AN	1750	51.43	0.0320	117.1	0.452	16.0	32.7	100.0	35.1	2.1
Integrated age ± 1σ		n = 39		K ₂ O = 10.68%		Age = 32.87 ± 0.12				
08ELK8 , kspars, 16.64 mg, J=0.00104±0.09%, D=1.0014±0.001, NM-222L, Lab#=58847-01										
X A	530	236.7	0.1331	639.3	0.629	3.8	20.2	0.1	87.6	3.2
X B	530	43.29	0.0898	90.24	1.57	5.7	38.4	0.4	30.94	0.62
X C	580	42.71	0.0959	72.78	1.74	5.3	49.7	0.7	39.36	0.64
X D	580	30.43	0.1048	44.75	2.27	4.9	56.6	1.1	32.03	0.46
X E	580	29.48	0.1226	39.59	2.57	4.2	60.3	1.6	33.07	0.39
X F	630	33.78	0.1521	49.64	1.64	3.4	56.6	1.9	35.53	0.60
X G	630	25.10	0.1600	25.87	2.59	3.2	69.6	2.4	32.48	0.28
X H	630	24.07	0.1335	22.17	3.68	3.8	72.8	3.1	32.60	0.25
X I	680	28.57	0.1296	31.43	2.65	3.9	67.5	3.6	35.84	0.38
X J	680	22.05	0.1178	14.42	4.37	4.3	80.7	4.4	33.09	0.21
X K	680	21.57	0.1019	13.21	6.16	5.0	81.9	5.5	32.85	0.16
X L	730	22.85	0.0928	16.40	3.93	5.5	78.8	6.3	33.49	0.24
X M	730	19.96	0.0794	7.799	6.29	6.4	88.5	7.4	32.83	0.14

Table A.4 (continued)

ID	Power (Watts)	⁴⁰ Ar/ ³⁹ Ar	³⁷ Ar/ ³⁹ Ar	³⁶ Ar/ ³⁹ Ar (x 10 ⁻³)	³⁹ Ar _K (x 10 ⁻¹⁵ mol)	K/Ca	⁴⁰ Ar* (%)	³⁹ Ar (%)	Age (Ma)	±1σ (Ma)
X N	780	21.29	0.0775	11.88	7.68	6.6	83.5	8.8	33.06	0.14
X O	780	19.16	0.0613	4.878	10.9	8.3	92.5	10.8	32.944	0.099
X P	830	20.17	0.0549	7.877	10.4	9.3	88.5	12.8	33.18	0.11
X Q	830	18.77	0.0452	3.039	13.8	11.3	95.2	15.3	33.232	0.091
X R	880	19.69	0.0416	6.356	11.4	12.3	90.5	17.4	33.11	0.11
X S	880	18.50	0.0336	2.294	14.8	15.2	96.3	20.2	33.130	0.077
X T	930	19.59	0.0343	5.899	11.8	14.9	91.1	22.3	33.18	0.11
X U	930	18.69	0.0284	3.124	15.0	18.0	95.1	25.1	33.045	0.075
X V	980	19.97	0.0249	7.169	11.5	20.5	89.4	27.3	33.18	0.10
X W	980	19.31	0.0204	4.849	14.1	25.1	92.6	29.9	33.245	0.088
X X	1030	21.18	0.0259	11.10	11.0	19.7	84.5	31.9	33.28	0.12
X Y	1030	20.32	0.0230	8.144	14.4	22.2	88.2	34.6	33.300	0.096
X Z	1080	23.27	0.0305	17.83	12.1	16.7	77.4	36.8	33.47	0.15
X AA	1080	22.04	0.0310	13.24	15.1	16.4	82.3	39.6	33.71	0.11
X AB	1130	25.65	0.0429	25.42	14.6	11.9	70.7	42.3	33.73	0.15
X AC	1130	24.17	0.0531	19.82	17.5	9.6	75.8	45.5	34.05	0.13
X AD	1180	25.38	0.0725	22.87	13.4	7.0	73.4	48.0	34.62	0.14
X AE	1180	24.97	0.0656	22.11	25.2	7.8	73.9	52.7	34.28	0.13
X AF	1180	24.86	0.0596	21.35	25.7	8.6	74.6	57.5	34.48	0.12
X AG	1230	24.52	0.0454	18.72	11.6	11.2	77.5	59.6	35.28	0.16
X AH	1280	24.09	0.0196	17.83	49.5	26.0	78.1	68.7	34.98	0.10
X AI	1330	25.47	0.0136	22.30	73.1	37.6	74.1	82.3	35.08	0.11
X AJ	1380	26.59	0.0198	25.43	33.5	25.7	71.7	88.5	35.44	0.14
X AK	1550	26.06	0.0259	23.66	31.6	19.7	73.2	94.3	35.44	0.12
X AL	1750	26.71	0.0122	25.71	30.8	41.7	71.6	100.0	35.51	0.13
Integrated age ± 1σ		n = 38	K ₂ O = 12.00%	Age = 34.339 ± 0.083						
Plateau ± 1σ steps E-M		n = 9	MSWD = 10.72	Age = 33.06 ± 0.246						
08ELK13 , kspar, 16.03 mg, J=0.0010133±0.11%, D=1.0014±0.001, NM-222L, Lab#=58852-01										
X A	530	337.4	0.0914	943.9	0.430	5.6	17.3	0.1	103.8	4.2
X B	530	38.93	0.0755	78.46	0.802	6.8	40.5	0.2	28.6	1.1
X C	580	51.56	0.0574	105.2	1.03	8.9	39.7	0.4	37.05	0.94
X D	580	27.80	0.0688	34.77	1.44	7.4	63.1	0.7	31.76	0.54
X E	580	24.95	0.0639	23.48	1.74	8.0	72.2	1.0	32.64	0.44
X F	630	29.61	0.0783	36.82	1.15	6.5	63.3	1.2	33.92	0.64
X G	630	23.29	0.0579	16.03	1.87	8.8	79.7	1.6	33.61	0.35
X H	630	22.57	0.0584	15.57	2.58	8.7	79.6	2.1	32.57	0.29
X I	680	29.20	0.0575	33.83	1.77	8.9	65.8	2.4	34.78	0.48
X J	680	21.67	0.0556	12.27	4.05	9.2	83.3	3.2	32.69	0.20
X K	730	25.87	0.0625	25.37	3.10	8.2	71.0	3.8	33.29	0.30
X L	730	20.08	0.0492	6.265	4.69	10.4	90.8	4.6	33.04	0.16
X M	780	21.85	0.0461	12.28	6.00	11.1	83.4	5.8	33.01	0.17
X N	780	19.23	0.0355	3.499	8.27	14.4	94.6	7.3	32.96	0.11
X O	830	20.56	0.0357	7.355	8.72	14.3	89.4	9.0	33.32	0.12
X P	830	18.99	0.0312	2.380	10.6	16.4	96.3	11.0	33.133	0.097
X Q	880	20.66	0.0324	7.483	9.16	15.7	89.3	12.7	33.43	0.11
X R	880	19.11	0.0269	2.479	10.5	19.0	96.2	14.7	33.283	0.086
X S	930	20.34	0.0278	6.851	8.47	18.3	90.1	16.3	33.17	0.12
X T	930	19.25	0.0222	3.163	9.20	23.0	95.2	18.0	33.19	0.11
X U	980	21.01	0.0215	9.599	7.29	23.7	86.5	19.4	32.93	0.13

Table A.4 (continued)

ID	Power (Watts)	$^{40}\text{Ar}/^{39}\text{Ar}$	$^{37}\text{Ar}/^{39}\text{Ar}$	$^{36}\text{Ar}/^{39}\text{Ar}$ ($\times 10^{-3}$)	$^{39}\text{Ar}_K$ ($\times 10^{-15}$ mol)	K/Ca	$^{40}\text{Ar}^*$ (%)	^{39}Ar (%)	Age (Ma)	$\pm 1\sigma$ (Ma)
X V	980	19.93	0.0191	5.668	9.22	26.7	91.6	21.1	33.07	0.12
X W	1030	22.21	0.0181	13.76	7.27	28.2	81.7	22.5	32.88	0.13
X X	1030	21.00	0.0177	9.878	9.81	28.8	86.1	24.3	32.76	0.13
X Y	1080	23.87	0.0219	19.68	8.78	23.3	75.6	26.0	32.70	0.15
X Z	1080	21.87	0.0223	12.33	11.5	22.9	83.4	28.2	33.03	0.12
X AA	1130	24.93	0.0344	22.02	12.0	14.8	73.9	30.4	33.37	0.15
X AB	1130	22.35	0.0336	14.25	14.0	15.2	81.2	33.1	32.87	0.12
X AC	1180	22.78	0.0393	15.09	13.1	13.0	80.4	35.5	33.19	0.12
X AD	1180	22.15	0.0341	13.25	24.2	14.9	82.3	40.1	33.03	0.11
X AE	1180	21.35	0.0262	10.62	29.4	19.5	85.3	45.6	33.002	0.081
X AF	1180	21.44	0.0199	10.62	34.5	25.6	85.4	52.1	33.159	0.091
X AG	1230	20.75	0.0154	8.430	11.5	33.1	88.0	54.3	33.08	0.11
X AH	1280	20.60	0.0068	7.474	90.0	75.4	89.3	71.3	33.317	0.068
X AI	1330	21.73	0.0074	11.06	84.1	69.2	85.0	87.1	33.446	0.071
X AJ	1380	22.87	0.0140	14.54	19.4	36.3	81.2	90.8	33.64	0.11
X AK	1550	21.92	0.0100	11.94	22.9	51.2	83.9	95.1	33.32	0.11
X AL	1750	22.59	0.0092	13.65	26.2	55.7	82.2	100.0	33.61	0.10
Integrated age $\pm 1\sigma$		n = 38	$\text{K}_2\text{O} = 12.55\%$	Age = 33.293 ± 0.071						
09ELK-R1 , K-Feldspar, 9.55 mg, J=0.0016113 \pm 0.08%, D=1.005 \pm 0.001, NM-233H, Lab#=59622-01										
X A	550	112.0	0.6969	345.1	2.72	0.73	9.0	1.3	29.2	1.6
X B	550	22.70	0.3156	51.28	3.43	1.6	33.3	3.0	21.85	0.48
X C	625	19.36	0.3425	37.42	5.29	1.5	43.0	5.6	24.03	0.34
X D	625	14.95	0.3410	21.18	3.76	1.5	58.3	7.5	25.13	0.34
X E	700	16.02	0.4065	23.57	5.50	1.3	56.7	10.2	26.21	0.27
X F	700	12.28	0.3528	9.204	4.45	1.4	78.1	12.4	27.64	0.24
G	800	12.37	0.4013	9.220	8.80	1.3	78.2	16.7	27.89	0.16
H	800	11.00	0.2825	4.691	6.73	1.8	87.6	20.0	27.78	0.17
I	900	11.19	0.1824	4.978	10.9	2.8	87.0	25.4	28.05	0.12
J	900	10.90	0.0896	3.289	8.18	5.7	91.1	29.4	28.62	0.13
K	1000	12.03	0.0526	7.653	11.5	9.7	81.2	35.1	28.17	0.13
L	1000	11.98	0.0361	6.866	9.02	14.1	83.1	39.5	28.67	0.14
M	1075	14.69	0.0424	16.61	10.7	12.0	66.6	44.8	28.19	0.21
N	1075	13.34	0.0414	11.98	9.10	12.3	73.5	49.3	28.24	0.17
O	1120	15.40	0.0475	19.02	8.68	10.7	63.5	53.5	28.18	0.21
P	1160	14.81	0.0413	16.98	20.1	12.3	66.1	63.5	28.23	0.13
Q	1200	15.99	0.0336	20.60	45.7	15.2	61.9	85.9	28.53	0.12
R	1250	18.92	0.0564	30.55	20.2	9.0	52.3	95.9	28.51	0.20
S	1300	34.05	0.1041	82.79	2.36	4.9	28.1	97.0	27.64	0.63
X T	1350	27.34	0.0765	59.56	4.38	6.7	35.6	99.2	28.09	0.43
X U	1650	86.52	0.1570	256.4	1.65	3.3	12.4	100.0	31.0	1.7
Integrated age $\pm 1\sigma$		n = 21	$\text{K}_2\text{O} = 5.07\%$	Age = 28.00 ± 0.12						
Plateau $\pm 1\sigma$ steps J-U		n = 12	MSWD = 1.82	Age = 28.392 ± 0.071						
09ELK-R6a , K-Feldspar, 10.95 mg, J=0.0016134 \pm 0.08%, D=1.005 \pm 0.001, NM-233H, Lab#=59623-02										
X A	550	83.52	0.5972	262.6	4.25	0.85	7.1	5.2	17.3	1.2
X B	550	21.00	0.4213	48.10	3.57	1.2	32.4	9.7	19.72	0.40
X C	625	40.05	0.5610	110.7	5.88	0.91	18.4	16.9	21.30	0.61
X D	625	16.76	0.6301	31.34	3.80	0.81	45.0	21.6	21.84	0.32
X E	700	21.19	0.9062	46.65	4.79	0.56	35.3	27.5	21.63	0.42

Table A.4 (continued)

ID	Power (Watts)	$^{40}\text{Ar}/^{39}\text{Ar}$	$^{37}\text{Ar}/^{39}\text{Ar}$	$^{36}\text{Ar}/^{39}\text{Ar}$ ($\times 10^{-3}$)	$^{39}\text{Ar}_K$ ($\times 10^{-15}$ mol)	K/Ca	$^{40}\text{Ar}^*$ (%)	^{39}Ar (%)	Age (Ma)	$\pm 1\sigma$ (Ma)
X F	700	14.59	0.7758	21.52	5.32	0.66	56.8	34.1	23.96	0.26
X G	800	19.39	1.097	38.45	5.64	0.46	41.8	41.0	23.47	0.31
X H	800	11.74	0.9687	11.16	3.10	0.53	72.6	44.9	24.63	0.30
X I	900	20.33	0.6517	39.34	4.48	0.78	43.1	50.4	25.32	0.33
X J	900	16.86	0.4124	27.00	3.07	1.2	52.9	54.2	25.75	0.43
X K	1000	22.95	0.2850	47.28	4.22	1.8	39.2	59.4	26.00	0.43
X L	1000	17.63	0.2707	28.91	2.84	1.9	51.6	62.9	26.29	0.44
X M	1075	21.14	0.2647	41.30	3.84	1.9	42.4	67.6	25.87	0.36
X N	1075	23.73	0.3163	49.47	2.83	1.6	38.5	71.1	26.37	0.57
X O	1120	26.51	0.3672	61.41	2.01	1.4	31.6	73.6	24.23	0.68
X P	1160	34.61	0.3906	85.29	3.68	1.3	27.2	78.1	27.23	0.58
X Q	1200	52.81	0.3906	148.9	7.07	1.3	16.7	86.9	25.56	0.75
X R	1250	69.63	0.6506	204.7	5.18	0.78	13.2	93.3	26.6	1.0
X S	1300	72.15	0.7856	211.2	2.81	0.65	13.6	96.7	28.3	1.2
X T	1350	116.5	1.061	353.8	1.53	0.48	10.4	98.6	34.8	1.7
X U	1650	214.6	2.720	693.7	1.12	0.19	4.6	100.0	28.4	3.4
Integrated age $\pm 1\sigma$		n = 21		K ₂ O = 1.76%	Age = 24.37 \pm 0.37					

Notes:

Isotopic ratios corrected for blank, radioactive decay, and mass discrimination, not corrected for interfering reactions.

Errors quoted for individual analyses include analytical error only, without interfering reaction or J uncertainties.

Integrated age calculated by summing isotopic measurements of all steps.

Integrated age error calculated by quadratically combining errors of isotopic measurements of all steps.

Plateau age is inverse-variance-weighted mean of selected steps.

Plateau age error is inverse-variance-weighted mean error (Taylor, 1982) times root MSWD where MSWD > 1.

Plateau error is weighted error of Taylor (1982).

Decay constants and isotopic abundances after Steiger and Jäger (1977).

X symbol preceding sample ID denotes analyses excluded from plateau age calculations.

Weight percent K₂O calculated from ^{39}Ar signal, sample weight, and instrument sensitivity.

Ages calculated relative to FC-2 Fish Canyon Tuff sanidine interlaboratory standard at 28.02 Ma (Renne et al., 1998).

Decay Constant (LambdaK (total)) = 5.543e-10/a

Correction factors:

$$(^{39}\text{Ar}/^{37}\text{Ar})_{\text{ca}} = 0.0007 \pm 5\text{e-}05$$

$$(^{36}\text{Ar}/^{37}\text{Ar})_{\text{ca}} = 0.00028 \pm 2\text{e-}05$$

$$(^{38}\text{Ar}/^{39}\text{Ar})_K = 0.013$$

$$(^{40}\text{Ar}/^{39}\text{Ar})_K = 0.01 \pm 0.002$$

APPENDIX B
LOW TEMPERATURE
THERMOCHRONOLOGY DATA

Appendix B contains the raw data collected during the apatite fission-track counting process, the AHe raw data, and the exhumation and cooling rates calculated for each sample. Table B.1 is the AFT data along with track length measurements. Table B.2 is the complete data table for the apatite (U-Th)/He analysis. Table B.3 is the exhumation rates estimated from the linear regression of the age data and included on Figure 3.4. Table B.4 is the cooling rates calculated for each pluton.

Table B.1: Apatite fission-track data.

Sample Number	Rock Type	Location (UTM)*	Elevation (m)	N_G	$\rho_s \times 10^5$ t/cm ²	$\rho_l \times 10^6$ t/cm ²	$\rho_d \times 10^6$ t/cm ²	Pooled Age (Ma) (± 1 S.E.)	$P(\chi)^2$ (%)	U (ppm)	Mean Track Length (μ m) (± 1 S.E.)	N_{TL}	S.D. (μ m) (TL)
Mount Sopris													
09Elk-S1	quartz	313272	3944	20	0.569	1.166	1.26787	30.0 \pm 4.2	99	11			
	monzonite	4347781			(61)	(625)	(4600)						
09Elk-S2	quartz	314178	3777	20	0.6684	1.299	1.25431	31.3 \pm 4.0	99	12			
	monzonite	4347276			(77)	(748)	(4600)						
09Elk-S3	quartz	314614	3649	20	0.4887	1.123	1.25504	26.5 \pm 4.9	99	11			
	monzonite	4347307			(33)	(379)	(4600)						
09Elk-S4	quartz	314800	3523	20	0.3984	0.8094	1.25689	30.0 \pm 4.6	99	8			
	monzonite	4347500			(51)	(518)	(4600)						
09Elk-S5	quartz	315067	3107	20	0.5938	1.67	1.24426	21.4 \pm 3.7	99	16			
	monzonite	4348880			(38)	(536)	(4600)						
Capitol Peak													
08Elk01	monzodiorite	320571	4151	20	1.06	2.44	1.07335	23.2 \pm 2.6	97	27			
		4335711			(99)	(1111)	(4600)						
08Elk02	monzodiorite	320921	3817	15	0.38	0.89	1.07372	22.3 \pm 4.7	99	10			
		4336665			(25)	(292)	(4600)						
08Elk05	monzodiorite	320118	3543	18	0.96	2.18	1.08089	23.1 \pm 3.9	99	24			
		4336869			(40)	(454)	(4600)						
08Elk06	diorite	320945	3386	20	1.00	2.21	1.08313	23.8 \pm 2.6	99	24	12.3 \pm 0.6	5	1.4
		4336595			(104)	(1148)	(4600)						
Snowmass Mountain													
08Elk08	granodiorite	321400	4295	20	1.03	1.88	1.0881	28.8 \pm 3.7	99	21	13.8 \pm 0.3	33	1.6
		4331780			(75)	(687)	(4600)						
08Elk09	granodiorite	321278	4201	20	0.62	1.24	1.09014	26.4 \pm 3.4	99	13	13.2 \pm 0.6	7	1.7
		4331773			(73)	(731)	(4600)						
08Elk10	granodiorite	321160	4107	20	0.71	1.38	1.09239	27.5 \pm 3.3	97	15	13.1 \pm 0.6	19	2.4
		4331748			(87)	(838)	(4600)						
08Elk11	granodiorite	321068	4020	20	0.56	1.23	1.09552	24.5 \pm 3.2	99	13	13.5 \pm 0.5	14	1.9
		4331674			(69)	(749)	(4600)						
08Elk12	granodiorite	320826	3827	20	0.78	1.76	1.09568	23.5 \pm 2.8	97	19			
		4331632			(87)	(983)	(4600)						
08Elk13	granodiorite	320616	3691	20	0.86	1.89	1.0991	24.4 \pm 2.7	99	20			
		4331516			(108)	(1180)	(4600)						
08Elk14	diorite	320209	3598	20	0.72	1.78	1.10412	21.7 \pm 2.9	99	19			
		4331326			(67)	(827)	(4600)						
08Elk 15	diorite	320029	3460	4	0.31	0.95	1.1009	17.6 \pm 8.1	50	10	13.0 \pm 2.6	4	5.2
		4330389			(5)	(76)	(4600)						

Table B.1 (continued)

Sample Number	Rock Type	Location (UTM)*	Elevation (m)	N_G	ρ_s $\times 10^5$ t/cm ²	ρ_i $\times 10^6$ t/cm ²	ρ_d $\times 10^6$ t/cm ²	Pooled Age (Ma) (± 1 S.E.)	$P(\chi)^2$ (%)	U (ppm)	Mean Track Length (μ m) (± 1 S.E.)	N_{TL}	S.D. (μ m) (TL)
Ragged Mountain													
09Elk-R2	porphyritic granodiorite	308470 4322419	3641	20	1.19 (128)	2.17 (1164)	1.16666 (4600)	31.1 \pm 3.2	99	22	13.7 \pm 0.3	78	2.6
09Elk-R1	porphyritic granodiorite	310628 4322428	3410	20	0.73 (94)	1.90 (1219)	1.17607 (4600)	22.0 \pm 2.5	99	19	14.1 \pm 0.4	47	2.4
09Elk-R3	porphyritic granodiorite	309806 4322976	3280	20	1.17 (138)	2.17 (1282)	1.15725 (4600)	30.2 \pm 3.0	99	22	12.9 \pm 0.3	100	2.6
09Elk-R4	porphyritic granodiorite	309790 4323388	3071	20	1.101 (118)	2.267 (1215)	1.15072 (4600)	27.1 \pm 2.8	99	23	13.7 \pm 0.5	17	2.1
09Elk-R5	porphyritic granodiorite	309554 4324477	2900	20	0.93 (117)	1.913 (1194)	1.1405 (4600)	27.1 \pm 2.9	99	20	13.5 \pm 0.3	45	2.0
09Elk-R6a	porphyritic granodiorite	307496 4327624	1882	20	0.5156 (66)	1.839 (1177)	1.13153 (4600)	15.4 \pm 2.0	70	19	12.8 \pm 0.6	33	3.2
Marcellina Mountain													
09Elk-M1	diorite	305549 4311177	3458	20	0.6029 (35)	1.416 (411)	1.24442 (4600)	25.7 \pm 4.6	99	13			
09Elk-M4	diorite	307181 4311005	2826	5	0.375 (6)	1 (80)	1.23122 (4600)	22.4 \pm 9.5	92	10			
East Beckwith Mountain													
09Elk-B1	granodiorite	307473 4302534	3530	20	0.97 (78)	1.88 (762)	1.21296 (4600)	30.5 \pm 3.8	99	18			
09Elk-B2	porphyritic granodiorite	307624 4302599	3401	20	0.96 (95)	2.022 (1003)	1.20174 (4600)	27.6 \pm 3.2	99	20			
09Elk-B3	porphyritic granodiorite	308017 4303109	3220	20	1.05 (135)	2.033 (1301)	1.18976 (4600)	30.0 \pm 3.0	99	20			
09Elk-B4	porphyritic granodiorite	308357 4303365	3045	20	1.13 (114)	2.16 (1090)	1.18317 (4600)	30.0 \pm 3.2	99	22			
Mount Gunnison													
09Elk-G4	porphyritic granodiorite	293147 4298419	3881	20	0.83 (85)	1.54 (789)	1.29452 (4600)	33.8 \pm 4.1	99	14			
09Elk-G3	porphyritic granodiorite	292720 4297113	3698	20	0.986 (123)	1.9 (1185)	1.29177 (4600)	32.5 \pm 3.4	97	17			
09Elk-G1	porphyritic granodiorite	292400 4297332	3503	20	0.82 (95)	1.73 (998)	1.3043 (4600)	30.1 \pm 3.5	96	16			
09Elk-G5	porphyritic granodiorite	291547 4297553	3149	20	0.65 (83)	1.386 (887)	1.27825 (4600)	29.0 \pm 3.5	99	13			

Notes:

*UTM datum is NAD 27, Zone 13S

ρ_s - spontaneous track density ρ_i = induced track density

ρ_d - track density in muscovite detector covering CN-5 (10 ppm); Reported value determined from interpolation of values for detectors covering standards at the top and bottom of the reactor packages (fluence gradient correction)

Number in parenthesis is the number of tracks counted for ages and fluence calibration or the number of track measured for lengths.

N.D. = no data $I_f = 1.551 \times 10^{-10} \text{ yr}^{-1}$, $g = 0.5$ $\zeta = 486 \pm 35$ (SAK)

S.E. = standard error S.D. = standard deviation TL = track length

N_G = number of grains dated N_{TL} = number of track lengths measured

Mean track lengths not corrected for length bias (Laslett and others, 1982)

Table B.2: Apatite (U-Th/He) data. Analyzed by D. Stockli and R. Kislitsyn at the University of Kansas. Gray highlighting indicates runs that were omitted during averaging.

Sample	Elevation [m]	Age [Ma]	$\pm 6\%$ [Ma]	U [ppm]	Th [ppm]	Sm [ppm]	He Th/U [nmo/mg]	mass [mg]	eU Ft	r [ppm]	comment		
Mt Sopris													
09Elk-S1-1		6.0	0.20	12.5	36.1	84.2	2.89	0.43	4.5	0.62	20.99	38.60	Incl?
09Elk-S1-2		12.3	0.32	5.1	23.2	32.6	4.57	0.46	6.9	0.64	10.55	39.63	
09Elk-S1-3		18.7	0.57	4.7	20.7	35.1	4.37	0.64	6.6	0.64	9.59	40.00	Incl?
09Elk-S1	3944	12.3	0.32	5.1	23.2	32.6	4.57	0.46	6.9	0.64	10.55	39.63	
09Elk-S2-1		12.4	0.57	4.0	18.9	48.4	4.72	0.40	9.3	0.67	8.46	45.01	
09Elk-S2-2		71.4	2.51	4.8	24.8	45.6	5.12	2.75	6.4	0.64	10.68	41.15	Incl?
09Elk-S2-3		20.5	0.66	4.7	22.1	37.7	4.74	0.71	5.4	0.63	9.85	40.97	Incl?
09Elk-S2	3777	12.4	0.57	4.0	18.9	48.4	4.72	0.40	9.3	0.67	8.46	45.01	
09Elk-S3-1		10.5	0.34	4.9	21.5	39.1	4.43	0.37	7.1	0.64	9.93	38.65	
09Elk-S3-2		10.7	0.27	2.5	10.9	11.1	4.31	0.18	4.9	0.61	5.11	35.91	
09Elk-S3-3		9.2	0.22	3.3	13.9	16.7	4.14	0.21	5.7	0.63	6.61	39.55	
09Elk-S3	3649	10.1	0.3	3.6	15.5	22.3	4.3	0.3	5.9	0.6	7.22	38.04	
09Elk-S4-1		11.1	0.29	5.3	25.8	35.7	4.86	0.45	7.3	0.65	11.36	40.46	
09Elk-S4-2		10.2	0.19	4.6	20.8	16.7	4.50	0.32	4.2	0.60	9.49	36.83	
09Elk-S4-3		9.2	0.36	5.6	21.4	50.5	3.80	0.34	4.7	0.62	10.66	40.72	
09Elk-S4	3523	10.2	0.3	5.2	22.6	34.3	4.4	0.4	5.4	0.6	10.50	39.34	
09Elk-S5-1		10.9	0.44	6.8	22.1	60.4	3.23	0.50	8.9	0.67	12.02	44.43	
09Elk-S5-2		7.4	0.41	5.2	21.4	70.4	4.11	0.26	3.8	0.60	10.24	38.66	
09Elk-S5-3		11.3	0.53	5.6	21.7	60.9	3.90	0.42	5.1	0.62	10.64	37.59	
09Elk-S5	3107	9.9	0.5	5.9	21.7	63.9	3.7	0.4	6.0	0.6	10.97	40.23	
Capitol Peak													
08Elk01-1		12.8	0.54	6.8	18.1	57.4	2.67	0.53	7.9	0.66	11.05	41.23	
08Elk01-2		9.6	0.49	6.1	14.4	60.1	2.35	0.35	9.5	0.67	9.50	42.51	
08Elk01	4151	11.2	0.5	6.5	16.3	58.7	2.5	0.4	8.7	0.7	10.27	41.87	
08Elk06-1		8.8	0.32	8.2	16.2	52.5	1.96	0.37	5.3	0.63	12.03	37.31	
08Elk06-2		7.7	0.30	5.7	15.2	44.4	2.66	0.27	10.6	0.69	9.28	59.32	
08Elk06-3		21.9	0.76	8.0	21.6	54.8	2.70	1.03	6.5	0.64	13.05	39.77	Incl?
08Elk06	3386	8.2	0.3	7.0	15.7	48.4	2.3	0.3	8.0	0.7	10.66	48.32	
Snowmass Mtn													
08Elk08-1		13.8	0.65	6.6	24.3	72.2	3.71	0.64	8.6	0.66	12.29	41.69	
08Elk08-2		14.9	0.84	5.2	21.3	72.0	4.07	0.60	11.7	0.69	10.21	46.44	
08Elk08-3		15.8	0.85	6.7	26.6	87.9	3.98	0.79	11.4	0.68	12.92	43.06	
08Elk08	4295	14.8	0.8	6.2	24.1	77.3	3.9	0.7	10.5	0.7	11.81	43.73	
08Elk09-1		14.9	0.86	5.5	24.6	81.6	4.51	0.68	15.3	0.70	11.23	47.45	
08Elk09-2		15.1	0.68	6.4	25.3	69.4	3.96	0.73	11.8	0.70	12.32	48.16	
08Elk09-3		32.0	1.68	4.8	20.0	62.6	4.15	1.23	12.5	0.71	9.52	52.19	Incl?
08Elk09	4201	15.0	0.8	5.9	24.9	75.5	4.2	0.7	13.5	0.7	11.77	47.81	
08Elk10-1		12.9	0.64	7.5	25.9	84.0	3.46	0.70	14.0	0.71	13.55	48.22	
08Elk10-2		12.7	0.56	8.2	24.7	77.2	3.01	0.68	8.2	0.67	14.04	45.21	
08Elk10-3		13.0	0.75	5.3	21.3	74.3	4.05	0.59	23.8	0.76	10.28	65.25	
08Elk10	4107	12.9	0.7	7.0	24.0	78.5	3.5	0.7	15.3	0.7	12.62	52.89	

Table B.2 (continued)

Sample	Elevation [m]	Age [Ma]	$\pm 6\%$ [Ma]	U [ppm]	Th [ppm]	Sm [ppm]	Th/U	He [nmo/mg]	mass [mg]	Ft	eU [ppm]	r [μm]	comment
08EIk11-1		12.9	0.57	6.6	23.8	65.8	3.58	0.55	4.9	0.61	12.22	37.21	
08EIk11-2		12.1	0.48	6.5	21.0	55.7	3.24	0.49	5.7	0.63	11.42	37.92	
08EIk11-3		19.5	0.98	5.4	18.8	60.4	3.47	0.67	4.6	0.61	9.83	37.25	Incl?
08EIk11	4020	12.5	0.5	6.6	22.4	60.8	3.4	0.5	5.3	0.6	11.82	37.57	
08EIk12-1		11.2	0.48	6.9	23.9	65.5	3.47	0.51	7.3	0.65	12.53	39.64	
08EIk12-2		18.3	0.74	7.2	26.1	66.1	3.62	0.88	6.6	0.64	13.35	39.30	Incl?
08EIk12-3		10.0	0.42	8.0	23.9	70.4	2.99	0.49	5.9	0.64	13.61	40.23	
08EIk12	3827	10.6	0.5	7.5	23.9	68.0	3.2	0.5	6.6	0.6	13.07	39.94	
08EIk13-1		12.3	0.46	9.8	28.4	75.1	2.90	0.72	5.7	0.63	16.47	39.56	
08EIk13-2		27.8	1.16	7.5	24.6	67.9	3.30	1.34	6.9	0.65	13.24	40.41	Incl?
08EIk13-3		22.9	0.91	10.1	28.7	82.1	2.83	1.56	16.8	0.72	16.87	51.61	Incl?
08EIk13	3691	12.3	0.46	9.8	28.4	75.1	2.90	0.72	5.7	0.63	16.47	39.56	
08EIk14-1		4.8	0.13	8.0	19.6	40.3	2.44	0.22	7.4	0.66	12.66	42.77	
08EIk14-2		8.1	0.22	9.8	24.5	51.5	2.50	0.43	5.3	0.62	15.55	37.77	
08EIk14-3		4.5	0.09	8.8	17.6	30.9	2.00	0.21	7.7	0.66	12.92	42.62	
08EIk14	3598	5.8	0.1	8.9	20.5	40.9	2.3	0.3	6.8	0.6	13.71	41.05	
Ragged Mtn													
09EIk-R2-1		11.2	0.49	7.1	17.2	59.5	2.42	0.48	9.1	0.69	11.13	47.38	
09EIk-R2-2		11.6	0.43	9.6	24.8	69.4	2.59	0.65	6.7	0.64	15.41	39.28	
09EIk-R2-3		9.3	0.23	9.6	22.4	44.0	2.34	0.55	14.4	0.72	14.83	53.55	
09EIk-R2	3641	10.7	0.4	8.7	21.5	57.6	2.5	0.6	10.1	0.7	13.79	46.74	
09EIk-R1-1		12.6	0.50	7.6	19.5	58.3	2.58	0.57	8.6	0.67	12.13	41.96	
09EIk-R1-2		10.5	0.31	7.8	20.4	44.2	2.63	0.47	6.3	0.63	12.58	37.43	
09EIk-R1-3		17.3	0.58	11.2	24.9	68.3	2.23	1.04	5.7	0.63	17.04	38.63	Incl?
09EIk-R1	3410	11.6	0.4	7.7	20.0	51.2	2.6	0.5	7.4	0.6	12.36	39.70	
09EIk-R3-1		8.8	0.33	11.0	23.1	75.8	2.10	0.56	10.0	0.70	16.42	48.41	
09EIk-R3-2		7.0	0.22	11.8	27.0	69.2	2.29	0.49	9.4	0.69	18.12	46.88	
09EIk-R3-3		9.2	0.45	8.0	21.4	79.5	2.69	0.43	6.5	0.64	12.98	40.00	
09EIk-R3	3280	8.3	0.3	10.2	23.8	74.8	2.4	0.5	8.6	0.7	15.84	45.10	
09EIk-R4-1		6.2	0.19	9.7	21.1	53.7	2.18	0.32	5.2	0.62	14.61	37.58	
09EIk-R4-2		6.6	0.24	6.6	16.9	45.6	2.54	0.25	6.6	0.65	10.61	40.88	
09EIk-R4-3		6.4	0.24	7.8	18.1	53.9	2.32	0.27	4.5	0.62	12.04	39.02	
09EIk-R4	3071	6.4	0.2	8.0	18.7	51.1	2.3	0.3	5.4	0.6	12.42	39.16	
09EIk-R5-1		9.6	0.47	5.6	15.7	56.3	2.79	0.35	8.5	0.68	9.31	47.49	
09EIk-R5-2		6.3	0.24	8.7	21.1	62.5	2.44	0.31	6.4	0.64	13.65	40.01	
09EIk-R5-3		4.7	0.19	8.5	22.5	69.0	2.66	0.24	7.4	0.65	13.78	40.00	
09EIk-R5	2900	6.9	0.3	7.6	19.8	62.6	2.6	0.3	7.4	0.7	12.24	42.50	
09EIk-R6a-1		7.0	0.25	7.5	21.0	54.8	2.81	0.35	11.7	0.71	12.38	53.17	
09EIk-R6a-2		4.2	0.19	7.1	21.7	65.9	3.05	0.19	7.3	0.64	12.20	39.02	
09EIk-R6a-3		15.8	0.76	2.2	10.2	26.7	4.60	0.27	6.8	0.66	4.60	44.78	Incl?
09EIk-R6a	1882	5.6	0.2	7.3	21.3	60.4	2.9	0.3	9.5	0.7	12.29	46.10	
E. Beckwith Mtn													
09EIk-B1-1		26.6	0.91	14.3	29.6	88.0	2.08	2.19	9.4	0.69	21.22	48.64	
09EIk-B1-2		32.3	0.98	20.3	41.8	110.4	2.06	3.34	4.6	0.61	30.15	36.95	
09EIk-B1-3		29.2	0.81	20.7	42.5	102.6	2.05	3.25	6.4	0.65	30.74	41.74	
09EIk-B1	3530	29.4	0.9	18.4	38.0	100.3	2.1	2.9	6.8	0.7	27.37	42.44	

Table B.2 (continued)

Sample	Elevation [m]	Age ± 6% [Ma]	Age ± 6% [Ma]	U [ppm]	Th [ppm]	Sm [ppm]	Th/U	He [nmo/mg]	mass [mg]	Ft	eU [ppm]	r [μm]	comment
09EIk-B2-1		13.9	0.42	10.5	27.5	61.9	2.63	0.98	20.5	0.75	16.93	57.50	
09EIk-B2-2		15.5	0.45	15.4	36.7	84.0	2.39	1.38	8.6	0.67	24.02	42.71	
09EIk-B2-3		15.9	0.48	14.7	32.2	81.8	2.19	1.32	7.0	0.67	22.28	45.05	
09EIk-B2	3401	15.1	0.5	13.5	32.1	75.9	2.4	1.2	12.1	0.7	21.07	48.42	
09EIk-B3-1		26.6	1.34	7.9	19.8	78.7	2.51	1.38	16.8	0.73	12.51	54.08	
09EIk-B3-2		32.4	1.03	10.6	24.1	62.6	2.27	1.97	8.7	0.67	16.25	42.68	
09EIk-B3-3		28.0	0.92	9.6	22.4	59.0	2.35	1.58	8.0	0.68	14.82	47.70	
09EIk-B3	3220	29.0	1.1	9.3	22.1	66.8	2.4	1.6	11.2	0.7	14.53	48.15	
09EIk-B4-1		14.7	0.32	9.8	22.1	39.3	2.25	0.89	15.6	0.73	15.01	55.68	
09EIk-B4-2		17.1	0.54	8.4	18.9	49.0	2.26	0.90	15.1	0.73	12.85	57.81	
09EIk-B4-3		15.7	0.48	10.7	24.6	60.1	2.30	0.94	6.9	0.65	16.47	41.58	
09EIk-B4	3045	15.8	0.4	9.6	21.9	49.5	2.3	0.9	12.6	0.7	14.78	51.69	
Mt Gunnison													
09EIk-G4-1		39.2	1.18	15.8	35.0	87.3	2.21	3.41	6.1	0.65	24.07	41.69	
09EIk-G4-2		29.6	0.97	14.9	32.3	88.3	2.17	2.28	4.4	0.61	22.44	37.92	
09EIk-G4-3		35.1	1.47	16.6	33.1	125.7	1.99	3.03	5.2	0.63	24.40	38.19	
09EIk-G4	3881	34.6	1.2	15.8	33.4	100.4	2.1	2.9	5.2	0.6	23.63	39.27	
09EIk-G3-1		32.9	1.03	13.0	28.5	74.7	2.18	2.74	18.5	0.75	19.73	65.92	
09EIk-G3-2		31.4	1.17	13.8	28.6	93.9	2.07	2.57	11.5	0.71	20.56	51.61	
09EIk-G3-3		31.5	0.90	17.5	35.0	88.6	2.01	3.02	7.6	0.67	25.69	45.09	
09EIk-G3	3698	32.0	1.0	14.8	30.7	85.7	2.1	2.8	12.5	0.7	21.99	54.21	
09EIk-G1-1		33.4	1.06	11.7	24.7	67.5	2.12	2.49	22.1	0.76	17.49	65.81	
09EIk-G1-2		35.5	1.30	13.5	27.8	89.4	2.06	2.68	8.2	0.67	20.03	44.29	
09EIk-G1-3		37.3	1.46	12.9	32.7	98.6	2.54	2.78	6.3	0.64	20.57	40.46	
09EIk-G1	3503	35.4	1.3	12.7	28.4	85.2	2.2	2.6	12.2	0.7	19.36	50.19	

Table B.3: Average exhumation rates calculated from linear regressions of the data plotted on the age vs. elevation plots (Figure 3.4).

Pluton Name	Exhumation Rates (m/Ma)	Corresponding Time Range (Ma)	Corresponding Dating Method
Mt Sopris	66.54	30 - 21.4	AFT
	199.41	12.3 - 9.9	AHe
Capitol Peak	256.27	11.2 - 8.2	AHe
Snowmass Mtn	78.71	28.8 - 17.6	AFT
	71.17	14.8 - 5.8	AHe
Ragged Mtn	85.14	31.1 - 15.4	AFT
	86.36	10.7 - 6.4	AHe
	875.81	6.4 - 5.6	AHe
Marcellina Mtn	191.47	25.7 - 22.4	AFT
Mt Gunnison	137.59	33.8 - 29.0	AFT

Table B.4: Cooling rates calculated for each sample between different isotherms.

Sample	Elevation (m)	Cooling Rates (°C/Ma)			
		(110° to 60°C)	(175° to 110°C)	(275° to 110°C)	(350° to 110°C)
Mt. Sopris					
09EIk-S1	3944	2.84	—	—	—
09EIk-S2	3777	2.65	—	—	72.95
09EIk-S3	3649	3.05	—	24.63	—
09EIk-S4	3523	2.53	—	—	—
09EIk-S5	3107	4.35	—	—	—
09EIk-S7	1622	—	—	—	—
Average		3		25	73
Capitol Peak					
08EIk01	4151	4.17	—	—	22.35
08EIk02	3817	—	—	—	—
08EIk03	3721	—	—	—	—
08EIk04	3762	—	—	—	—
08EIk05	3543	—	16.35	—	—
08EIk06	3386	3.21	—	—	22.77
08EIk07	3229	—	—	—	—
Average		4	16		23
Snowmass Mountain					
08EIk08	4295	3.75	15.25	—	48.68
08EIk09	4201	4.39	—	—	31.66
08EIk10	4107	3.42	—	—	37.33
08EIk11	4020	4.17	—	—	26.06
08EIk12	3827	3.88	—	—	23.83
08EIk13	3691	4.13	7.88	—	25.56
08EIk14	3598	3.14	—	—	19.64
08EIk15	3460	—	—	—	14.73
Average		4	12		28
Ragged Mountain					
09EIk-R2	3641	2.45	—	—	—
09EIk-R1	3410	4.81	—	25.82	—
09EIk-R3	3280	2.28	—	—	—
09EIk-R4	3071	2.42	—	—	—
09EIk-R5	2900	2.48	—	—	—
09EIk-R6a	1882	5.10	34.21	—	—
Average		3	34	26	
Marcellina Mountain					
09EIk-M1	3458	—	—	—	47.43
09EIk-M2	3284	—	—	—	—
09EIk-M3	3156	—	—	—	—
09EIk-M4	2826	—	—	—	—
Average					47
E. Beckwith Mountain					
09EIk-B1	3530	45.45	—	—	—
09EIk-B2	3401	4.00	—	—	118.81
09EIk-B3	3220	50.00	—	—	—
09EIk-B4	3045	3.52	—	—	—
Average		26			119
Mt. Gunnison					
09EIk-G4	3881	—	—	—	—
09EIk-G3	3698	—	—	—	—
09EIk-G1	3503	—	—	—	—
09EIk-G2	3328	—	—	—	—
09EIk-G5	3149	—	—	—	307.69
Average					308

APPENDIX C
ADDITIONAL DATA

Appendix C contains the sample description table (Table C.1), the sample photographs (Figures C.1 – C.7), the regional AFT data table (Table C.2) and the Oligocene plutons data table (Table C.3). The sample descriptions in Table C.1 were collected in the field and by further inspection of the samples with a hand lens. Figures C.1 – C.7 are separated by mountain with a photograph of each sample. Table C.2 contains the age data that was used in Figure 4.8. Table C.3 contains the age data used in Figure 4.7.

Table C.1: Sample Description. Both the fresh (F) and weathered (W) color is given for each sample.

Sample	Location (UTM)*	Color	Texture	General Mineralogy	Other Properties	Alteration	Rock Type
Mount Sopris							
09EIk-S1	313272 4347781	light grayish white (F), reddish brown (W)	porphyritic phaneritic	plagioclase, K-feldspar, quartz, biotite	—	chlorite	quartz monzonite
09EIk-S2	314178 4347276	light brownish gray (F), coppery gray (W)	phaneritic, equigranular	plagioclase, K-feldspar, quartz, biotite	mafic enclaves	chlorite, hematite	quartz monzonite
09EIk-S3	314614 4347307	light-medium pinkish gray (F), reddish brown (W)	porphyritic phaneritic	plagioclase, K-feldspar, quartz, biotite, hornblende	—	chlorite	quartz monzonite
09EIk-S4	314800 4347500	brownish gray (F), dark reddish brown (W)	porphyritic phaneritic	plagioclase, K-feldspar, quartz, biotite, hornblende	—	chlorite	quartz monzonite
09EIk-S5	315067 4348880	light brownish gray (F), medium brownish gray (W)	phaneritic, equigranular	plagioclase, K-feldspar, quartz, biotite, hornblende	—	hematite	quartz monzonite
09EIk-S7	307314 4345606	light gray (F), light brownish gray (W)	phaneritic, equigranular	plagioclase, K-feldspar, quartz, biotite	—	chlorite	quartz monzonite
Capitol Peak							
08EIk01	320571 4335711	light gray (F), light brownish gray (W)	phaneritic, equigranular	plagioclase, K-feldspar, quartz, biotite	aplite vein, slight foliation of mafic minerals	weathered biotites	granodiorite
08EIk02	320921 4336665	pinkish gray (F), brown (W)	porphyritic phaneritic	plagioclase, K-feldspar, quartz, biotite	slight foliation of mafic minerals	weathered biotites	granodiorite
08EIk03	319710 4335754	pinkish gray (F), pinkish brown (W)	phaneritic, equigranular	plagioclase, K-feldspar, biotite, trace quartz	foliation of mafic minerals	chlorite	monzodiorite

Table C.1 (continued)

Sample	Location (UTM)*	Color	Texture	General Mineralogy	Other Properties	Alteration	Rock Type
08EIk04	319612 4336044	medium gray (F), light orange brown (W)	phaneritic, equigranular	plagioclase, K-feldspar, biotite, trace quartz	—	weathered biotites	monzodiorite
08EIk05	320118 4336869	light gray (F), light brown (W)	phaneritic, equigranular	plagioclase, K-feldspar, biotite, trace quartz	—	chlorite	monzodiorite
08EIk06	320945 4336595	medium-dark gray (F), brownish gray (W)	phaneritic, equigranular	plagioclase, biotite	foliation of mafic minerals (dipping 20°E)	weathered biotites	diorite
08EIk07	319528 4338489	light gray (F), brown (W)	phaneritic, equigranular	plagioclase, K-feldspar, biotite, trace quartz	—	chlorite, iron-oxides	monzodiorite
Snowmass Mountain							
08EIk08	321400 4331780	grayish white (F), light brown (W)	phaneritic, equigranular	plagioclase, K-feldspar, quartz, biotite	—	some weathered biotites	granodiorite
08EIk09	321278 4331773	grayish white (F), light brown (W)	phaneritic, equigranular	plagioclase, K-feldspar, quartz, biotite, hornblende	—	chlorite	granodiorite
08EIk10	321160 4331748	grayish white (F), light brown (W)	phaneritic, equigranular	plagioclase, K-feldspar, quartz, biotite, hornblende	—	chlorite	granodiorite
08EIk11	321068 4331674	grayish white (F), light brown (W)	phaneritic, equigranular	plagioclase, K-feldspar, quartz, biotite, hornblende	—	chlorite	granodiorite
08EIk12	320826 4331632	light pinkish gray (F), light brown (W)	phaneritic, equigranular	plagioclase, K-feldspar, quartz, biotite, hornblende	—	chlorite	granodiorite

Table C.1 (continued)

Sample	Location (UTM)*	Color	Texture	General Mineralogy	Other Properties	Alteration	Rock Type
08Elk13	320616 4331516	grayish white (F), light brown (W)	phaneritic, equigranular	plagioclase, K-feldspar, quartz, biotite, hornblende	biotite schist xenoliths	chlorite	granodiorite
08Elk14	320209 4331326	dark gray (F), brown (W)	phaneritic, equigranular	plagioclase, biotite	foliation of mafic minerals	—	diorite
08Elk15	320029 4330389	medium-dark gray (F), brownish gray (W)	phaneritic, equigranular	plagioclase, biotite, trace K-feldspar	—	weathered biotites	diorite
Ragged Mountain							
09Elk-R2	308470 4322419	light gray (F), light brown (W)	porphyritic phaneritic	plagioclase, K-feldspar, quartz, biotite, hornblende	—	weathered biotites, chlorite?	porphyritic granodiorite
09Elk-R1	310628 4322428	light brownish gray (F), medium brown (W)	porphyritic phaneritic	plagioclase, K-feldspar, quartz, biotite, hornblende	—	chlorite	porphyritic granodiorite
09Elk-R3	309806 4322976	light-medium brown (F), medium brown (W)	porphyritic phaneritic	plagioclase, K-feldspar, quartz, biotite, hornblende	—	weathered biotites	porphyritic granodiorite
09Elk-R4	309790 4323388	light grayish white (F), light brown (W)	porphyritic phaneritic	plagioclase, K-feldspar, quartz, biotite, hornblende	—	chlorite	porphyritic granodiorite
09Elk-R5	309554 4324477	grayish white (F), medium brown (W)	porphyritic phaneritic	plagioclase, K-feldspar, quartz, biotite, hornblende	mafic enclaves	weathered biotites	porphyritic granodiorite
09Elk-R6a	307496 4327624	light gray (F), light brown (W)	porphyritic phaneritic	plagioclase, K-feldspar, quartz, biotite, hornblende	mafic enclaves	weathered biotites, chlorite?	porphyritic granodiorite

Table C.1 (continued)

Sample	Location (UTM)*	Color	Texture	General Mineralogy	Other Properties	Alteration	Rock Type
Marcellina Mountain							
09Elk-M1	305549 4311177	medium gray (F), brown (W)	phaneritic, equigranular	plagioclase, biotite, hornblende, trace K-feldspar & quartz	mafic enclaves	weathered biotites	diorite
09Elk-M2	306433 4311255	light brownish gray (F), light brown (W)	phaneritic, equigranular	plagioclase, biotite, hornblende	mafic enclaves	weathered biotites	diorite
09Elk-M3	306696 4311286	medium gray (F), brown (W)	phaneritic, equigranular	plagioclase, biotite, trace quartz	mafic enclaves	weathered biotites	diorite
09Elk-M4	307181 4311005	light brownish gray (F), light brownish gray (W)	phaneritic, equigranular	plagioclase, biotite, hornblende	mafic enclaves	weathered biotites	diorite
East Beckwith Mountain							
09Elk-B1	307473 4302534	light gray (F), brown (W)	phaneritic, equigranular	plagioclase, K-feldspar, quartz, biotite	mafic enclaves	—	granodiorite
09Elk-B2	307624 4302599	gray (F), light brown (W)	porphyritic phaneritic	plagioclase, K-feldspar, quartz, biotite, hornblende	quartz phenocrysts	fine grained matrix slightly chalky	porphyritic granodiorite
09Elk-B3	308017 4303109	purple brown (F), reddish brown (W)	porphyritic phaneritic	plagioclase, K-feldspar, quartz, biotite, hornblende	—	hornblende alteration	porphyritic granodiorite
09Elk-B4	308357 4303365	purple brown (F), brown (W)	porphyritic phaneritic	plagioclase, K-feldspar, quartz, biotite, hornblende	quartz & K-spar phenocrysts	—	porphyritic granodiorite
Mount Gunnison							
09Elk-G4	293147 4298419	light grayish brown (F), brown (W)	porphyritic phaneritic	plagioclase, K-feldspar, quartz, biotite	—	—	porphyritic granodiorite

Table C.1 (continued)

Sample	Location (UTM)*	Color	Texture	General Mineralogy	Other Properties	Alteration	Rock Type
09Elk-G3	292720 4297113	light grayish brown (F), brown (W)	porphyritic phaneritic	plagioclase, K-feldspar, quartz, biotite	—	weathered biotites	porphyritic granodiorite
09Elk-G1	292400 4297332	light brown (F), brown (W)	porphyritic phaneritic	plagioclase, K-feldspar, quartz, biotite	xenoliths	weathered biotites	porphyritic granodiorite
09Elk-G2	292060 4297494	light brown (F), pinkish brown (W)	porphyritic phaneritic	plagioclase, K-feldspar, quartz, biotite	—	weathered biotites	porphyritic granodiorite
09Elk-G5	291547 4297553	medium brown (F), dark brown (W)	porphyritic phaneritic	plagioclase, K-feldspar, quartz, biotite, hornblende	plagioclase & quartz stained brown	weathered biotites	porphyritic granodiorite

*UTM datum is NAD27, zone 13S



(a) 09Elk-S1 (3944m), quartz monzonite



(d) 09Elk-S4 (3523m), quartz monzonite



(b) 09Elk-S2 (3777m), quartz monzonite



(e) 09Elk-S5 (3107m), quartz monzonite



(c) 09Elk-S3 (3649m), quartz monzonite



(f) 09Elk-S7 (1622m), quartz monzonite

Figure C.1: Mount Sopris sample photographs.



(a) 08Elk01 (4151m), granodiorite



(e) 08Elk05 (3543m), monzodiorite



(b) 08Elk02 (3817m), granodiorite



(f) 08Elk06 (3386m), diorite



(c) 08Elk03 (3721m), monzodiorite



(g) 08Elk07 (3229m), monzodiorite



(d) 08Elk04 (3763m), monzodiorite

Figure C.2: Capitol Peak sample photographs.



(a) 08Elk08 (4295m), granodiorite



(e) 08Elk12 (3827m), granodiorite



(b) 08Elk09 (4201m), granodiorite



(f) 08Elk13 (3691m), granodiorite



(c) 08Elk10 (4107m), granodiorite



(g) 08Elk14 (3598m), diorite



(d) 08Elk11 (4020m), granodiorite



(h) 08Elk15 (3460m), diorite

Figure C.3: Snowmass Mountain sample photographs.



(a) 09Elk-R2 (3641m), porphyritic granodiorite



(d) 09Elk-R4 (3071m), porphyritic granodiorite



(b) 09Elk-R1 (3410m), porphyritic granodiorite



(e) 09Elk-R5 (2900m), porphyritic granodiorite



(c) 09Elk-R3 (3280m), porphyritic granodiorite



(f) 09Elk-R6a (1882m), porphyritic granodiorite

Figure C.4: Ragged Mountain sample photographs.



(a) 09Elk-M1 (3458m), diorite



(c) 09Elk-M3 (3156m), diorite



(b) 09Elk-M2 (3284m), diorite



(d) 09Elk-M4 (2826m), diorite

Figure C.5: Marcellina Mountain sample photographs.



(a) 09Elk-B1 (3530m), granodiorite



(c) 09Elk-B3 (3220m), porphyritic granodiorite



(b) 09Elk-B2 (3401m), porphyritic granodiorite



(d) 09Elk-B4 (3045m), porphyritic granodiorite

Figure C.6: East Beckwith Mountain sample photographs.



(a) 09Elk-G4 (3881m), porphyritic granodiorite



(d) 09Elk-G2 (3328m), porphyritic granodiorite



(b) 09Elk-G3 (3698m), porphyritic granodiorite



(e) 09Elk-G5 (3149m), porphyritic granodiorite



(c) 09Elk-G1 (3503m), porphyritic granodiorite

Figure C.7: Mount Gunnison sample photographs.

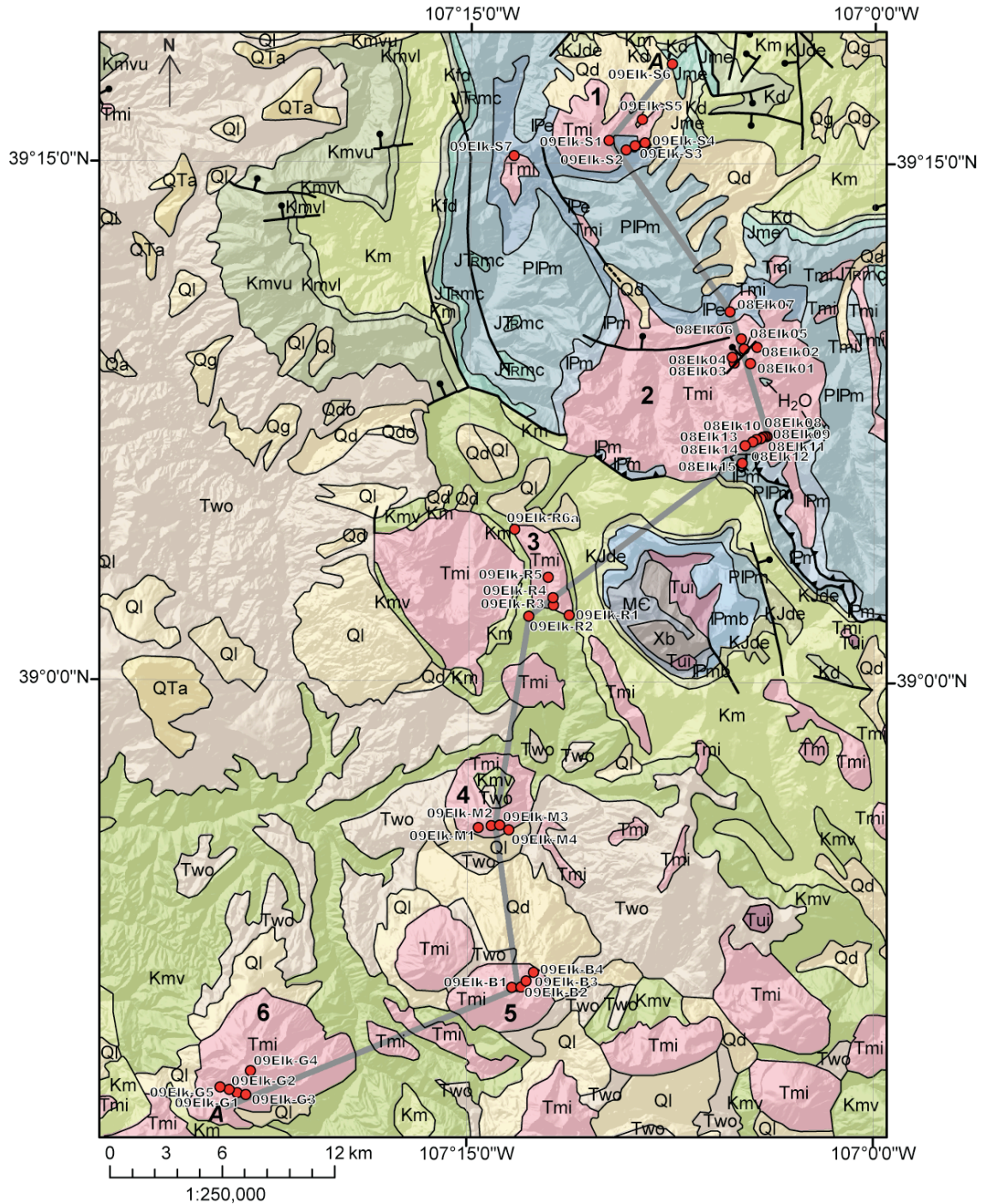


Figure C.8: Sample location map. Geology from Tweto (1979).

Table C.2: Regional apatite fission-track data. Ages mostly compiled from Klein et al. (2009). Data used for Figure 4.8.

Latitude	Longitude	Elevation	Age (Ma)	Error (Ma)	Rock Type	Location	Reference
39.58670	-105.84100	--	40.2	17.6	Granite	--	Bookstrom et al., 1987
39.06556	-106.39972	2819	16.0	2.40	Aplite	Sawatch Range	Bryant and Naeser, 1980
39.07250	-106.45083	3005	19.9	4.40	Granodiorite	Sawatch Range	Bryant and Naeser, 1980
39.07056	-106.40306	2926	20.0	2.90	Granodiorite	Sawatch Range	Bryant and Naeser, 1980
39.03056	-106.76861	3450	27.9	3.90	Basement	Sawatch Range	Bryant and Naeser, 1980
39.06917	-106.50972	3109	29.9	4.20	Granodiorite	Sawatch Range	Bryant and Naeser, 1980
39.50167	-105.93278	3145	45.1	5.90	Basement	South Park to Swan River	Bryant and Naeser, 1980
39.41361	-105.75889	3048	49.8	4.00	Monzonite	South Park to Swan River	Bryant and Naeser, 1980
39.23583	-106.75139	2966	51.1	5.50	Monzonite	Sawatch Range	Bryant and Naeser, 1980
39.19972	-106.77444	3091	52.5	12.80	Basement	Sawatch Range	Bryant and Naeser, 1980
39.63389	-105.55028	3350	57.8	8.70	Granodiorite	Front Range -- Mt Evans and East	Bryant and Naeser, 1980
39.63639	-105.52194	2929	66.5	4.00	Granodiorite	Front Range -- Mt Evans and East	Bryant and Naeser, 1980
39.61278	-105.43056	2401	68.5	5.00	Monzonite	Front Range -- Mt Evans and East	Bryant and Naeser, 1980
39.45944	-105.40583	3651	79.0	38.00	Basement	South Park to Swan River	Bryant and Naeser, 1980
39.58000	-105.63056	4017	90.2	12.70	Granodiorite	Front Range -- Mt Evans and East	Bryant and Naeser, 1980
39.63222	-105.60361	3703	98.0	5.00	Granodiorite	Front Range -- Mt Evans and East	Bryant and Naeser, 1980
39.30694	-105.75278	2800	124.0	18.00	Monzonite	South Park to Swan River	Bryant and Naeser, 1980
39.29722	-105.70833	2761	130.0	25.00	Monzonite	South Park to Swan River	Bryant and Naeser, 1980
39.57111	-105.64167	4312	134.0	7.00	Monzonite	Front Range -- Mt Evans and East	Bryant and Naeser, 1980
39.32278	-105.75833	2822	148.0	1.90	Monzonite	South Park to Swan River	Bryant and Naeser, 1980
39.30917	-105.76806	2859	245.0	30.00	Monzonite	South Park to Swan River	Bryant and Naeser, 1980
39.09139	-105.71806	2804	352.0	18.00	Granite	South Park to Swan River	Bryant and Naeser, 1980
39.18611	-105.79778	2910	473.0	100.00	Monzonite	South Park to Swan River	Bryant and Naeser, 1980
39.06560	-106.40000	--	16	4.8	Aplite	--	Bryant and Naeser, 1980
39.07250	-106.45100	--	19.9	8.8	--	--	Bryant and Naeser, 1980
39.07060	-106.40300	--	20	5.8	--	--	Bryant and Naeser, 1980
39.03060	-106.76900	--	27.9	7.8	Migmatite	--	Bryant and Naeser, 1980
39.06920	-106.51000	--	29.9	8.4	--	--	Bryant and Naeser, 1980
39.50170	-105.93300	--	45.1	11.8	Gneiss	--	Bryant and Naeser, 1980

Table C.2 (continued)

Latitude	Longitude	Elevation	Age (Ma)	Error (Ma)	Rock Type	Location	Reference
39.41360	-105.75900	--	49.8	8	Monzonite	--	Bryant and Naeser, 1980
39.23580	-106.75100	--	51.1	11	Monzonite	--	Bryant and Naeser, 1980
39.19970	-106.77400	--	52.5	25.6	Monzonite	--	Bryant and Naeser, 1980
39.63390	-105.55000	--	57.8	17.4	Gneiss	--	Bryant and Naeser, 1980
39.63640	-105.52200	--	66.5	8	Gneiss	--	Bryant and Naeser, 1980
39.61280	-105.43100	--	68.5	10	GNEISS	--	Bryant and Naeser, 1980
39.45940	-105.40600	--	79	76	Amphibolite	--	Bryant and Naeser, 1980
39.58000	-105.63100	--	90.2	25.4	GNEISS	--	Bryant and Naeser, 1980
39.63220	-105.60400	--	98	10	Gneiss	--	Bryant and Naeser, 1980
39.30690	-105.75300	--	124	36	Monzonite	--	Bryant and Naeser, 1980
39.29720	-105.70800	--	130	60	Monzonite	--	Bryant and Naeser, 1980
39.29720	-105.70800	--	130	30	Monzonite	--	Bryant and Naeser, 1980
39.57110	-105.64200	--	134	7	Gneiss	--	Bryant and Naeser, 1980
39.32280	-105.75800	--	148	19	Monzonite	--	Bryant and Naeser, 1980
39.30920	-105.76800	--	245	30	Monzonite	--	Bryant and Naeser, 1980
39.09140	-105.71800	--	352	18	Granite	--	Bryant and Naeser, 1980
39.18610	-105.79800	--	473	100	Monzonite	--	Bryant and Naeser, 1980
39.14030	-106.82300	--	22.3	18.4	--	--	Bryant, 1990
39.76330	-105.72200	--	37.3	4.4	--	--	Cunningham, 1977
37.98470	-107.71100	--	7.8	7	--	--	Cunningham et al., 1994
37.99440	-107.70400	--	14.9	11.4	--	--	Cunningham et al., 1994
37.63970	-108.05600	--	20.3	14.8	--	--	Cunningham et al., 1994
39.25000	-106.24100	--	34.8	9.8	--	--	Cunningham et al., 1994
40.11110	-105.39200	--	47.1	11.6	--	--	Cunningham et al., 1994
39.95170	-105.58800	--	58.6	18.8	--	--	Cunningham et al., 1994
37.27970	-108.78100	--	66.8	16.2	--	--	Cunningham et al., 1994
39.86750	-105.55500	--	66.8	15	--	--	Cunningham et al., 1994
39.86750	-105.55500	--	71.3	36	--	--	Cunningham et al., 1994
37.43690	-108.01500	--	79	42	--	--	Cunningham et al., 1994
38.99100	-106.41326	3053	10.2	1.9	Granite	Twin Lakes Batholith	Feldman et al., 2010
38.94506	-106.45770	3289	13.1	2	Granite	Twin Lakes Batholith	Feldman et al., 2010
38.98955	-106.41515	3059	13.3	1.8	Granite	Twin Lakes Batholith	Feldman et al., 2010
38.94852	-106.43664	4104	18.5	1.7	Granite	Twin Lakes Batholith	Feldman et al., 2010
38.95357	-106.44267	3884	21.2	1.6	Granite	Twin Lakes Batholith	Feldman et al., 2010
38.99739	-106.56186	4120	22.8	6.3	Granite	Twin Lakes Batholith	Feldman et al., 2010

Table C.2 (continued)

Latitude	Longitude	Elevation	Age (Ma)	Error (Ma)	Rock Type	Location	Reference
38.95511	-106.45600	3506	22.8	2.3	Granite	Twin Lakes Batholith	Feldman et al., 2010
38.94550	-106.43807	4268	34.5	3	Granite	Twin Lakes Batholith	Feldman et al., 2010
39.26115	-107.16424	3944	30	4.2	quartz monzonite	Mount Sopris	Garcia et al., 2011
39.25680	-107.15360	3777	31.3	4	quartz monzonite	Mount Sopris	Garcia et al., 2011
39.25717	-107.14856	3649	26.5	4.9	quartz monzonite	Mount Sopris	Garcia et al., 2011
39.25895	-107.14646	3523	30	4.6	quartz monzonite	Mount Sopris	Garcia et al., 2011
39.27143	-107.14375	3107	21.4	3.7	quartz monzonite	Mount Sopris	Garcia et al., 2011
39.15400	-107.07649	4151	23.2	2.6	granodiorite	Capitol Peak	Garcia et al., 2011
39.16266	-107.07269	3817	22.3	4.7	granodiorite	Capitol Peak	Garcia et al., 2011
39.16433	-107.08203	3543	23.1	3.9	granodiorite	Capitol Peak	Garcia et al., 2011
39.16203	-107.07240	3386	23.8	2.6	granodiorite	Capitol Peak	Garcia et al., 2011
39.11877	-107.06587	4295	28.8	3.7	granodiorite	Snowmass Mountain	Garcia et al., 2011
39.11868	-107.06727	4201	26.4	3.4	granodiorite	Snowmass Mountain	Garcia et al., 2011
39.11843	-107.06863	4107	27.5	3.3	granodiorite	Snowmass Mountain	Garcia et al., 2011
39.11774	-107.06968	4020	24.5	3.2	granodiorite	Snowmass Mountain	Garcia et al., 2011
39.11732	-107.07246	3827	23.5	2.8	granodiorite	Snowmass Mountain	Garcia et al., 2011
39.11623	-107.07486	3691	24.4	2.7	granodiorite	Snowmass Mountain	Garcia et al., 2011
39.11443	-107.07951	3598	21.7	2.9	diorite	Snowmass Mountain	Garcia et al., 2011
39.10596	-107.08135	3460	17.6	8.1	diorite	Snowmass Mountain	Garcia et al., 2011
39.03173	-107.21269	3641	31.1	3.2	porphyritic granodiorite	Ragged Mountain	Garcia et al., 2011
39.03228	-107.18778	3410	22	2.5	porphyritic granodiorite	Ragged Mountain	Garcia et al., 2011
39.03703	-107.19742	3280	30.2	3	porphyritic granodiorite	Ragged Mountain	Garcia et al., 2011
39.04074	-107.19772	3071	27.1	2.8	porphyritic granodiorite	Ragged Mountain	Garcia et al., 2011
39.05050	-107.20075	2900	27.1	2.9	porphyritic granodiorite	Ragged Mountain	Garcia et al., 2011
39.07838	-107.22541	1882	15.4	2	porphyritic granodiorite	Ragged Mountain	Garcia et al., 2011
38.92985	-107.24321	3458	25.7	4.6	granodiorite	Marcellina Mountain	Garcia et al., 2011
38.92866	-107.22435	2826	22.4	9.5	granodiorite	Marcellina Mountain	Garcia et al., 2011
38.85245	-107.21861	3530	30.5	3.8	granodiorite	E. Beckwith Mountain	Garcia et al., 2011

Table C.2 (continued)

Latitude	Longitude	Elevation	Age (Ma)	Error (Ma)	Rock Type	Location	Reference
38.85307	-107.21689	3401	27.6	3.2	granodiorite	E. Beckwith Mountain	Garcia et al., 2011
38.85774	-107.21251	3220	30	3	granodiorite	E. Beckwith Mountain	Garcia et al., 2011
38.86012	-107.20866	3045	30	3.2	granodiorite	E. Beckwith Mountain	Garcia et al., 2011
38.81214	-107.38233	3881	33.8	4.9	porphyritic granodiorite	Mount Gunnison	Garcia et al., 2011
38.80028	-107.38685	3698	32.5	3.4	porphyritic granodiorite	Mount Gunnison	Garcia et al., 2011
38.80218	-107.39060	3503	30.1	3.5	porphyritic granodiorite	Mount Gunnison	Garcia et al., 2011
38.80397	-107.40048	3149	29	3.5	porphyritic granodiorite	Mount Gunnison	Garcia et al., 2011
40.33000	-106.25000	--	24	10	--	--	Karimpour, 1982
40.33000	-106.25000	--	24.04	10	--	--	Karimpour, 1982
39.23330	-107.87000	686	42.8	8.20	SS/Shale/Conglom	MWX Well	Kelley and Blackwell, 1990
39.23330	-107.87000	463	27.7	4.30	SS/Shale/Conglom	MWX Well	Kelley and Blackwell, 1990
39.23330	-107.87000	340	3.6	0.60	SS/Shale/Conglom	MWX Well	Kelley and Blackwell, 1990
39.23330	-107.87000	324	21.0	4.40	SS/Shale/Conglom	MWX Well	Kelley and Blackwell, 1990
39.23330	-107.87000	247	6.3	0.90	SS/Shale/Conglom	MWX Well	Kelley and Blackwell, 1990
39.23330	-107.87000	133	6.7	1.40	SS/Shale/Conglom	MWX Well	Kelley and Blackwell, 1990
39.23330	-107.87000	97	3.0	0.40	SS/Shale/Conglom	MWX Well	Kelley and Blackwell, 1990
39.23330	-107.87000	-55	3.8	0.60	SS/Shale/Conglom	MWX Well	Kelley and Blackwell, 1990
39.23330	-107.87000	-110	3.7	0.90	SS/Shale/Conglom	MWX Well	Kelley and Blackwell, 1990
39.23330	-107.87000	-215	2.2	0.40	SS/Shale/Conglom	MWX Well	Kelley and Blackwell, 1990
39.23330	-107.87000	-270	2.6	0.30	SS/Shale/Conglom	MWX Well	Kelley and Blackwell, 1990
39.23330	-107.87000	-349	1.9	0.50	SS/Shale/Conglom	MWX Well	Kelley and Blackwell, 1990
39.23330	-107.87000	-409	3.5	0.60	SS/Shale/Conglom	MWX Well	Kelley and Blackwell, 1990
39.23330	-107.87000	-442	2.5	0.50	SS/Shale/Conglom	MWX Well	Kelley and Blackwell, 1990
39.23330	-107.87000	-535	2.5	0.60	SS/Shale/Conglom	MWX Well	Kelley and Blackwell, 1990
39.23330	-107.87000	-576	1.3	0.60	SS/Shale/Conglom	MWX Well	Kelley and Blackwell, 1990
39.23330	-107.87000	-766	1.8	0.60	SS/Shale/Conglom	MWX Well	Kelley and Blackwell, 1990
39.23330	-107.87000	-788	1.4	0.50	SS/Shale/Conglom	MWX Well	Kelley and Blackwell, 1990
39.23330	-107.87000	-837	1.0	0.20	SS/Shale/Conglom	MWX Well	Kelley and Blackwell, 1990
38.70267	-105.12467	2963	26.9	4	Granodiorite	Pikes Peak	Kelley and Chapin, 2004
38.04633	-105.00400	1900	31.1	7.4	Migmatitic gneiss	Wet Mountains	Kelley and Chapin, 2004

Table C.2 (continued)

Latitude	Longitude	Elevation	Age (Ma)	Error (Ma)	Rock Type	Location	Reference
38.07650	-104.99150	1940	31.3	5.8	Migmatitic gneiss	Wet Mountains	Kelley and Chapin, 2004
40.13850	-105.67400	3389	41	10.8	Granitic gneiss	Indean Peaks	Kelley and Chapin, 2004
39.63583	-105.81117	4139	43	7.4	Gneiss	Grays Peak	Kelley and Chapin, 2004
40.68917	-105.42867	2034	44.4	10.4	Granite breccia	Cache la Poudre River	Kelley and Chapin, 2004
38.58833	-104.94833	2055	44.5	8.6	Quartz	Pikes Peak	Kelley and Chapin, 2004
40.26027	-105.62153	4023	45.1	17	Granite	Longs Peak/St. Vrain River	Kelley and Chapin, 2004
40.42250	-105.23217	1720	45.4	6.8	Granite	Big Thompson Canyon	Kelley and Chapin, 2004
38.49233	-105.76217	2865	46.7	6.6	Granodiorite	Royal Gorge Arkansas River	Kelley and Chapin, 2004
40.16905	-105.46310	2499	46.9	11.8	Granite	Longs Peak/St. Vrain River	Kelley and Chapin, 2004
40.68450	-105.77250	2524	47.1	14.2	Granodiorite	Cache la Poudre River	Kelley and Chapin, 2004
39.43883	-105.12367	1798	47.1	12.8	Gneiss	North Fork, South Platte River	Kelley and Chapin, 2004
40.27127	-105.55483	2835	47.3	8.4	Granite	Longs Peak/St. Vrain River	Kelley and Chapin, 2004
40.20467	-105.30633	1725	47.5	10.4	Granite porphyry	Longs Peak/St. Vrain River	Kelley and Chapin, 2004
39.74683	-105.43600	2207	47.7	13	Gneiss	Clear Creek	Kelley and Chapin, 2004
40.55600	-105.77833	2835	47.8	9.4	Gneiss	Cache la Poudre River	Kelley and Chapin, 2004
40.37367	-105.48817	2300	48.7	13.6	Granitic gneiss	Big Thompson Canyon	Kelley and Chapin, 2004
39.80183	-105.25833	2012	48.8	13.8	Gneiss	Von Bibber Creek	Kelley and Chapin, 2004
40.27250	-105.58625	3383	49.2	10.2	Granite	Longs Peak/St. Vrain River	Kelley and Chapin, 2004
40.21517	-105.27617	1650	49.5	6.8	Sandstone	Longs Peak/St. Vrain River	Kelley and Chapin, 2004
40.83600	-105.31233	2000	50	10.2	Granitic gneiss	Front Range -- Northeast	Kelley and Chapin, 2004
39.87950	-105.27300	2012	50.8	10.4	Meta Rhyolite	Boulder Canyon Coal Creek	Kelley and Chapin, 2004
40.29273	-105.52262	3292	50.9	8.4	Granitic gneiss	Longs Peak/St. Vrain River	Kelley and Chapin, 2004
40.92767	-105.27467	2150	51	10.6	Granite	Front Range -- Northeast	Kelley and Chapin, 2004
39.41083	-105.16417	1878	51.0	11.2	Amphibolite	North Fork, South Platte River	Kelley and Chapin, 2004

Table C.2 (continued)

Latitude	Longitude	Elevation	Age (Ma)	Error (Ma)	Rock Type	Location	Reference
40.34783	-105.66667	2682	51.1	10.4	Granodiorite	Longs Peak/St. Vrain River	Kelley and Chapin, 2004
40.25517	-105.61498	4343	51.7	8.6	Granite	Longs Peak/St. Vrain River	Kelley and Chapin, 2004
37.91833	-104.97333	2329	51.7	13.6	Migmatitic gneiss	Wet Mountains	Kelley and Chapin, 2004
39.74300	-105.40650	2140	52.4	11.6	Gneiss	Clear Creek	Kelley and Chapin, 2004
40.69817	-105.59150	2191	52.5	7.4	Granodiorite	Cache la Poudre River	Kelley and Chapin, 2004
39.84717	-105.35450	2310	52.6	8.2	Gneiss	Von Bibber Creek	Kelley and Chapin, 2004
39.83333	-105.32833	2493	52.8	11.8	Gneiss	Von Bibber Creek	Kelley and Chapin, 2004
40.12550	-105.67200	2926	53	8.6	Granitic gneiss	Indean Peaks	Kelley and Chapin, 2004
40.18220	-105.34163	1900	53.1	11.6	Granite	Longs Peak/St. Vrain River	Kelley and Chapin, 2004
40.27475	-105.60518	3688	53.3	10.8	Granite	Longs Peak/St. Vrain River	Kelley and Chapin, 2004
39.73450	-105.36733	2218	53.3	7.8	Granitic gneiss	Clear Creek	Kelley and Chapin, 2004
38.17500	-105.14833	2256	53.4	11	Migmatitic gneiss	Wet Mountains	Kelley and Chapin, 2004
40.73867	-105.37367	2150	54	11.4	Granite	Front Range -- Northeast	Kelley and Chapin, 2004
39.75200	-105.35867	2645	54.0	8.6	Granitic gneiss	Clear Creek	Kelley and Chapin, 2004
40.29517	-105.53217	2938	54.1	8.4	Granitic gneiss	Longs Peak/St. Vrain River	Kelley and Chapin, 2004
40.43400	-105.72550	3463	54.5	7.4	Mica schist	Longs Peak/St. Vrain River	Kelley and Chapin, 2004
40.17132	-105.37960	2100	54.6	9	Granite	Longs Peak/St. Vrain River	Kelley and Chapin, 2004
38.37133	-105.68300	1951	54.7	9	Granodiorite	Royal Gorge Arkansas River	Kelley and Chapin, 2004
38.49633	-105.78600	2633	54.9	10.2	Granodiorite	Royal Gorge Arkansas River	Kelley and Chapin, 2004
39.41550	-105.64067	3334	55.1	22.4	Gneiss	North Fork, South Platte River	Kelley and Chapin, 2004
40.25495	-105.61902	4121	55.1	8.4	Granite	Longs Peak/St. Vrain River	Kelley and Chapin, 2004
40.42983	-105.31867	1900	55.3	19.6	Granite	Big Thompson Canyon	Kelley and Chapin, 2004
39.74617	-105.43817	2207	55.6	11.8	Gneiss	Clear Creek	Kelley and Chapin, 2004

Table C.2 (continued)

Latitude	Longitude	Elevation	Age (Ma)	Error (Ma)	Rock Type	Location	Reference
39.74517	-105.28233	2097	56	7.6	Granitic gneiss	Clear Creek	Kelley and Chapin, 2004
40.66483	-105.21483	1609	56.4	7.8	Schist	Cache la Poudre River	Kelley and Chapin, 2004
40.13267	-105.66900	3548	56.8	8.6	Granitic gneiss	Indean Peaks	Kelley and Chapin, 2004
38.54867	-105.10367	2054	56.8	17.8	Migmatitic gneiss	Pikes Peak	Kelley and Chapin, 2004
38.50400	-105.10483	1777	57.1	14.2	Migmatitic gneiss	Pikes Peak	Kelley and Chapin, 2004
39.74800	-105.36100	2518	57.2	12	Granitic gneiss	Clear Creek	Kelley and Chapin, 2004
40.63283	-105.80550	2569	57.3	9.8	Granodiorite	Cache la Poudre River	Kelley and Chapin, 2004
40.43383	-105.70033	3780	57.6	6.8	Schist	Longs Peak/St. Vrain River	Kelley and Chapin, 2004
39.46200	-105.67833	2700	57.6	8.2	Granite	North Fork, South Platte River	Kelley and Chapin, 2004
40.14133	-105.50217	2682	57.6	9.4	Granite	Longs Peak/St. Vrain River	Kelley and Chapin, 2004
40.69183	-105.25533	1655	57.6	7.8	Gneiss	Cache la Poudre River	Kelley and Chapin, 2004
40.38133	-105.46867	2250	57.9	13.4	Granitic gneiss	Big Thompson Canyon	Kelley and Chapin, 2004
39.87900	-105.27067	2012	58.1	14.2	Granite	Boulder Canyon Coal Creek	Kelley and Chapin, 2004
39.50183	-105.68333	2875	58.5	8.2	Biotite gneiss	North Fork, South Platte River	Kelley and Chapin, 2004
38.43617	-105.71650	2512	59	8.6	Granodiorite	Royal Gorge Arkansas River	Kelley and Chapin, 2004
39.80383	-105.25867	1951	59.3	9.8	Gneiss	Von Bibber Creek	Kelley and Chapin, 2004
39.74267	-105.28283	1951	59.4	9.6	Granitic gneiss	Clear Creek	Kelley and Chapin, 2004
39.40600	-105.47233	2365	59.6	15.4	Diorite	North Fork, South Platte River	Kelley and Chapin, 2004
39.74233	-105.29333	1877	59.7	8	Granite	Clear Creek	Kelley and Chapin, 2004
38.51950	-105.12483	1866	59.7	11	Migmatitic gneiss	Pikes Peak	Kelley and Chapin, 2004
39.78533	-105.35517	2390	60.1	8.2	Granitic lens	Golden Gate Canyon	Kelley and Chapin, 2004
40.16808	-105.44777	2350	60.2	18.6	Granite (more mafic)	Longs Peak/St. Vrain River	Kelley and Chapin, 2004
39.41433	-105.51867	2414	60.5	13.6	Granite	North Fork, South Platte River	Kelley and Chapin, 2004
38.61983	-105.44867	2268	60.6	14.4	quartz diorite	Currant Creek Shear Zone	Kelley and Chapin, 2004
39.74350	-105.28483	1938	61.0	9.8	Granitic gneiss	Clear Creek	Kelley and Chapin, 2004

Table C.2 (continued)

Latitude	Longitude	Elevation	Age (Ma)	Error (Ma)	Rock Type	Location	Reference
39.74633	-105.28100	2152	61.8	9	Granitic gneiss	Clear Creek	Kelley and Chapin, 2004
40.67683	-105.42900	1938	61.9	10.2	Schist	Cache la Poudre River	Kelley and Chapin, 2004
39.74133	-105.32767	2005	62.3	9.2	Gneiss	Clear Creek	Kelley and Chapin, 2004
40.01317	-105.30167	1675	62.3	7.6	Granitic gneiss	Boulder Canyon Coal Creek	Kelley and Chapin, 2004
38.43883	-105.67700	2362	62.4	8.8	Granodiorite	Royal Gorge Arkansas River	Kelley and Chapin, 2004
38.43700	-105.66633	2515	62.5	9.2	Granodiorite	Royal Gorge Arkansas River	Kelley and Chapin, 2004
40.42250	-105.35483	2000	62.5	9.4	Granite (2 mica)	Big Thompson Canyon	Kelley and Chapin, 2004
39.78433	-105.33000	2360	62.5	8.4	Schist	Golden Gate Canyon	Kelley and Chapin, 2004
39.82200	-105.28433	2256	63.1	14.2	Schist	Von Bibber Creek	Kelley and Chapin, 2004
39.74317	-105.28233	2030	63.1	11.2	Granitic gneiss	Clear Creek	Kelley and Chapin, 2004
40.69617	-105.43717	1975	63.4	9.8	Gneiss	Cache la Poudre River	Kelley and Chapin, 2004
38.60617	-105.21883	1915	63.6	8	Granodiorite	Pikes Peak	Kelley and Chapin, 2004
38.43083	-105.70717	2396	63.9	10.4	Arkose	Royal Gorge Arkansas River	Kelley and Chapin, 2004
39.47750	-105.12950	1762	64.4	8.2	Granite	North Fork, South Platte River	Kelley and Chapin, 2004
40.43067	-105.23167	1700	64.8	16.8	Granite porphyry	Big Thompson Canyon	Kelley and Chapin, 2004
39.44617	-105.12167	1768	65.2	9	Gneiss	North Fork, South Platte River	Kelley and Chapin, 2004
39.46883	-105.24050	2219	65.9	11.4	Granite	North Fork, South Platte River	Kelley and Chapin, 2004
39.48283	-105.69267	2750	66	9	Granitic gneiss	North Fork, South Platte River	Kelley and Chapin, 2004
39.47200	-105.13450	1719	66.1	12.4	Schist	North Fork, South Platte River	Kelley and Chapin, 2004
38.61400	-105.13333	2482	66.2	7.8	Granodiorite	Pikes Peak	Kelley and Chapin, 2004
38.57150	-105.08600	2183	66.6	12.6	Granodiorite	Pikes Peak	Kelley and Chapin, 2004
39.74350	-105.36717	2316	66.8	11.6	Granitic gneiss	Clear Creek	Kelley and Chapin, 2004
38.61417	-105.21267	1994	66.9	8.8	Granodiorite	Pikes Peak	Kelley and Chapin, 2004
39.81483	-105.29067	2469	67.3	9.6	Schist	Von Bibber Creek	Kelley and Chapin, 2004
40.14083	-105.67233	3450	67.4	12	Granitic gneiss	Indean Peaks	Kelley and Chapin, 2004

Table C.2 (continued)

Latitude	Longitude	Elevation	Age (Ma)	Error (Ma)	Rock Type	Location	Reference
39.82600	-105.40117	2800	67.8	9.2	Monzonite	Von Bibber Creek	Kelley and Chapin, 2004
40.68983	-105.32483	1743	68.7	10.2	Gneiss	Cache la Poudre River	Kelley and Chapin, 2004
39.42650	-105.12550	2073	69.2	23.6	Gneiss	North Fork, South Platte River	Kelley and Chapin, 2004
39.43367	-105.11850	1813	69.3	10.6	Sandstone dike float	North Fork, South Platte River	Kelley and Chapin, 2004
40.68833	-105.29500	1719	70.5	10	Schist/gneiss	Cache la Poudre River	Kelley and Chapin, 2004
39.42833	-105.12200	2012	70.6	10.4	Gneiss	North Fork, South Platte River	Kelley and Chapin, 2004
39.42567	-105.12117	1963	70.8	18.6	Gneiss	North Fork, South Platte River	Kelley and Chapin, 2004
39.46833	-105.74700	2850	71.5	13.8	Granite	North Fork, South Platte River	Kelley and Chapin, 2004
39.51583	-105.66000	3275	71.7	10	Granitic gneiss	North Fork, South Platte River	Kelley and Chapin, 2004
40.82583	-105.30167	1900	72.3	14.2	Granite	Front Range -- Northeast	Kelley and Chapin, 2004
39.42850	-105.11817	1902	74.2	9.6	Gneiss	North Fork, South Platte River	Kelley and Chapin, 2004
40.69167	-105.37050	1810	74.4	9.2	Schist	Cache la Poudre River	Kelley and Chapin, 2004
39.82733	-105.39733	2896	74.7	10.4	Monzonite	Von Bibber Creek	Kelley and Chapin, 2004
39.22250	-105.62733	2743	74.9	18.6	Monzonite	Agate Creek Tarryall Reservoir	Kelley and Chapin, 2004
38.41467	-105.57400	1902	74.9	13	Gneiss	Royal Gorge Arkansas River	Kelley and Chapin, 2004
38.40867	-105.59333	1920	75.8	14.4	Granite/quartzite	Royal Gorge Arkansas River	Kelley and Chapin, 2004
40.69950	-105.24850	1655	75.8	9.2	Schist	Cache la Poudre River	Kelley and Chapin, 2004
39.47700	-105.14617	2085	76.8	12	Granite	North Fork, South Platte River	Kelley and Chapin, 2004
38.35983	-105.73717	1981	77.5	9.4	Granodiorite	Royal Gorge Arkansas River	Kelley and Chapin, 2004
39.23583	-105.60417	2737	78.4	9.8	Monzonite	Agate Creek Tarryall Reservoir	Kelley and Chapin, 2004
39.43617	-105.59083	2560	78.9	11.2	Gneiss	North Fork, South Platte River	Kelley and Chapin, 2004

Table C.2 (continued)

Latitude	Longitude	Elevation	Age (Ma)	Error (Ma)	Rock Type	Location	Reference
39.47500	-105.14067	1981	79.8	11.6	Granitic gneiss	North Fork, South Platte River	Kelley and Chapin, 2004
38.29667	-105.26083	2311	80.8	42.4	Granite	Wet Mountains	Kelley and Chapin, 2004
38.93100	-105.49700	2615	80.9	14.4	Granite	Elevenmile Reservoir	Kelley and Chapin, 2004
40.92950	-105.33900	2080	81.2	9.2	Biotite schist	Front Range -- Northeast	Kelley and Chapin, 2004
38.66033	-105.47517	2408	84.8	11.0	Gneiss	Currant Creek Shear Zone	Kelley and Chapin, 2004
38.61183	-105.44900	2280	85.4	16.0	quartz diorite	Currant Creek Shear Zone	Kelley and Chapin, 2004
38.45700	-105.58450	2516	87.9	12.0	Quartz Monzonite	Royal Gorge Arkansas River	Kelley and Chapin, 2004
38.44500	-105.52733	1853	91.7	19.8	Gneiss	Royal Gorge Arkansas River	Kelley and Chapin, 2004
39.47933	-105.12700	1713	93.4	17.6	Granitic gneiss	North Fork, South Platte River	Kelley and Chapin, 2004
38.93417	-105.55867	2670	94.1	14.8	Granite	Elevenmile Reservoir	Kelley and Chapin, 2004
38.45283	-105.59233	2219	95.9	12.6	Gneiss	Royal Gorge Arkansas River	Kelley and Chapin, 2004
38.83833	-105.77717	2880	97.5	30.4	Granite	Agate Creek Tarryall Reservoir	Kelley and Chapin, 2004
39.74750	-105.25033	1770	98.9	14	Migmatitic gneiss	Clear Creek	Kelley and Chapin, 2004
39.74933	-105.23883	1976	100.8	11.2	Gneiss	Golden/Lookout Mountain	Kelley and Chapin, 2004
39.41333	-105.65600	3560	104.5	15.2	Gneiss	North Fork, South Platte River	Kelley and Chapin, 2004
38.16000	-105.26000	2741	109.5	22.4	Granite	Wet Mountains	Kelley and Chapin, 2004
38.65383	-105.22050	2061	110.9	13.4	Granodiorite	Pikes Peak	Kelley and Chapin, 2004
39.44967	-105.11817	2060	111.9	15.4	Granite	North Fork, South Platte River	Kelley and Chapin, 2004
39.43883	-105.22633	1999	114.1	15.2	Granite	North Fork, South Platte River	Kelley and Chapin, 2004
38.43350	-105.26483	1650	115	13.6	Gneiss	Royal Gorge Arkansas River	Kelley and Chapin, 2004
39.38333	-105.44517	2353	115.7	18.6	Schist	North Fork, South Platte River	Kelley and Chapin, 2004

Table C.2 (continued)

Latitude	Longitude	Elevation	Age (Ma)	Error (Ma)	Rock Type	Location	Reference
39.75417	-105.23700	1755	115.7	38.8	Granitic gneiss	Clear Creek	Kelley and Chapin, 2004
39.41550	-105.68033	3743	115.9	16.8	Quartz Monzonite	North Fork, South Platte River	Kelley and Chapin, 2004
38.00000	-105.16833	2390	115.9	21.2	Migmatitic gneiss	Wet Mountains	Kelley and Chapin, 2004
39.42400	-105.46633	2521	117.1	25.6	Granite	North Fork, South Platte River	Kelley and Chapin, 2004
38.09833	-105.14500	2860	118.8	17.2	Migmatitic gneiss	Wet Mountains	Kelley and Chapin, 2004
39.45067	-105.11850	2012	118.9	17.6	Granitic gneiss	North Fork, South Platte River	Kelley and Chapin, 2004
39.39717	-105.52050	2603	119.6	21.4	Granitic gneiss	North Fork, South Platte River	Kelley and Chapin, 2004
39.48333	-105.11917	1707	119.6	24.4	Gneiss/schist	North Fork, South Platte River	Kelley and Chapin, 2004
38.17617	-105.12950	2175	122.3	16.6	Migmatitic gneiss	Wet Mountains	Kelley and Chapin, 2004
39.41333	-105.47300	2432	122.8	20.2	Gneiss	North Fork, South Platte River	Kelley and Chapin, 2004
38.16500	-105.19167	2561	123	17.6	Migmatitic gneiss	Wet Mountains	Kelley and Chapin, 2004
38.68733	-105.05233	2680	123.6	22.4	Granodiorite	Pikes Peak	Kelley and Chapin, 2004
38.44733	-105.52083	1853	126.2	20	Granite/pegmatite	Royal Gorge Arkansas River	Kelley and Chapin, 2004
38.90200	-105.50217	2639	127.6	24.2	Granite	Elevenmile Reservoir	Kelley and Chapin, 2004
38.45233	-105.49433	1829	128.8	21.6	Pegmatite	Royal Gorge Arkansas River	Kelley and Chapin, 2004
39.38250	-105.54267	3042	130.9	18.8	Granodiorite	North Fork, South Platte River	Kelley and Chapin, 2004
38.45467	-105.50000	1841	134	23.6	Gneiss	Royal Gorge Arkansas River	Kelley and Chapin, 2004
39.49550	-105.63083	3923	134.7	25.4	Granitic gneiss	North Fork, South Platte River	Kelley and Chapin, 2004
39.54417	-105.16883	1886	135	31.2	Granite	Deer Creek	Kelley and Chapin, 2004
38.11500	-105.12667	2687	138.4	22.4	Migmatitic gneiss	Wet Mountains	Kelley and Chapin, 2004
38.97400	-105.44783	2643	138.7	36	Gneiss	Elevenmile Reservoir	Kelley and Chapin, 2004
38.20500	-105.36667	2469	140.6	20.4	Migmatitic gneiss	Wet Mountains	Kelley and Chapin, 2004
39.78483	-105.24233	1859	142.8	20.4	Phyllite/schist	Golden Gate Canyon	Kelley and Chapin, 2004

Table C.2 (continued)

Latitude	Longitude	Elevation	Age (Ma)	Error (Ma)	Rock Type	Location	Reference
38.95217	-105.47117	2758	143.0	18.0	Pegmatite	Elevenmile Reservoir	Kelley and Chapin, 2004
39.75383	-105.24200	1768	149.7	38	Gneiss	Golden/Lookout Mountain	Kelley and Chapin, 2004
39.39367	-105.53050	2749	149.9	16.8	Granitic gneiss	North Fork, South Platte River	Kelley and Chapin, 2004
39.41883	-105.47183	2463	151.9	32.2	Granite	North Fork, South Platte River	Kelley and Chapin, 2004
39.36917	-105.54683	3554	155.8	22	Granite	North Fork, South Platte River	Kelley and Chapin, 2004
38.60983	-105.20400	2329	156.3	23.2	Granodiorite	Pikes Peak	Kelley and Chapin, 2004
38.43917	-105.53917	1877	164	26.4	Granite	Royal Gorge Arkansas River	Kelley and Chapin, 2004
37.91583	-104.99500	2521	166.5	18.8	Gneiss	Wet Mountains	Kelley and Chapin, 2004
38.48417	-105.40667	1768	169.8	22.6	Diorite	Royal Gorge Arkansas River	Kelley and Chapin, 2004
38.60917	-105.19867	2512	170.5	37	Granodiorite	Pikes Peak	Kelley and Chapin, 2004
38.70333	-104.84333	1951	171	19.8	Quartz Monzonite	Pikes Peak	Kelley and Chapin, 2004
38.47183	-105.44700	1780	171.3	30.6	Granodiorite	Royal Gorge Arkansas River	Kelley and Chapin, 2004
38.62750	-105.21883	1994	172.2	35.8	Granodiorite	Pikes Peak	Kelley and Chapin, 2004
38.48683	-105.37067	1756	173.8	23.8	Diorite	Royal Gorge Arkansas River	Kelley and Chapin, 2004
38.18167	-105.40667	2411	180.8	22.8	Migmatitic gneiss	Wet Mountains	Kelley and Chapin, 2004
38.62300	-105.48650	2396	183.9	32	Gneiss	Currant Creek Shear Zone	Kelley and Chapin, 2004
37.93333	-105.06667	3445	187.4	26.4	Granite	Wet Mountains	Kelley and Chapin, 2004
38.22667	-105.34500	2414	188.6	22.8	Migmatitic gneiss	Wet Mountains	Kelley and Chapin, 2004
38.61083	-105.20933	2122	194.6	35.4	Granodiorite	Pikes Peak	Kelley and Chapin, 2004
38.34500	-105.23333	1911	195.1	23.6	Granodiorite	Wet Mountains	Kelley and Chapin, 2004
39.74717	-105.24383	2036	196.0	26.4	Gneiss	Golden/Lookout Mountain	Kelley and Chapin, 2004
39.48517	-105.10750	1708	197.4	25.4	Granodiorite	North Fork, South Platte River	Kelley and Chapin, 2004
37.90083	-105.01333	3116	199.1	25.8	Granite	Wet Mountains	Kelley and Chapin, 2004
38.61500	-105.46650	2329	199.7	33.4	Gneiss	Currant Creek Shear Zone	Kelley and Chapin, 2004

Table C.2 (continued)

Latitude	Longitude	Elevation	Age (Ma)	Error (Ma)	Rock Type	Location	Reference
38.00083	-105.18250	3171	210.7	25.2	Granite	Wet Mountains	Kelley and Chapin, 2004
38.65400	-105.11583	2771	211.7	42.6	Granodiorite	Pikes Peak	Kelley and Chapin, 2004
38.45783	-105.58900	2390	212.1	24.4	Gneiss	Royal Gorge Arkansas River	Kelley and Chapin, 2004
37.89333	-105.04000	3506	219.8	25.8	Granite	Wet Mountains	Kelley and Chapin, 2004
37.90000	-105.02333	3564	228.3	33.2	Migmatitic gneiss	Wet Mountains	Kelley and Chapin, 2004
38.55933	-105.42317	1999	230	35.8	Granodiorite	Currant Creek Shear Zone	Kelley and Chapin, 2004
39.54617	-105.16000	1829	233.1	26.6	Granite	Deer Creek	Kelley and Chapin, 2004
38.98917	-105.38883	2463	252.1	31.6	Gneiss	Elevenmile Reservoir	Kelley and Chapin, 2004
38.93333	-105.56000	2650	264.7	78	Granite	Elevenmile Reservoir	Kelley and Chapin, 2004
38.33000	-105.23500	2108	290.2	29	Granodiorite	Wet Mountains	Kelley and Chapin, 2004
38.33167	-105.24333	2241	298.8	40.2	Granodiorite	Wet Mountains	Kelley and Chapin, 2004
38.50042	-107.02622	2295	177.4	10	granite	Black Canyon of the Gunnison	Kelley, unpublished
38.48625	-107.04350	2295	158.8	8.2	granite	Black Canyon of the Gunnison	Kelley, unpublished
38.48685	-107.06717	2299	83.1	5.1	granite	Black Canyon of the Gunnison	Kelley, unpublished
38.44948	-107.34560	2256	55.8	4	granite	Black Canyon of the Gunnison	Kelley, unpublished
38.44750	-107.34252	2359	69.6	4.3	granite	Black Canyon of the Gunnison	Kelley, unpublished
38.40458	-107.40742	2498	40.7	3.2	granite	Black Canyon of the Gunnison	Kelley, unpublished
38.71733	-106.22317	2640	12.3	1.5	granite	Mt. Princeton	Kelley et al., 1992
38.74200	-106.20067	3146	14.1	1.8	granite	Mt. Princeton	Kelley et al., 1992
38.74217	-106.19283	3055	13.2	1.5	granite	Mt. Princeton	Kelley et al., 1992
38.74283	-106.18650	2969	9.5	0.8	granite	Mt. Princeton	Kelley et al., 1992
38.74850	-106.18733	2899	9.6	1.2	granite	Mt. Princeton	Kelley et al., 1992
38.74250	-106.35150	3896	22.9	2.5	granite	Mt. Princeton	Kelley et al., 1992
38.74133	-106.34933	3846	22.9	2.5	granite	Mt. Princeton	Kelley et al., 1992
38.74000	-106.34633	3747	23.1	2.8	granite	Mt. Princeton	Kelley et al., 1992
38.71900	-106.34417	3396	17.8	1.8	granite	Mt. Princeton	Kelley et al., 1992

Table C.2 (continued)

Latitude	Longitude	Elevation	Age (Ma)	Error (Ma)	Rock Type	Location	Reference
38.70600	-106.33983	3041	20.1	2.3	granite	Mt. Princeton	Kelley et al., 1992
38.70633	-106.30083	2902	15.3	1.9	granite	Mt. Princeton	Kelley et al., 1992
38.71583	-106.25567	2768	14.8	1.9	granite	Mt. Princeton	Kelley et al., 1992
37.74700	-105.45667	3299	12.8	2.3	gneiss	Sangre de Cristo Mountains	Kelley et al., 1992
37.73067	-105.46117	2927	10.4	1.3	granite	Sangre de Cristo Mountains	Kelley et al., 1992
37.73333	-105.50600	2536	5.6	1.4	metasediment	Sangre de Cristo Mountains	Kelley et al., 1992
37.28900	-105.16417	4121	37.2	5.9	sandstone	Sangre de Cristo Mountains	Kelley et al., 1992
37.29783	-105.16367	3847	31.4	4.1	sandstone	Sangre de Cristo Mountains	Kelley et al., 1992
37.31833	-105.12750	3082	18.6	2.5	siltstone	Sangre de Cristo Mountains	Kelley et al., 1992
37.33200	-105.09483	2829	19.4	2.3	siltstone	Sangre de Cristo Mountains	Kelley et al., 1992
37.61367	-105.18900	2870	38.9	4	arkose sandstone	Sangre de Cristo Mountains	Kelley et al., 1992
37.53150	-105.29483	2536	28.5	2.6	sandstone	Sangre de Cristo Mountains	Kelley et al., 1992
37.49450	-105.34183	2530	22	2	gneiss	Sangre de Cristo Mountains	Kelley et al., 1992
37.57733	-105.48517	4373	18	2	gabbro	Sangre de Cristo Mountains	Kelley et al., 1992
37.56867	-105.51167	3591	20.3	3.5	gneiss	Sangre de Cristo Mountains	Kelley et al., 1992
37.55100	-105.55633	2732	16	2.7	granite	Sangre de Cristo Mountains	Kelley et al., 1992
37.28833	-105.31167	2911	29.3	3.7	tuff	Sangre de Cristo Mountains	Kelley et al., 1992
37.29250	-105.27950	3280	29.3	7.1	granitic gneiss	Sangre de Cristo Mountains	Kelley et al., 1992
37.28400	-105.25817	3268	11.3	1.9	gneiss	Sangre de Cristo Mountains	Kelley et al., 1992

Table C.2 (continued)

Latitude	Longitude	Elevation	Age (Ma)	Error (Ma)	Rock Type	Location	Reference
37.24800	-105.27850	3226	10.6	1.5	pegmatite granite	Sangre de Cristo Mountains	Kelley et al., 1992
37.23733	-105.31067	2878	32.5	3.9	granitic gneiss	Sangre de Cristo Mountains	Kelley et al., 1992
37.25317	-105.33317	2646	11.5	2.7	quartzite	Sangre de Cristo Mountains	Kelley et al., 1992
37.12217	-105.18517	4283	42.3	7.9	granitic gneiss	Sangre de Cristo Mountains	Kelley et al., 1992
37.60317	-105.47533	3300	13.4	2.7	granite	Sangre de Cristo Mountains	Kelley et al., 1992
37.59483	-105.49000	3775	17.5	3.7	granite	Sangre de Cristo Mountains	Kelley et al., 1992
37.59167	-105.48183	3525	12.7	3.1	granite	Sangre de Cristo Mountains	Kelley et al., 1992
40.72133	-106.60017	3048	54.6	4.7	Proterozoic Mt. Ethel granite	Park Range	Kelley, 2005
40.76900	-106.91467	3075	53.8	5.8	Proterozoic metasediment	Park Range	Kelley, 2005
40.38267	-106.68867	2847	69.2	5.3	Proterozoic granite	Park Range	Kelley, 2005
40.36917	-106.74083	2865	70.3	5.3	Proterozoic gneiss and granite	Park Range	Kelley, 2005
40.34867	-106.74733	2658	63.8	4.7	Proterozoic migmatite	Park Range	Kelley, 2005
40.36083	-106.77300	2499	68.9	6.7	Proterozoic granite lens	Park Range	Kelley, 2005
40.36967	-106.79150	2347	63.8	6.4	Proterozoic granitic gneiss	Park Range	Kelley, 2005
40.37750	-106.79800	2280	73.5	4.1	Proterozoic granite lens	Park Range	Kelley, 2005
40.38733	-106.80833	2158	64.1	3.7	Proterozoic granite	Park Range	Kelley, 2005
40.52983	-106.71967	3075	69.2	5.4	Proterozoic gneiss	Park Range	Kelley, 2005
40.59117	-106.69783	3316	55.1	7	Proterozoic Mt. Ethel granite	Park Range	Kelley, 2005
40.55833	-106.70033	3261	57.6	13.6	Proterozoic gneiss	Park Range	Kelley, 2005

Table C.2 (continued)

Latitude	Longitude	Elevation	Age (Ma)	Error (Ma)	Rock Type	Location	Reference
40.65033	-106.78083	2926	63.2	4.8	Proterozoic Mt. Ethel granite	Park Range	Kelley, 2005
40.61667	-106.83150	2536	46.5	3.9	Proterozoic Mt. Ethel granite	Park Range	Kelley, 2005
40.60417	-106.84500	2353	53.8	4	Proterozoic gneiss	Park Range	Kelley, 2005
40.57367	-106.88083	2134	58.9	4.2	Proterozoic gneiss	Park Range	Kelley, 2005
40.56767	-106.88533	2073	60.1	3.9	Proterozoic gneiss	Park Range	Kelley, 2005
40.52717	-106.76000	2743	54.5	4.2	Proterozoic gneiss	Park Range	Kelley, 2005
40.52883	-106.77817	2548	64.6	5	Proterozoic gneiss	Park Range	Kelley, 2005
40.52583	-106.80783	2268	68.8	4.7	Proterozoic gneiss	Park Range	Kelley, 2005
40.51483	-106.81283	2164	71	4.8	Proterozoic gneiss	Park Range	Kelley, 2005
40.76983	-106.77483	2438	76.1	4.4	Proterozoic gneiss	Park Range	Kelley, 2005
40.76483	-106.78933	2390	67.8	5.7	Proterozoic gneiss	Park Range	Kelley, 2005
40.75833	-106.80800	2365	70.9	11.1	Proterozoic gneiss	Park Range	Kelley, 2005
40.74750	-106.84617	2316	51.5	5.3	Proterozoic schist	Park Range	Kelley, 2005
40.72567	-106.88767	2256	50.8	4.8	Proterozoic gneiss	Park Range	Kelley, 2005
40.73950	-106.90917	2286	66.8	5	Triassic Chugwater siltstone	Park Range	Kelley, 2005
39.07060	-106.40300	--	18.5	8	Granodiorite	--	Marvin et al., 1974
38.01338	-107.79273	3937	23.1	2.8	Precambrian crystalline rocks	Mt. Sneffles Stock	McKeon, 2009
38.02080	-107.78120	3262	29.4	4.1	Precambrian crystalline rocks	Mt. Sneffles Stock	McKeon, 2009
37.79455	-107.73270	3954	19.6	1.7	Precambrian crystalline rocks	Bear Peak	McKeon, 2009
37.80403	-107.72392	3651	19.1	3.4	Precambrian crystalline rocks	Bear Peak	McKeon, 2009
37.80883	-107.72070	3373	21	2.4	Precambrian crystalline rocks	Bear Peak	McKeon, 2009
37.81652	-107.72920	2966	11.5	1.2	Precambrian crystalline rocks	Bear Peak	McKeon, 2009
39.82860	-106.31000	2642	4.8	2.60	Gneiss	Gore Range East	Naeser et al., 2002
39.63030	-106.14310	3152	5.7	1.50	Granite	Gore Range East	Naeser et al., 2002
39.53110	-106.10580	2929	6.4	2.00	Granofels	Gore Range East	Naeser et al., 2002

Table C.2 (continued)

Latitude	Longitude	Elevation	Age (Ma)	Error (Ma)	Rock Type	Location	Reference
39.57500	-106.07970	2791	7.5	1.60	Granite	Gore Range East	Naeser et al., 2002
39.69080	-106.19780	3100	9.2	1.80	Granite	Gore Range East	Naeser et al., 2002
39.63190	-106.14920	3364	10.9	2.40	Migmatite	Gore Range East	Naeser et al., 2002
39.62140	-106.13500	3621	11.0	2.80	Gneiss	Gore Range East	Naeser et al., 2002
39.69170	-106.20190	3230	11.7	2.00	Granite	Gore Range East	Naeser et al., 2002
39.69360	-106.20750	3433	11.9	1.50	Migmatite	Gore Range East	Naeser et al., 2002
39.78420	-106.27690	2810	12.8	3.50	Granite	Gore Range -- Mt Powell	Naeser et al., 2002
39.69530	-106.21500	3755	13.5	2.20	Granite	Gore Range East	Naeser et al., 2002
39.76830	-106.28920	3011	14.1	1.90	Granite	Gore Range -- Mt Powell	Naeser et al., 2002
39.69170	-106.21810	3911	15.9	2.20	Granite	Gore Range East	Naeser et al., 2002
39.62890	-106.26970	2727	16.7	3.40	Arkose	Gore Range West	Naeser et al., 2002
39.69420	-106.21140	3603	16.8	3.40	Granite	Gore Range East	Naeser et al., 2002
39.68190	-106.34250	3410	17.8	3.30	Granite	Gore Range West	Naeser et al., 2002
39.72390	-105.90140	3959	19.0	7.90	MonzoGranite	Front Range -- Pettingel Peak	Naeser et al., 2002
39.61810	-106.14190	3871	19.2	6.70	Gneiss	Gore Range East	Naeser et al., 2002
39.61610	-106.14250	3889	19.4	5.10	Gneiss	Gore Range East	Naeser et al., 2002
39.72530	-105.89420	3670	19.5	3.30	Amphibolite	Front Range -- Pettingel Peak	Naeser et al., 2002
39.81250	-106.34580	3042	20.4	6.60	Diorite	Gore Range West	Naeser et al., 2002
39.62530	-106.21940	3032	21.0	2.50	MonzoGranite	Gore Range West	Naeser et al., 2002
39.82580	-106.10690	2993	21.0	4.50	Granodiorite Gneiss	Front Range West	Naeser et al., 2002
39.75720	-106.31830	3261	21.4	2.60	MetaGabbro	Gore Range -- Mt Powell	Naeser et al., 2002
39.70640	-105.84110	3316	21.7	4.50	MonzoGranite	Front Range -- Mount Parnassus	Naeser et al., 2002
39.70080	-105.79250	2987	21.8	5.80	MonzoGranite	Front Range -- Mount Parnassus	Naeser et al., 2002
39.75420	-106.33580	3658	22.4	2.20	MonzoGranite	Gore Range -- Mt Powell	Naeser et al., 2002
39.62890	-106.24420	2920	22.4	2.90	Tonalite	Gore Range West	Naeser et al., 2002
39.67140	-106.33970	3340	22.9	3.80	Granite	Gore Range West	Naeser et al., 2002
39.65110	-106.28250	2902	23.4	3.40	Granite	Gore Range West	Naeser et al., 2002
39.70390	-105.85060	3182	23.4	6.20	Tonalite	Front Range -- Mount Parnassus	Naeser et al., 2002
39.53390	-106.22360	3337	24.2	4.30	Arkose	Gore Range West	Naeser et al., 2002

Table C.2 (continued)

Latitude	Longitude	Elevation	Age (Ma)	Error (Ma)	Rock Type	Location	Reference
39.76000	-106.34030	4139	24.4	2.50	Granite	Gore Range -- Mt Powell	Naeser et al., 2002
39.75560	-106.34080	3865	24.7	4.50	Granite Gneiss	Gore Range -- Mt Powell	Naeser et al., 2002
39.50170	-106.16310	2993	25.4	5.50	Granofels	Gore Range West	Naeser et al., 2002
39.54000	-106.19890	3487	25.5	4.90	Granodiorite	Gore Range West	Naeser et al., 2002
39.71110	-105.83060	3554	25.9	6.30	Granodiorite	Front Range -- Mount Parnassus	Naeser et al., 2002
39.54420	-106.21080	3401	26.5	4.30	Arkose	Gore Range West	Naeser et al., 2002
39.83220	-106.11690	3252	27.5	5.70	Granodiorite	Front Range West	Naeser et al., 2002
39.65140	-106.24250	3746	28.9	3.10	Tonalite	Gore Range West	Naeser et al., 2002
39.67140	-106.33970	3325	30.2	3.70	Arkose	Gore Range West	Naeser et al., 2002
39.55670	-106.19560	3804	30.8	5.00	Granite	Gore Range West	Naeser et al., 2002
39.82890	-106.42140	3267	31.4	3.60	Granite	Gore Range West	Naeser et al., 2002
39.64310	-106.24530	3438	32.3	5.10	Tonalite	Gore Range West	Naeser et al., 2002
39.71810	-105.91110	3975	32.3	5.80	Amphibolite	Front Range -- Pettingel Peak	Naeser et al., 2002
39.55170	-106.19690	3716	32.6	4.60	Tonalite	Gore Range West	Naeser et al., 2002
39.56830	-107.29170	1871	34.2	4.50	MonzoGranite	White River Uplift	Naeser et al., 2002
39.71830	-105.82890	3795	34.3	5.50	MonzoGranite	Front Range -- Mount Parnassus	Naeser et al., 2002
39.82280	-106.05440	2690	35.9	4.70	Schist	Front Range West	Naeser et al., 2002
39.80250	-106.40390	3557	37.0	4.30	Granite	Gore Range West	Naeser et al., 2002
39.56220	-107.24890	1817	40.9	4.70	Granodiorite Gneiss	White River Uplift	Naeser et al., 2002
39.71860	-105.82190	4135	43.4	14.30	MonzoGranite	Front Range -- Mount Parnassus	Naeser et al., 2002
39.66890	-107.52310	2084	45.3	5.80	MonzoGranite Gneiss	White River Uplift	Naeser et al., 2002
39.73190	-107.79610	2371	48.2	4.20	Tonalite	White River Uplift	Naeser et al., 2002
39.72060	-105.82640	4029	48.3	6.80	MonzoGranite	Front Range -- Mount Parnassus	Naeser et al., 2002
39.78000	-107.41780	3243	50.9	6.80	Tonalite	White River Uplift	Naeser et al., 2002
39.84500	-107.33440	2761	53.2	5.70	Granitic	White River Uplift	Naeser et al., 2002
39.78000	-107.41780	3243	62.8	7.00	Tonalite	White River Uplift	Naeser et al., 2002
39.75670	-106.34060	3962	283.0	29.00	Gneiss	Gore Range -- Mt Powell	Naeser et al., 2002
38.84080	-105.04420	4300	458.0	58.00	Granite	Front Range -- Pikes Peak	Naeser et al., 2002

Table C.2 (continued)

Latitude	Longitude	Elevation	Age (Ma)	Error (Ma)	Rock Type	Location	Reference
37.68330	-108.03300	--	4.6	5.8	Latite	--	Naeser et al., 1980
37.70000	-108.03300	--	5.6	6.4	Latite	--	Naeser et al., 1980
37.69170	-108.05800	--	6.6	4.6	Monzonite	--	Naeser et al., 1980
37.69170	-108.02500	--	7	6.6	Latite	--	Naeser et al., 1980
37.72500	-108.02500	--	7.8	7.4	Latite	--	Naeser et al., 1980
37.65000	-108.03300	--	10.3	8.2	Latite	--	Naeser et al., 1980
37.63330	-108.05800	--	20.2	14.8	Latite	--	Naeser et al., 1980

Table C.3: Regional Oligocene pluton LTT data. Mapped on Figure 4.7.

Latitude	Longitude	Elevation (m)	AFT: Age	AHe:Age	Location	Reference
39.26115	-107.16424	3944 - 3107	31.3 - 21.4 Ma	12.4 - 9.9 Ma	Mt. Sopris	This Study
39.15400	-107.07649	4151 - 3386	23.8 - 22.3 Ma	11.2 - 8.2 Ma	Capitol Peak	This Study
39.11877	-107.06587	4295 - 3460	28.8 - 17.6 Ma	15.0 - 5.8 Ma	Snowmass Mtn.	This Study
39.03173	-107.21269	3641 - 1882	31.1 - 15.4 Ma	11.6 - 5.6 Ma	Ragged Mtn.	This Study
38.92985	-107.24321	3458 - 2826	25.7 - 22.4 Ma	--	Marcellina Mtn.	This Study
38.85245	-107.21861	3530 - 3045	30.5 - 27.6 Ma	29.4 - 15.1 Ma	E. Beckwith Mtn.	This Study
38.81214	-107.38233	3881 - 3149	33.8 - 29.0 Ma	35.4 - 32.0 Ma	Mt. Gunnison	This Study
37.34208	-106.49433	3381 - 2985	--	28.3 - 22.3 Ma	Alamosa River	McKeon, 2009
37.38042	-106.69960	3803 - 3623	--	21.0 - 19.2 Ma	Bear Creek	McKeon, 2009
37.28210	-106.58833	3734	--	31.9 Ma	Diablo Canyon	McKeon, 2009
38.30343	-106.58915	2929	--	38.6 Ma	Needle Creek	McKeon, 2009
38.01338	-107.79273	3937 - 3084	29.4 - 23.1 Ma	9.4 - 2.8 Ma	Mt. Sneffles	McKeon, 2009
37.79455	-107.73270	3954 - 2966	21 - 11.5 Ma	10 - 4.2 Ma	Bear Peak	McKeon, 2009
37.86038	-107.98467	4272 - 3747	--	21.9 - 20.1 Ma	Mt. Wilson	McKeon, 2009
37.35213	-106.94428	2412	--	5.8 Ma	Jackson Mtn.	McKeon, 2009

REFERENCES

- Bookstrom, A.A., Naeser, C.W. & Shannon, J.R., 1987. Isotopic age determinations, unaltered and hydrothermally altered igneous rocks, north-central Colorado mineral belt. *Isochron/West*, 49, pp.13-20.
- Bryant, B., 1979. Geology of the Aspen 15-Minute Quadrangle, Pitkin and Gunnison Counties, Colorado. *US Geological Survey Professional Paper*, 1073, pp.1-146.
- Bryant, B. & Martin, P.L., 1988. The geologic story of the Aspen region: mines, glaciers, and rocks. *US Geological Survey Bulletin*, 1603, p.53.
- Bryant, B. & Naeser, C.W., 1980. The significance of fission-track ages of apatite in relation to the tectonic history of the Front and Sawatch Ranges, Colorado. *Geological Society of America Bulletin*, 91(3), p.156.
- Bryant, B., Naeser, C.W. & Stegen, R.J., 1990. Reconnaissance fission-track geochronology of the Aspen mining district, central Colorado, in Beaty, D.W., Landis, G.P., and Thompson, T.B., eds., Carbonate-hosted sulfide deposits of the central Colorado mineral belt. *Economic Geology Monograph*, (no. 7), pp.301-307.
- Chapin, Charles E., 1979. Evolution of the Rio Grande rift - A summary. *Rio Grande Rift: Tectonics and Magmatism, American Geophysical Union*, pp.1-5.
- Chapin, Charles E., Origin of the Colorado mineral belt (in press). *Geological Society of America Bulletin*.
- Chapin, Charles E. & Cather, S.M., 1994. Tectonic setting of the axial basins of the northern and central Rio Grande rift. *GSA SPECIAL PAPERS*, 291, pp.5-25.
- Coney, P.J. & Reynolds, S.J., 1977. Cordilleran Benioff zones. *Nature*, 270(5636), pp.403-406.
- Cunningham, C.G., Naeser, C.W. & Marvin, R.F., 1977. New ages for intrusive rocks in the Colorado mineral belt. *U.S. Geological Survey*, (Open-File Report 77-573), p.8.
- Cunningham, C.G. et al., 1994. Age of selected intrusive rocks and associated ore deposits in the Colorado Mineral Belt. *U.S. Geological Survey Bulletin*, 2109, p.31.

- Cunningham, Charles G., J., 1976. Petrogenesis and postmagmatic geochemistry of the Italian Mountain Intrusive Complex, eastern Elk Mountains, Colorado. *Geological Society of America Bulletin*, 87(6), pp.897-908.
- Cunningham, Charles G., J. & Naeser, C.W., 1975. The Italian Mountain Intrusive Complex, west-central Colorado, in Cohee, G.V., and Wright, W. B., Changes in stratigraphic nomenclature by the U. S. Geological Survey. *U.S. Geological Survey Bulletin*, 1405-A, p.A27-A28.
- Cunningham, Charles G., J. et al., 1994. Ages of selected intrusive rocks and associated ore deposits in the Colorado mineral belt. *U.S. Geological Survey Bulletin*, 2109, pp.1-31.
- Decker, E.R. et al., 1988. Significance of past and recent heat-flow and radioactivity studies in the Southern Rocky Mountains region. *Geological Society of America Bulletin*, 100(12), pp.1851-1885.
- Donelick, R.A., 1991. Crystallographic orientation dependence of mean etchable fission track length in apatite: An empirical model and experimental observations. *American Mineralogist; (United States)*, 76:1-2.
- Farley, K.A., 2000. Helium diffusion from apatite: General behavior as illustrated by Durango fluorapatite. *Journal of Geophysical Research*, 105(B2), pp.2903-2914.
- Farmer, G. Lang, Bailey, T. & Elkins-Tanton, L.T., 2008. Mantle source volumes and the origin of the mid-Tertiary ignimbrite flare-up in the southern Rocky Mountains, western U.S. *Lithos*, 102(1-2), pp.279-294.
- Feldman, J.D., 2010. *The emplacement and exhumation history of the Twin Lakes batholith and implications for the Laramide orogeny and flat slab subduction [M.S. thesis]*. Socorro, New Mexico Institute of Mining and Technology, p.185.
- Flowers, R.M. & Kelley, Shari A., Compatible apatite (U-Th/He) and fission-track data from cratons: Explaining data dispersion and “inverted” dates in a cratonic dataset (in press). *Earth and planetary science letters*.
- Flowers, R.M. et al., 2009. Apatite (U-Th)/He thermochronometry using a radiation damage accumulation and annealing model. *Geochimica et Cosmochimica Acta*, 73(8), pp.2347-2365.
- Foster, D. et al., 1990. Effects of excess argon within large diffusion domains on K-feldspar age spectra. *Geochimica et Cosmochimica Acta*, 54(6), pp.1699-1708.
- Galbraith, R.F., 1981. On statistical models for fission track counts. *Journal of the International Association for Mathematical Geology*, 13(6), pp.471-478.

- Gaskill, D.L. & Godwin, L.H., 1966a. *Geologic map of the Marble quadrangle, Gunnison and Pitkin Counties, Colorado*, U.S. Geological Survey, GQ-512, scale 1:24000.
- Gaskill, D.L. & Godwin, L.H., 1966b. *Geologic map of the Marcellina Mountain quadrangle, Gunnison County, Colorado*, U.S. Geological Survey, GQ-511, scale 1:24000.
- Gehrels, G.E., Valencia, V.A. & Ruiz, J., 2008. Enhanced precision, accuracy, efficiency, and spatial resolution of U-Pb ages by laser ablation–multicollector–inductively coupled plasma–mass spectrometry. *Geochemistry Geophysics Geosystems*, 9(Q03017), p.13.
- Gleadow, A.J.W. et al., 1986. Confined fission track lengths in apatite: a diagnostic tool for thermal history analysis. *Contributions to Mineralogy and Petrology*, 94(4), pp.405-415.
- Godwin, L.H., 1968. *Geologic map of the Chair Mountain quadrangle, Gunnison and Pitkin Counties, Colorado*, U.S. Geological Survey, GQ-704, scale 1:24000.
- Heizler, M.T., Lux, D.R. & Decker, E.R., 1988. The age and cooling history of the Chain of Ponds and Big Island Pond plutons and the Spider Lake Granite, west-central Maine and Quebec. *American Journal of Science*, 288(9), pp.925-952.
- Hoffman, M. et al., 2010. Mio-Pliocene erosional exhumation of the central Colorado Plateau, eastern Utah: New insights from apatite (U-Th)/He thermochronometry, in Beard, S., Karlstrom, K.E., House, K., Young, D., Aslan, A., Billingsley, G., and Pederson, J., eds. *USGS*, (Open File Report 2011-x).
- Humphreys, E. et al., 2003. How Laramide-Age Hydration of North American Lithosphere by the Farallon Slab Controlled Subsequent Activity in the Western United States. *International Geology Review*, 45(7), pp.575-595.
- Isaacson, L.B. & Smithson, S.B., 1976. Gravity anomalies and granite emplacement in west-central Colorado. *Geological Society of America Bulletin*, 87(1), p.22.
- Jones, C.H. et al., 2011. Hydrodynamic mechanism for the Laramide orogeny. *Geosphere*, 7(1), pp.183-201.
- Karimpour, M.H., 1982. *Petrology, geochemistry, and genesis of the A.O. porphyry copper complex in Jackson and Grand Counties, northwestern Colorado [Ph.D. thesis]*. Boulder, University of Colorado, p.251.
- Karlstrom, Karl E. & Bowring, S.A., 1988. Early Proterozoic Assembly of Tectonostratigraphic Terranes in Southwestern North America. *The Journal of Geology*, 96(5), pp.561 - 576.

- Kelley, S., 2005. Low-temperature cooling histories of the Cheyenne belt and laramie peak shear zone, Wyoming, and the soda creek-fish creek shear zone, Colorado. *Geophysical monograph*, 154, pp.55-70.
- Kelley, S.A. & Blackwell, D.D., 1990. Thermal history of the multi-well experiment (MWX) site, Piceance Creek Basin Northwestern Colorado, derived from fission-track analysis. *International Journal of Radiation Applications and Instrumentation. Part D. Nuclear Tracks and Radiation Measurements*, 17(3), pp.331-337.
- Kelley, S.A. & Chapin, C.E., 2004. Denudation history and internal structure of the Front Range and Wet Mountains, Colorado, based on apatite-fission-track thermochronology. *Tectonics, Geochronology and Volcanism in the Southern Rocky Mountains and Rio Grande Rift: Socorro, New Mexico, New Mexico Bureau of Geology and Mineral Resources Bulletin*, 160, pp.41-78.
- Kelley, S.A., Chapin, C.E. & Corrigan, J., 1992. *Late Mesozoic to Cenozoic cooling histories of the flanks of the northern and central Rio Grande rift, Colorado and New Mexico*, New Mexico Bureau of Mines & Mineral Resources (Socorro).
- Ketcham, R.A., 2005. Forward and inverse modeling of low-temperature thermochronometry data. *Reviews in Mineralogy and Geochemistry*, 58(1), p.275.
- Ketcham, R.A. et al., 2007. Improved modeling of fission-track annealing in apatite. *American Mineralogist*, 92(5-6), p.799.
- Klein, T.L., Evans, K.V. & DeWitt, E.H., 2009. Geochronology database for central Colorado. *U.S. Geological Survey*, (Data Series 489), p.13.
- Lipman, P.W. et al., 1976. Multiple ages of mid-Tertiary mineralization and alteration in the western San Juan Mountains, Colorado. *Economic Geology*, 71(3), pp.571-588.
- Lipman, P.W., Prostka, H.J. & Christiansen, R.L., 1971. Evolving subduction zones in the Western United States, as interpreted from igneous rocks. *Science (New York, N.Y.)*, 174(4011), pp.821-5.
- Lipman, Peter W., 2007. Incremental assembly and prolonged consolidation of Cordilleran magma chambers: Evidence from the Southern Rocky Mountain volcanic field. *Geosphere*, 3(1), p.42.
- Lipman, Peter W. & McIntosh, W.C., 2008. Eruptive and noneruptive calderas, northeastern San Juan Mountains, Colorado: Where did the ignimbrites come from? *Geological Society of America Bulletin*, 120(7), p.771.
- Lipman, Peter W. et al., 1969. Similarity of Cenozoic igneous activity in the San Juan and Elk Mountains, Colorado, and its regional significance. *US Geological Survey Professional Paper*, 650-D, p.D33-D42.

- Lipman, Peter W., Steven, Thomas A. & Mehnert, Harald H., 1970. Volcanic History of the San Juan Mountains, Colorado, as Indicated by Potassium–Argon Dating. *Geological Society of America Bulletin*, 81(8), p.2329.
- Lo, C.-H. & Onstott, T.C., 1989. ^{39}Ar recoil artifacts in chloritized biotite. *Geochimica et Cosmochimica Acta*, 53(10), pp.2697-2711.
- Lovera, O.M., Richter, F.M. & Harrison, T.M., 1989. The $^{40}\text{Ar}/^{39}\text{Ar}$ Thermochronometry for Slowly Cooled Samples Having a Distribution of Diffusion Domain Sizes. *Journal of Geophysical Research*, 94(B12), pp.17917-17935.
- Ludwig, K., 2003. *User's manual for Isoplot 3.00: a geochronological toolkit for Microsoft Excel*, Kenneth R. Ludwig.
- MacCarthy, J.K. et al., 2010. Mantle Lithosphere Support of Colorado Rocky Mountain Elevation: 3D Tomography from CREST. *American Geophysical Union, Fall Meeting*, (abstract #T21E-2217).
- Marvin, R.F. et al., 1974. Summary of radiometric age determinations on Mesozoic and Cenozoic igneous rocks and uranium and base metal deposits in Colorado. *Isochron/West*, (no. 11), pp.1-41.
- McCoy, A.M. et al., 2005. The proterozoic ancestry of the Colorado mineral belt: 1.4 Ga shear zone system in central Colorado. *Geophysical monograph*, 154, pp.71-90.
- McKeon, R.E., 2009. *The interaction between tectonics, topography, and climate in the San Juan Mountains, Southwestern Colorado [M.S. thesis]*. Bozeman, Montana State University, p.86.
- Moucha, R. et al., 2008. Mantle convection and the recent evolution of the Colorado Plateau and the Rio Grande Rift valley. *Geology*, 36(6), p.439.
- Mutschler, F.E., 1970. *Geologic map of the Snowmass Mountain quadrangle, Pitkin and Gunnison Counties, Colorado*, U.S. Geological Survey, GQ-853, scale 1:24000.
- Naeser, C.W. et al., 2002. Late Cenozoic Evaporite Tectonism and Volcanism in West-Central Colorado. *Geological Society of America Special Papers*, 366, pp.31-54.
- Naeser, C.W. et al., 1980. Pliocene intrusive rocks and mineralization near Rico, Colorado. *Economic Geology*, 75, pp.122-127.
- Obradovich, John D., Mutschler, F.E. & Bryant, B., 1969. Potassium-Argon Ages Bearing on the Igneous and Tectonic History of the Elk Mountains and Vicinity, Colorado: A Preliminary Report. *Geological Society of America Bulletin*, 80(9), p.1749.

- Reiter, M., 2008. Geothermal anomalies in the crust and upper mantle along Southern Rocky Mountain transitions. *Geological Society of America Bulletin*, 120(3-4), pp.431-441.
- Reiter, M. et al., 1975. Terrestrial Heat Flow along the Rio Grande Rift, New Mexico and Southern Colorado. *Geological Society of America Bulletin*, 86(6), p.811.
- Renne, P.R., 1998. Intercalibration of standards, absolute ages and uncertainties in $^{40}\text{Ar}/^{39}\text{Ar}$ dating. *Chemical Geology*, 145(1-2), pp.117-152.
- Roy, M. et al., 2004. Middle Tertiary buoyancy modification and its relationship to rock exhumation, cooling, and subsequent extension at the eastern margin of the Colorado Plateau. *Geology*, 32(10), p.925.
- Schmandt, B. & Humphreys, E., 2010. Complex subduction and small-scale convection revealed by body-wave tomography of the western United States upper mantle. *Earth and Planetary Science Letters*, 297(3-4), pp.435-445.
- Shuster, D. & Farley, K.A., 2009. The influence of artificial radiation damage and thermal annealing on helium diffusion kinetics in apatite. *Geochimica et Cosmochimica Acta*, 73(1), pp.183-196.
- Shuster, D.L., Flowers, R.M. & Farley, Kenneth A., 2006. The influence of natural radiation damage on helium diffusion kinetics in apatite. *Earth and Planetary Science Letters*, 249(3-4), pp.148-161.
- Snyder, W.S., Dickinson, W.R. & Silberman, M.L., 1976. Tectonic implications of space-time patterns of Cenozoic magmatism in Western United States. *Earth and Planetary Science Letters*, 32, pp.91-106.
- Stacey, J.S. & Kramers, J.D., 1975. Approximation of terrestrial lead isotope evolution by a two-stage model. *Earth and Planetary Science Letters*, 26(2), pp.207-221.
- Steiger, R.H. & Jager, E., 1977. Subcommittee on geochronology: convention on the use of decay constants in geo- and cosmochronology. *Earth and planetary science letters*, 36, pp.359-362.
- Streufert, R.K., 1999. *Geologic map of the Mount Sopris quadrangle, Garfield and Pitkin Counties, Colorado*, Colorado Geological Survey, Open-File Report 99-7, scale 1:24000.
- Taylor, J.R., 1982. *An introduction to error analysis: the study of uncertainties in physical measurements* 2nd ed., Sausalito: University Science Books.
- Thomas, J.A. & Galey, J.T., 1982. Exploration and geology of the Mt. Emmons molybdenite deposits, Gunnison County, Colorado. *Economic Geology*, 77(5),

pp.1085-1104.

Tweto, O. & Schoenfeld, R.E., 1979. *Geologic map of Colorado*, U.S. Geological Survey, scale 1:500000.

Tweto, O. & Sims, P.K., 1963. Precambrian Ancestry of the Colorado Mineral Belt. *Geological Society of America Bulletin*, 74(8), p.991.

van Wijk, J.W. et al., 2010. Small-scale convection at the edge of the Colorado Plateau: Implications for topography, magmatism, and evolution of Proterozoic lithosphere. *Geology*, 38(7), pp.611-614.

Wohletz, K., 2008. KWare Heat3D.

York, D., 1969. Least squares fitting of a straight line with correlated errors: *Earth Planet. Sci. Letters*, 5, pp.320–324.